Dissertation

Exploring thiol-based chemistry for photopolymerizable inkjet inks and for advanced surface functionalization

by

Florian Hermann Mostegel

Chair of Chemistry of Polymeric Materials

Montanuniversität Leoben

Leoben, September 2015

Affidavit

I declare in lieu of oath, that I wrote this thesis and performed the associated research myself, using only the support indicated in the acknowledgements and literature cited in this volume.

Date	Dipl.-Ing. Florian H. Mostegel

“I’m still confused—but on a higher level”

Enrico Fermi

Acknowledgements

First and foremost I express my gratitude to my family for all their support, not just during the time of my PhD thesis, but every moment leading up to this date as well, as I wouldn't be here without them.

I would like to thank Assoc. Prof. Dr. techn. Thomas Grießer for providing me with the opportunity to work at the Christian Doppler Laboratory for Functional and Polymer Based Inkjet Inks and thus, giving me the opportunity for this thesis. Furthermore, I want to thank him for all his support, guidance and friendship in the last couple of years. Additionally, I want to thank Univ.-Prof. Mag.rer.nat. Dr. techn. Wolfgang Kern for the supervision of this work. I want to thank all other employees of the CD lab for their scientific advices, helpful discussion and for the eventful time. In particular, I want to express my gratitude to our secretary Heike Noll.
Furthermore, I want to thank all members of the Chair of Chemistry of Polymeric Materials and in particular Claudia Wieser for their support.
Moreover, I want to thank Prof. Graham J. Leggett for the opportunity to spend time at the University of Sheffield. Additionally, I want to thank Dr. Robert Ducker and all other members of the Nanoscale Analytical Science Group at the University of Sheffield for their support during my stays.
I would also like to thank all employees of Durst Phototechnik GmbH, Lienz, for their support and advice.

Thanks go in particular to:
Dr. Matthias Edler for his help with the stabilization experiments and XPS measurements
Dr. Josef Spreitz and DI Meinhart Roth for their contribution in the thiol synthesis
Dr. Anna Maria Coclite and DI Baris Kaynak for the ellipsometry measurements
Dr. Simone Radl for the preliminary polymer brush experiments
Paul Rieger for his contribution to the polymer brush and photo-oxidation experiments
Ing. Josefine Hobisch for conducting the GPC measurements
Dr. Osama El Zubir for the fluorescence microscope imaging and for his help in IL patterning
Prof. C. Neil Hunter and Dr. Michael L. Cartron for providing the His-tagged GFP

Financial support by the Durst Phototechnik AG, the Christian Doppler research association and the Austrian Federal Ministry of Science, Research and Economy (BMWFW) is gratefully acknowledged.

Kurzfassung

Bedenken gegenüber Acrylsäureestern auf Grund möglicher gesundheitsschädlicher Auswirkungen verhindern deren Einsatz in einigen Gebieten, wie dem Bedrucken von Nahrungsmittelverpackungen. Der erste Teil dieser Arbeit beschäftigt sich mit der Evaluierung eines alternativen Monomersystems zu den derzeit gebräuchlichen Acrylsäureestern in UV härtenden Druckertinten. Eine interessante Alternative präsentiert sich in der Verwendung von Vinylcarbonaten.

Im Zuge dieser Arbeit wurden verschiedene Vinylcarbonatmonomere synthetisiert und hinsichtlich der Eignung für UV härtende Druckertinten evaluiert. Obwohl die physikalischen Eigenschaften der Vinylcarbonate sich für den Druck als geeignet erwiesen, stellte sich heraus, dass deren Aushärtung für den industriellen Einsatz zu lange benötigt. Durch die Zugabe von multifunktionellen Thiolen konnte das Aushärteverhalten signifikant verbessert werden. Bei der Herstellung von pigmentierten Systemen zeigte sich, dass die kommerziell verfügbaren multifunktionellen Thiole eine zu hohe Viskosität aufweisen, um sie für den digitalen Tintenstrahldruck einzusetzen. Folglich wurde ein tetrafunktionelles Thiol synthetisiert, welches eine geringere Viskosität und nur einen geringen Geruch aufweist. Der Einsatz dieses Thiols für Tintenformulierungen ermöglichte die Entwicklung einer grundlegenden Druckertinte mit ausgezeichnetem Druckverhalten. In weiterer Folge wurde diese Tintenformulierung für den Einsatz auf PET-Folien evaluiert. Weiterführend wurde die Lagerstabilität von Thiol-Vinylcarbonatsystemen untersucht, um sie hinsichtlich ihrer industriellen Einsetzbarkeit zu evaluieren.

Der zweite Teil dieser Arbeit beschäftigt sich mit weiterführenden Untersuchungen von Reaktionen basierend auf Thiolen. Speziell die photochemische Oxidation immobilisierter Mercaptogruppen auf Siliziumoberflächen, welche eine genaue Untersuchung der Reaktionen mittels analytischer Methoden (XPS, AFM) erlaubt, und deren Anwendungen wurden untersucht. Durch photolithographische Verfahren konnte eine strukturierte Photo-Oxidation der Mercaptogruppen zu Sulfonsäuregruppen nachgewiesen werden. Die Möglichkeit einer zusätzlichen Derivatisierung der gebildeten Sulfonsäuregruppen mit Aminen durch eine Aktivierung mittels Triphenylphosphintrifluormethansulfonat wurde erforscht. Eine weitere untersuchte Möglichkeit der Derivatisierung von Mercaptogruppen ist die photo-induzierte Polymerisation. Die Anwendung lithographischer Methoden ermöglichte die Bildung strukturierter „Polymer Brushes“. Die Kombination dieser unterschiedlichen Derivatisierungsmethoden ermöglichte die selektive Immobilisierung von Proteinen im Sub-Mikrometerbereich.

Diese neu entwickelte Strukturierungsmethode jenseits der Thiol-en Reaktion erweitert die bisher bekannten Strategien für die Herstellung von komplexen Protein-Nanostrukturen.

Abstract

Concerns over deleterious effects of acrylate monomers limit their applicability in promising fields like food packaging materials. The first part of this work covers the investigation of an alternative system to the commonly used acrylate system in UV curable inkjet inks. One interesting alternative system is based on vinyl carbonates.

Several monomers based on vinyl carbonate building blocks were synthesized and evaluated regarding their application in UV curable digital inks. Although the physical properties of these monomers were appropriate for inkjet printing, the curing speed turned out to be too slow for industrial use. The addition of multifunctional thiols improved the curing behavior (e.g. curing speed and conversion) similar to those for acrylates. However, commercially available multifunctional thiols proved to be of too high viscosity for the use in pigmented ink formulations. Consequently, a multifunctional thiol providing a lower viscosity and low odor was synthesized. Its application enabled the formulation of a basic inkjet ink offering an excellent printing behavior. The ink was further evaluated for its use on PET-substrates. Moreover, the shelf life of thiol-vinyl carbonate inks was investigated to evaluate their applicability in an industrial context.

The second part of this work covers the investigation of thiol-reactions beyond the thiol-ene reaction used in the first part. In particular the photochemical oxidation of immobilized thiol groups and its applicability were investigated. For this matter thiol groups were immobilized on silicon substrates facilitating the monitoring of the reactions through analytical methods. The photo-oxidation of the thiol groups yielded sulfonic acid groups. Using photolithography or interference lithography patterned samples with oxidized and non-oxidized areas were obtained. Remaining thiol groups were evaluated for a photo-induced polymerization reaction under ambient conditions for a facilitated polymer brush patterning. The generated sulfonic acid groups were evaluated for further derivatization with amino-functionalized molecules after activation with triphenylphosphine ditriflate. The combination of both reactions enabled the site-specific immobilization of green fluorescent protein in previously photo-oxidized regions, while the thiol groups in the non-photo-oxidized regions were exploited for the growth of non-specific adsorption inhibiting polymer brushes.

The investigated thiol chemistry beyond the thiol-ene reaction, starting with the photo-oxidation and the subsequent derivatization steps, expand the known strategies for the fabrication of complex protein nanopatterns.

Table of content

Abbreviations

AFM	Atomic force microscopy
AIBN	Azobis(isobutyronitrile)
ATRP	Atom transfer radical polymerization
b	Minimal resolution limit
BD-VC	Butane-1,4-diyl divinyl dicarbonate
BTAF	Benzyltrimethylammonium fluoride
C	Cyan
CIJ	Continuous inkjet
Cy	Cyclohexane
d	Diameter of the orifice
DBC	Double bond conversion
DBN	1,5-Diazabicyclo[4.3.0]non-5-ene
DBU	1,8-Diazabicyclo[5.4.0]undec-7-ene
DEGME-VC	2-(2-Ethoxyethoxy)ethyl vinyl carbonate
Diisooctyl PA	Diisooctylphosphinic acid
DMAP	4-Dimethylaminopyridine
DMEM	Dulbecco's modified Eagle's medium
DMP	Dimatix material printer
DMPhPh	Dimethylphenlyphosphine
DMSO	Dimethyl sulfoxide
DNA	Deoxyribonucleic acid
DoD	Drop-on-demand inkjet
DPG-VC	Oxybis(propane-2,1-diyl) divinyl dicarbonate
DTMP-VC	(Oxybis(methylene))bis(2-ethylpropane-3,2,1-triyl) tetravinyl tetracarbonate
EA	Ethyl acetate
$\mathbf{E_b}$	Binding energy
$\mathbf{E_{kin}}$	Kinetic energy
$\mathbf{EC_{50}}$	Cell viability
EDM-VC	(5-Ethyl-1,3-dioxan-5-yl)methyl vinyl carbonate
EO	Ethoxy group
EPET-VC	Ethoxylated (3/4 **EO**/**VC**) 2,2-bis(methyl vinyl carbonate)1,3-propanediyl divinyl dicarbonate
Eq.	Equivalent
Ethoxy PA	6-[2-[2-(2-Methoxyethoxy)ethoxy]ethoxy]-hexylphosphonic acid
ETTMP	Ethoxylated trimethylolpropan trimercaptopropionate (**MW** 708)
EWG	Electron withdrawing group
FFM	Friction force microscopy
FTIR	Fourier transform infrared spectroscopy
FWHM	Full width at half maximum
GFP	Green fluorescent protein
HALS	Hindered amine light stabilizers
HDFA	Heptadecafluoroundecylamine

HDFDA	Heptadecafluorodecyl acrylate
IB-VC	1,7,7-Trimethylbicyclo[2.2.1]heptan-2-yl vinyl carbonate
IgG	Immunoglobulin G
IL	Interference lithography
ISO	International organization for standardization
K	Black
l.o.	Low odor
M	Magenta
MDPhPh	Methyldiphenylphosphine
MEHQ	Monomethyl ether hydroquinone
MeOH	Methanol
MPTMS	(3-Mercaptopropyl)trimethoxysilane
MW	Molecular weight
M_w	Mass average molar mass
M_n	Number average molar mass
NMR	Nuclear magnetic resonance spectroscopy
NTA	Nitrilotriacetic acid
OEGA	Oligoethylene glycol acrylate
OEGMA	Oligoethylene glycol methacrylate
P	Polarization direction
PBS	Phosphate buffered saline
PDMS	Polydimethylsiloxane
PET	Polyethylene terephthalate
PETMP	Pentaerythritol tetra(3-mercaptopropionate
PE-VC	2-Phenoxyethyl vinyl carbonate
PI blend 50/50	Blend (50 wt%/ 50 wt%) of diphenyl(2,4,6-trimethylbenzoyl)-phosphine oxide and 2-hydroxy-2-methyl-propiophenone
PTFE	Polytetrafluoroethylene
R_a	Arithmetic average roughness
R_{RMS}	Root mean square roughness
ROMP	Ring-opening metathesis polymerization
SAM	Self-assembled monolayer
SIMS	Secondary ion mass spectrometry
SNOM	Near-field scanning optical microscopy
SNP	Scanning near-field scanning photolithography
SPL	Scanning probe lithography
SPM	Scanning probe microscopy
STED	Stimulated emission depletion
STM	Scanning tunneling microscopy
TDET	2,2'-Thiodiethanethiol
TEA	Triethylamine
THF	Tetrahydrofuran
THF-VC	(Tetrahydrofuran-2-yl)methyl vinyl carbonate
t_{max}	The time to reach the maximum heat of polymerization (photo-DSC)

TMPMP	Trimethylolpropan trimercaptopropionate
TMP-VC	2-(Methyl vinyl carbonate)-2-ethylpropane-1,3-diyl divinyl dicarbonate
TPP	Triphenylphosphite
TPPDTF	Triphenlyphoshine ditriflate
UV	Ultraviolet (wavelength between 400 and 100 nm)
VC	Vinyl carbonate
Y	Yellow
z	Photoresist thickness

γ	Interfacial tension
Δ	Phase difference
ΔH	Reaction enthalpy
Δp	Pressure difference
µCP	Micro contact printing
η	Viscosity
θ	Opening angle
θ_c	Contact angle
θ_t	Tilt angle
λ	Wave length
ρ	Density
ρ_s	Complex reflectance ratio
σ	Surface tension
Φs	Spectrometer work function
Ψ	Amplitude ratio

Motivation and outline

The first part of my PhD thesis covers the investigation of an alternative system to the commonly used acrylate system in UV curable inkjet inks. Acrylates are used in many different fields of application. Consequently, they have been exhaustively investigated, and are well understood. Recently however, especially for acrylate monomers, which are in use in the low-viscous inkjet inks, several considerable drawbacks have surfaced concerning some deleterious effects.[1–5] The increasing focus on health issues in industries has produced significant interest in alternative systems. One of the possible alternative systems is based on vinyl carbonates. The group of Professor Liska at the Technical University of Vienna investigated this system for its application in 3D-printing and successfully implemented it for the fabrication of bone scaffolds.[6] However, the addition of thiols is necessary to improve the curing behavior of vinyl carbonates,[7] which is necessary for suitable inks for the industrial high speed printing process.

The aim of this work in collaboration with Durst Phototechnik GmbH in the framework of the Christian Doppler Laboratory for Functional and Polymer Based Inkjet Inks was to investigate a system based on vinyl carbonates for its application in inkjet inks. The main goal was to find a new chemical composition for UV curing inks for the industrial high speed printing process. It is supposed to feature a lower toxicity than the commonly used acrylate-based inks without the necessity of changes to the hardware on the industrial printers.

The aim of the second part of this thesis was to expand the known thiol reactions for surface modifications. Ensuing from the experience from the application of thiol-ene chemistry in the first part of this thesis, further thiol reactions, in particular the photochemical oxidation and its applications, were pursued. For this matter thiol groups were immobilized on silicon substrates. Silicon surfaces do not interact with thiols, as gold would for example, and allow a precise evaluation of chemical changes on the surface through analytical methods due to their smooth surfaces. New patterning strategies using the photo-oxidation of immobilized thiol groups were evaluated. Furthermore, a new derivatization route for the photo-oxidized species was to be investigated in an attempt to make it accessible for further utilization.

One of the possible applications for new surface reactions is the fabrication of DNA-chips and the imitation of cell behavior on surfaces. Those rely on the combination of different surface modification techniques to obtain spatially defined patterns of proteins, genes and gene-sequences.[8–11] Especially for the imitation of the cell behavior, modifications at the nanoscale have to be performed to ensure a cell behavior, which correlates to the one *in vivo*. Thus, the application of the new reaction pathway was tested for the site-specific binding of green fluorescent protein at the sub-micron scale.

1. Inkjet inks with low toxicity based on vinyl carbonates and thiols

Parts of the work in this chapter have been submitted to Progress in Organic Coatings and have been published in Journal Polymer Science Part A (see list of publications).
Dr. Matthias Edler contributed to the thiol-ene stabilization investigation and Dr. Josef Spreitz and Meinhart Roth (PhD student) contributed to the thiol synthesis.

1.1. Introduction

Modern printing is based on the visualization of digitalized information onto a substrate. This "digital printing" and "printing on demand" enables the flexible realization of high quality prints favored and needed in today's industry.[12] In recent years research on new digital inks increased with the endeavor to open up new markets. One highly potential market booming right now is the one for printed electronics, for example. Another promising market is printing on food packaging, textiles and garments. However, the composition of today's commercially available inks limits or even prevents their application in the latter fields due to precarious substances or solvents. Especially UV curable inks with their advantage of instantaneous drying, which is very beneficial in an industrial context, consist of harmful monomers, e.g. acrylates, and photoinitators. The ink is printed on a substrate and a subsequent irradiation with UV light starts a polymerization reaction through photoinitiators. The free radical polymerization of the monomers and oligomers leads to an almost instantaneous crosslinking (e.g. curing), which enables the immediate stacking of the imprinted surfaces.

One of the major issues of irritant chemicals in printing inks concerns the health of the operator of the printer.[13,14] They are consistently subjected to vapors and aerosols of the ink generated during the printing process. The predominately applied acrylic monomers are known to have high irritancy levels and cause skin sensitization upon contact.[2–5] Another aspect for certain applications is the migration of uncured monomers, unreacted photoinitiators and their residuals. In general, monomer conversions of around 80% have been reported for acrylate systems.[6,15,16] Especially the inhibition of the polymerization reaction through oxygen presents a problem in the inkjet inks.[17] To address this issue prevalently high amounts of photoinitiators are used. All molecules (e.g. monomers and photoinitiators), which are not built into the polymeric network upon curing can potentially migrate. Especially for the application on food packaging materials this is not desirable.

In recent years an increase in research on alternative monomer systems to the well-established (meth)acrylates has been observed, especially the works by the group of Liska covering vinyl carbonate and vinyl ester monomers.[6,18] Like acrylates, those monomers may be polymerized by a free radical initiation using photoinitiators.[6] The huge interest in those

monomers is especially owed to their low cytotoxicity and high stability in the uncured state and superior biocompatibility in the cured state, as well as their beneficial degradation behavior compared to acrylate-based systems.[19] One considerable drawback of vinyl carbonates is their significantly lower rate of polymerization compared to acrylates.[6] However, Mautner et al.[7] showed that the addition of multifunctional thiols to vinyl carbonate formulations enhances the curing speed up to values usually reserved for acrylates.

In this work thiol-vinyl carbonate systems are investigated for their applicability as “low-toxic” UV curable inks for digital printing. In previous studies only thiol-vinyl carbonate formulations with viscosities not suitable for pigmented inkjet inks were reported. Consequently, the application of the multifunctional thiol tetra(3-mercaptopropyl)silane was investigated to lower the viscosities of suitable ink formulations to acceptable values. Besides the reactivity, conversion and printability of the thiol-vinyl carbonate system, further important considerations for its industrial use, such as pot life, film forming properties and adhesion behavior, were evaluated.

1.2. Fundamentals

1.2.1. Inkjet printing

Inkjet is a printing technology, in which droplets of ink are jetted from very small orifices directed at a specific position on a substrate. The control of the drop position allows a flexibility not known of other printing methods, which use physical image carrier or plates to transfer the ink to the media. For this reason there is a great variety of applications and technologies on the market today using inkjet technology.

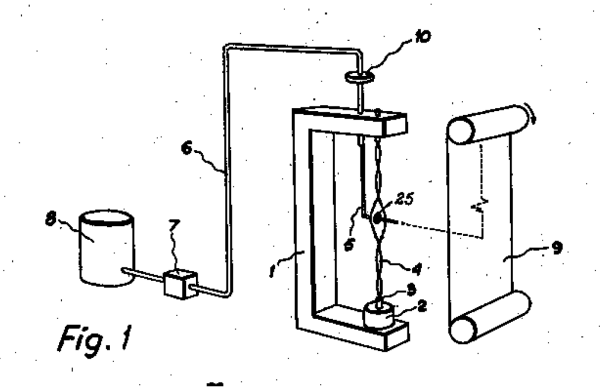

Figure 1: First inkjet printer patented by Rune Elmquist[20]

Although the mechanism by which a liquid stream is broken up into small droplets was already described by Lord Rayleigh in 1878,[21] it was not until 1951, that the first inkjet printing device was patented by Rune Elmquist (Figure 1).[20] His invention describes a recording oscillograph, where the position of a single movable orifice is influenced by a recorded magnitude. Using a continuous ink flow onto a medium, this setup allowed the visualization and recording of the changes of the observed magnitude. A decade later Richard G. Sweet improved the oscillgraph by controlling the droplet size and spacing and, thus, enabled records of higher frequencies.[22] Furthermore, he was able to electrically charge specific droplets selectively and, consequently, he was capable of deflecting them independently by passing them through a deflection field. Uncharged droplets pass the electric field unchanged, while the charged ones are deflected depending on their respective charge.[23] This principle is still used today and is called continuous inkjet (**CIJ**). As the name suggests, the drops are being formed continuously and unnecessary drops are being deflected into a collector and reused (Figure 2). The disadvantages of CIJ systems are their relatively low resolution, high maintenance costs and the prerequisite of an electrically chargeable ink.[24]

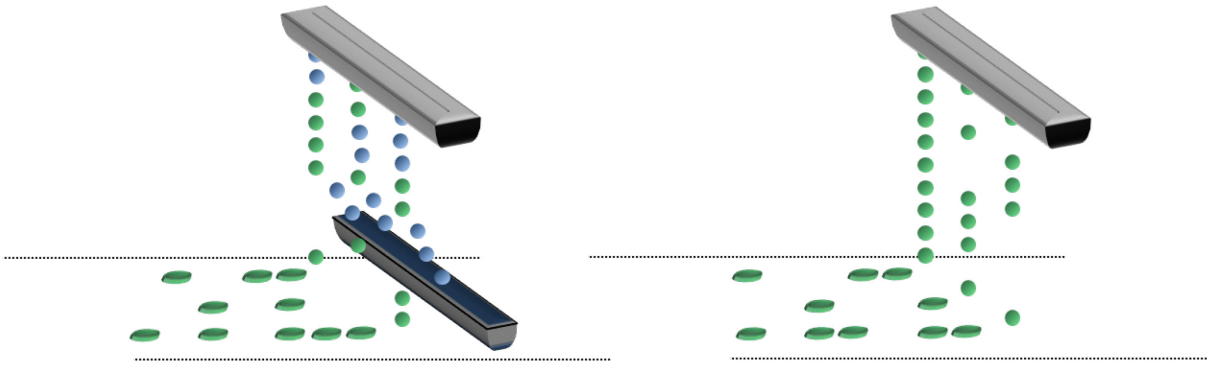

Figure 2: **Left**: continuous inkjet, charged drops (**blue**) are deflected into a pan, while uncharged droplets (**green**) hit the substrate; **right**: drop-on-demand inkjet, the drops are only ejected, when needed

The alternative to CIJ is called drop-on-demand inkjet (**DoD**). A DoD device does only eject ink when it is used on the media (Figure 2). This is beneficial as the unnecessary drops do not have to be collected and recycled. Furthermore, the flexibility of the ink composition increases with the disappearance of the requirements for a chargeable ink. DoD dates back to the 1970s, when Steven Zoltan and Edmond Kyser filed applications for patents regarding their inventions[25,26]. In their printers the fluid is ejected through the mechanical response of a piezoelectric ceramic to an applied voltage (Figure 3). The piezo allows sudden changes in the volume of the fluid reservoir and, thus, starts a pressure wave that ejects a defined droplet by overcoming the surface tension at the orifice. Although this concept was still in its infancy, it triggered several commercial products, but the reliability of DoD inkjet printer remained poor at that time.[12]

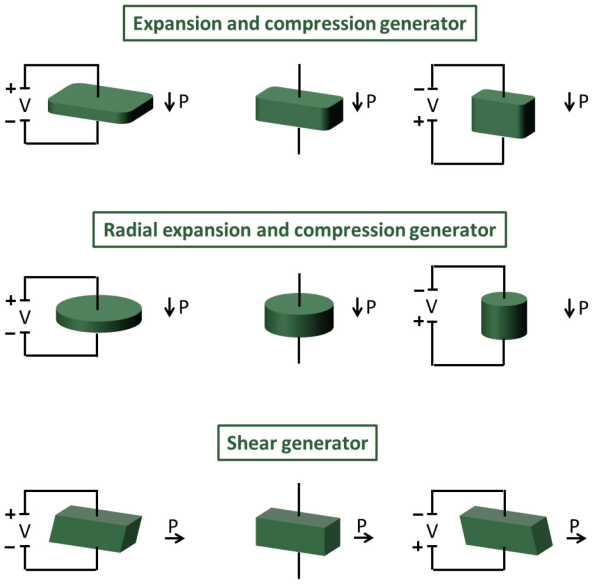

Figure 3: Piezoelectric changes to an applied voltage; P is the polarization direction of the piezoelectric ceramic

In 1979 Canon invented a new DoD technology called thermal inkjet.[27] They used a small heater in the ink chamber to induce a local state change of the used ink and thereby causing a sudden volume change, that triggers the ejection of a droplet. This technology was called “bubble jet” and started the popularity of inkjet printers due to its simple design and low costs. With the cheap fabrication of thermal inkjet print heads the reliability was no criterion anymore as the print heads could be replaced each time the cartridge was emptied.[12]

1.2.2. Industrial drop-on-demand technologies

The primarily used inkjet printing method in today's industry is DoD. Modern printing is based on the visualization of digitalized information onto a substrate, pixel by pixel. This digital printing in combination with DoD offers a high flexibility favored and sometimes needed for industrial applications. The DoD can further be categorized in four different methods, depending on their ejection principle: 1.) thermal; 2.) piezoelectric; 3.) electrostatic; 4.) acoustic.[12]

1.2.2.1. Thermal inkjet

In thermal inkjet a local state change of the ink is used to trigger the ejection of a droplet. Depending on its configuration thermal inkjet can be divided into two categories, either roof- or side-shooter.[12] In a roof-shooter setup the heater is located opposite the orifice in the ink chamber (Figure 4, A). A side-shooter's heater is situated on the side of the wall close to the orifice (Figure 4, B). Although thermal inkjet is the most successful printing method on the market today due to its use in consumer desktop printers,[12] it is still limited in other applications, because of its specific ink requirements, such as the ability to withstand extremely high local temperatures. If the used ink is poorly suited, residues may deposit on the heater and reduce its efficiency.[24]

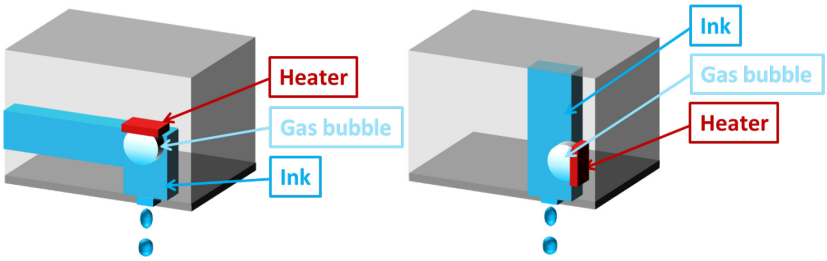

Figure 4: Thermal inkjet setups; **left**: roof-shooter thermal inkjet; **right**: side-shooter thermal inkjet

1.2.2.2. Piezoelectric inkjet

Piezoelectric inkjet printers are the commonly used technology nowadays in industrial applications attributed to the great range of possible inks.[24] Four different setups are being used primarily, depending on the utilization of the piezoelectric ceramic:

Bend-mode actuator

In a bend-mode piezoelectric inkjet design a piezoelectric ceramic is attached to a diaphragm forming one ink-chamber-wall. The chamber has an inlet for ink supply, which is connected to a reservoir, and an orifice as an outlet for the drop ejection (Figure 5). As a result of an applied voltage the piezoelectric material changes its shape (Figure 3) and causes the diaphragm to flex inwardly into the ink chamber. This induces a volume change in the chamber that causes a droplet to be ejected. By the variation of the electric pulse (i.e. voltage, length) the size of the droplet can be adjusted. When the piezoelectric transducer relaxes again, the surface tension at the orifice prevents the volume to be filled with air from the outside. Thus, the volume is only refilled with ink from the reservoir.[28]

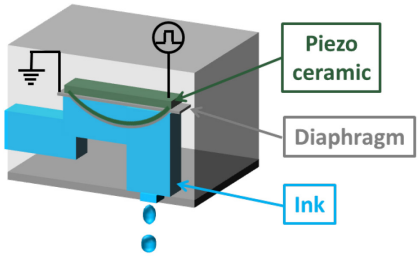

Figure 5: Piezoelectric drop-on-demand inkjet with a bend-mode actuator

Push-mode actuator

A piezo ceramic rod that pushes against the diaphragm into the ink chamber, while expanding due to an applied voltage, is called push-mode design (Figure 6). Although theoretically it is not obligatory to use a diaphragm in this setup, it is commonly used to avoid undesirable interaction between the ink and the piezoelectric material.[12]

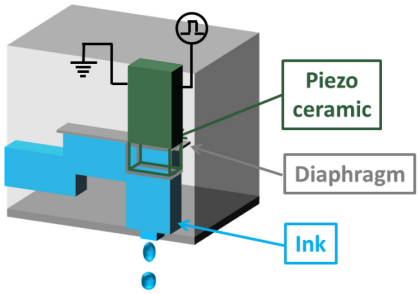

Figure 6: Piezoelectric drop-on-demand inkjet with a push-mode actuator

Shear-mode actuator

The third design is called shear-mode and features a generated electric field, which is perpendicular to its piezo ceramic polarization direction. This is in contrast to push- and bend mode actuators, whose field is parallel to its polarization direction (Figure 3). Due to the fact that there is no diaphragm to shield the piezo from the ink in the shear-mode setup, the compatibility between ink and piezo ceramic accrues to the ink requirements (Figure 7).[12,28]

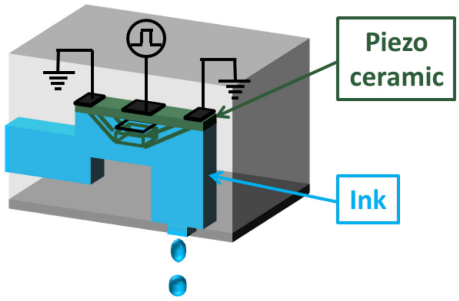

Figure 7: Piezoelectric drop-on-demand inkjet with a shear-mode actuator

Squeeze-mode actuator

The fourth setup is called squeeze mode. Herein a piezoelectric ceramic tubing is used that is polarized radially (Figure 3) with electrodes on the outer and inner surface. An applied voltage leads to the contraction of the tube and consequently a decrease in volume that forces the ejection of a droplet (Figure 8). Although upon contraction some ink is forced back into the chamber as well, the quantity is very small due to the high acoustic impedance owed to the high aspect ratio of the tube. Upon the removal of the voltage, the piezo ceramic relaxes and the resulting void is refilled with ink from the reservoir.[28]

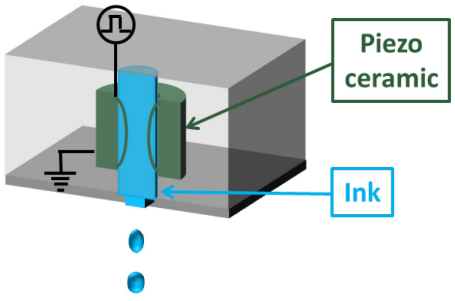

Figure 8: Piezoelectric drop-on-demand inkjet with a squeeze-mode actuator

1.2.2.3. Electrostatic inkjet

Electrostatic DoD inkjet has just been industrialized in recent years, although a patent describing the innovation was already published in 1993. In this method chargeable pigments are used in a non-conductive liquid. By applying an electric field pigment agglomerates are being formed and ejected. Using this method, no nozzles are needed on the printheads (Figure 9). The size of the ejected agglomerate is controllable by the applied electric field, point geometry and the properties of the used pigments and solvents.[29]

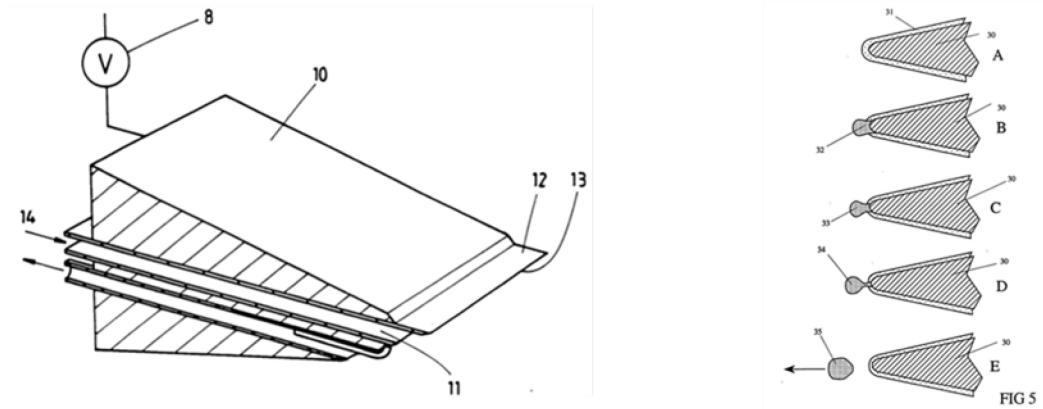

Figure 9: **Left**: electrostatic Drop-on-Demand Inkjet setup;[29] **right**: drop formation[29]

1.2.2.4. Acoustic inkjet

In an acoustic inkjet setup a focused sound beam is used to release a droplet from a liquid surface (Figure 10). Hence, as for the electrostatic inkjet, a nozzle is not needed. Albeit the method and applicability was already described in detail in 1992,[30] it has not yet established itself in an industrial context.

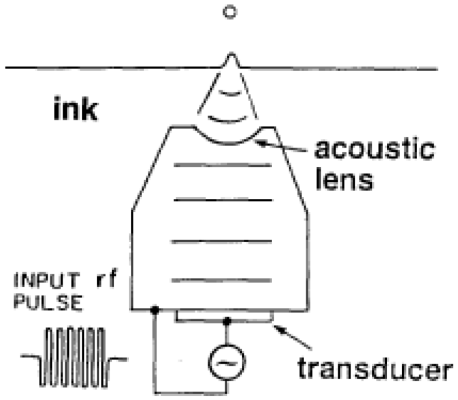

Figure 10: Acoustic inkjet[30]

1.2.1. Composition of inkjet inks

There are four main categories that inkjet inks can be divided into: Aqueous inks, solvent-based inks, phase-change inks and UV curable inks. As the name suggests, aqueous inks are based on water, where the other ink components can either be solved, dispersed or micro-emulsified in. These inks are widely used in home and small-office printers predominantly using the thermal inkjet process. They are fairly inexpensive and environmentally friendly. Nevertheless, its industrial use has been limited. This can mainly be attributed to its ink-substrate interaction and drying behavior. The adhesion on non-porous substrates is weak. A porous or specially treated substrate is required as the drying mechanism is based on the penetration and adsorption of the ink. Evaporation of the water component is slow and its acceleration is energy consuming. In contrast, the evaporation of solvent-based inks can be fairly quick. The latter are suitable for a wide range of substrate materials, even non-porous materials like plastic, glass and metal. Furthermore, the solvent-based inks are inexpensive and possess good print quality and image durability. Consequently, they have been used for wide and large format applications. In recent years environmental concerns have increased the importance of alternatives. Phase-change inks are solid at room temperature. They are printed in their molten form and solidify almost immediately upon contact with the substrate. Hence they offer good image quality as the ink is limited to little spreading on the medium. The main disadvantage is their poor durability and abrasion resistance. UV curing inks have gained significant importance in recent years. UV curable inks are liquid compositions, which are instantaneously dried when irradiated with ultraviolet (**UV**) light (electromagnetic radiation in the wavelengths between 400 and 100 nm).[12,24]

As this work centers on UV curable inks, this topic is discussed in further detail.

1.2.1.1. Composition of UV curable inks

UV curable inks possess many advantages to other printing inks (e.g. solvent-based inks). One example is the instant curing upon irradiation that allows for an almost instantaneous piling and reeling of the printed medium. Another economical factor that favors UV curable inks is the lower energy consumption of UV lamps compared to conventional dryers. Moreover, they offer a longer open time while printing. The open time is the permissible idle time in between consecutive droplet ejections of one nozzle. If the open time is short, additional cleaning cycles (i.e. purge or spit) are needed to keep nozzles fully functional. UV curable inks reduce the frequency of the needed cleaning steps. As a consequence, the wasted ink is minimized and higher printing speeds are obtainable. Another benefit of UV curable inks is their durability and solvent and abrasion resistance. This is attributed to their

curing mechanics, in which a cross-linked network is being formed. These advantages among others lead to the largest growth rate among the different printing inks in recent years.[31] Disadvantages include acquisition costs and facility requirements.[24] For piezoelectric DoD printers several ink requirements have to be fulfilled. Viscosity, density, surface tension and particle size have to comply with the printhead in use. Specific working ranges vary from one model to another.

Commercially available UV curable inks cure either through radical or cationic polymerization. Both systems are initiated by UV-light. The combination of both systems is occasionally used and called “Dual-Cure” system.

For the cationic systems photoinitiators are used that generate strong Brønsted acids upon irradiation. As reactive monomers epoxy and vinylether monomers are feasible.[32] In the presence of epoxy monomers those acids cause a ring-opening reaction of the epoxy groups forming carbocations. The formed cation itself attacks another epoxy group starting a ring-opening cationic addition polymerization.[17]
One specific feature of the cationic reaction compared to a radical reaction is that the reaction proceeds even when the irradiation is intermitted. This behavior is beneficial for a thorough cure. However, even stray light can initiate a significant polymerization in the ink before its actual curing step. Therefore, high caution has to be exercised to keep the ink away from light before its intended curing. Another disadvantage of this reaction is the influence of moisture as water significantly inhibits the cationic reaction.[31]

The predominately used reaction mechanism in UV curable inks is the free radical polymerization. The mechanism of this chain addition polymerization involves four steps:

(1) **Initiation**: When illuminated, photoinitiators absorb light. If the absorbed energy is sufficient radicals are being formed. The formation of these radicals is the starting point of the free radical polymerization (Figure 11).

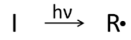

Figure 11: Generation of radicals through UV-light

These radicals react with monomers and form monomer radicals (Figure 12).

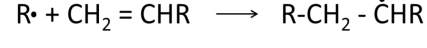

Figure 12: Formation of monomer radicals

(2) **Propagation**: A chain growth reaction occurs. The monomer radicals react with monomers and oligomers in the formulation and form polymer radicals with increasing chain lengths (Figure 13).

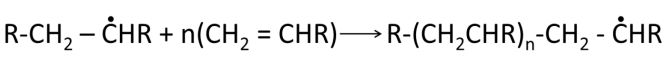

Figure 13: Chain growth

(3) **Chain transfer**: In a chain transfer reaction a (polymer) radical abstracts a hydrogen atom from a polymer chain stopping the growth of the former polymer chain (Figure 14). The newly formed radical in latter polymer chain is now a new starting point for the chain growth reaction leading to the formation of a side chain.

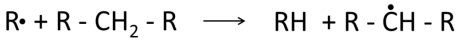

Figure 14: Chain transfer reaction

(4) **Termination**: The stop of the polymerization can occur via two different mechanisms. The first one is called combination reaction (Figure 15): Two radicals combine to form an unreactive species.

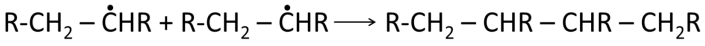

Figure 15: Combination reaction

The second path is called disproportionation reaction (Figure 16): One (polymer) radical abstracts a hydrogen atom from another (polymer) radical. This leads to the formation of a saturated chain of the former and the formation of a carbon-carbon double bond in the latter polymer chain.

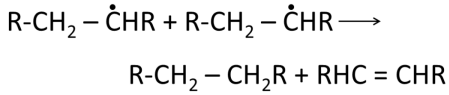

Figure 16: Disproportionation reaction

The composition of UV curable inks is described in further detail below. In general, UV curable inks based on free radical polymerization consist of four component groups: Monomers (and oligomers), pigments/dyes, photoinitiators and additives.

1.2.1.2. Radical photoinitiators

Radical photoinitiators are molecules that yield radicals upon irradiation, which initiate a free radical polymerization in the presence of monomers.[33] For the initiation process the photoinitiator has to absorb energy in a sufficient extent to form the excited species. Depending on the used chromophore the absorbed wavelength ranges vary.[17] Most photoinitiators absorb in the region between 200 and 400 nm. The most commonly used chromophore is the aryl ketone group (Figure 17). The absorbed wavelength can be altered by the substitution of R_2 (e.g. an electron donating substitution of R_2 shifts the absorption to higher wavelengths).

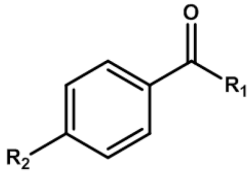

Figure 17: Structure of aromatic ketones with R_1 being an aliphatic or aromatic unit

Absorption of UV light excites the carbonyl group via a singlet state to the triplet state. Depending on the substitution of R_1, the mechanism of the generation of radicals follows one of two different paths and is, depending on its mechanism, either called a Type I or Type II photoinitiator[17]:

Type I photoinitiator: If the energy, acquired through the absorbance of UV light, is higher than an intramolecular bond energy, a scission occurs. In that case, the photoinitiator is called a Type I photoinitiator. One typical Type I photoinitiator in the form of 2-hydroxy-2-methyl-propiophenone is illustrated in Figure 18. If the scission takes place at the α-carbon (as in the case of 2-hydroxy-2-methyl-propiophenone), the reaction is called Norrish Type I.[17]

In the event of an existing weak bond between the alpha carbon to a hetero atom (Cl, S or N) a β-scission may occur.[17]

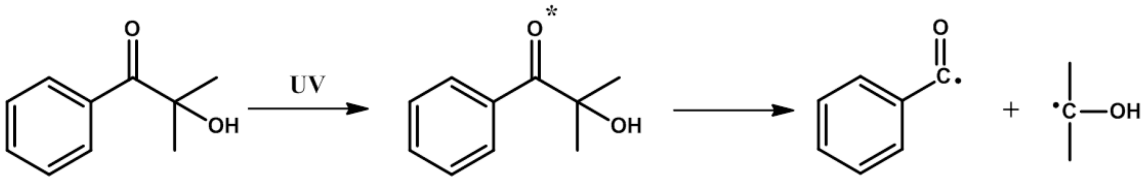

Figure 18: The mechanism of a Type I photoinitiation on the example of 2-hydroxy-2-methyl-propiophenone[34]

Type II photoinitiator: In the case of R_1 (Figure 17) being an aryl group, the energy inserted by UV light is not sufficiently high to break the bond anymore. The photoinitiator is exited to its triplet state, however, the abstraction of a hydrogen atom from a donor molecule is now needed to generate free radicals. Hydrogen donors are molecules with active hydrogen atoms, like tertiary amines, thiols, ethers or esters, among others. The hydrogen abstraction leads to ketyl radicals with low reactivity, and highly reactive donor radicals. An example of a Type II based photoinitiation using benzophenone is illustrated in Figure 19. In the special case of an active hydrogen atom in the γ-position of the photoinitiator, the hydrogen abstraction can also occur intramolecularly and yield a biradical. This distinctive Type II photoinitiation is called Norrish Type II reaction.[17]

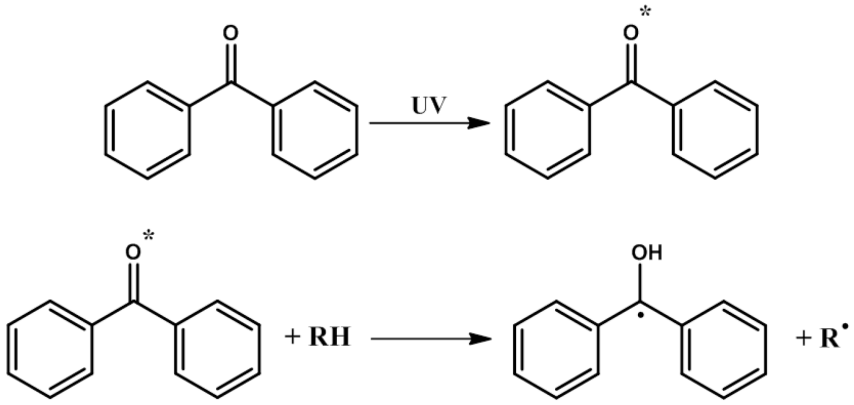

Figure 19: The Type II photoinitiation of benzophenone [33]

Several aspects have to be considered, when using a photoinitiator:

The radical polymerization reaction can be severely affected by the presence of oxygen. Oxygen acts twofold. First, oxygen will quench the excited state of the photoinitiator and prevent the formation of radicals (Figure 20). Oxygen quenching is more prominent when Type II photoinitiators are used as their triplet lifetimes are longer than those of Type I photoinitiators.[17]

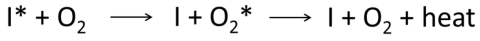

Figure 20: Oxygen quenching

Second, oxygen acts as a radical scavenger. Oxygen can react with radicals and form peroxy radicals with low reactivity towards acrylate monomers (Figure 21), which results in shorter polymer chain lengths. Especially in inkjet inks, where low viscosities in the single and low double-digit-mPa*s range are prevalent and thin layers are applied, oxygen from the air can be absorbed to the full depth of the film. As a countermeasure high amounts of photoinitiators are used in inkjet inks to ensure thorough curing.[17]

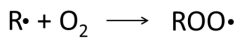

Figure 21: Formation of a peroxy radical

High photoinintiator concentrations are especially concerning in printed mediums, which come in contact with food. In the most cases health risks of individual photointiators are not yet fully assessed. Although there is no European legislation specifically covering inkjet inks, there are specific demands on materials and articles with prints on the non-food-contact side intended for food contact. One of the best investigated photoinitiators regarding its migration is the Type II photoinitiator benzophenone. An investigation of forty beverages from the Italian market revealed that benzophenone could be detected in every single analyzed sample.[35] Its health risk was evaluated by the European Food Safety Authority in 2009 and, as a result, a tolerable daily intake of 0.03 mg/kg bodyweight was determined.[36]
In general, ink components (photoinitiators, monomers and additives) have to comply with specific migration limits (e.g. for benzophenone the specific migration limit is 0.6 mg/L). The main regulations are outlined in Regulation (EU) No. 10/2011 on plastic materials and articles intended to come in contact with food. Therein a specific migration limit for substances (photoinitiators, monomers, etc.) of 60 mg/kg food is specified. However, substances with evidentially health damaging behavior, like benzophenone, are specifically

listed with narrower restrictions. Furthermore, products intended for children are subjected to even tighter restrictions.

Because not all photoinitiator content is immobilized in the cured inks, all unreacted photoinitiator content and migrating photoinitiator residues have to be assessed through time consuming and expensive measurements. Alternatively, quite often a worst case scenario is assumed, where all photoinitiator in the formulation is presumed to migrate into the food. For the inkjet printing on food packaging material a low content of photoinitiator is therefore desirable, opposing the high photoinitiator content needed for thorough curing.

In general, monomer conversions of around 80% have been reported for photocured monomer-photoinitiator model formulations,[6,15,16] although higher conversions have been reported for individual acrylate monomers that minimize the hydrogen abstraction reaction.[37] Taking the effect of pigments and curing under ambient conditions in industrial high speed printing processes under consideration, a lower conversion in inkjet inks has to be expected. As for the photoinitiators, the migration of unreacted monomers in printed food packaging has to be accounted for the respective migration limits (*vide supra*).

The chain growth polymerization stops when (a) no new radicals are being formed, (b) all the monomer is consumed or gelation stops the reaction, (c) there is a severe quenching by oxygen and/or (d) chain termination occurs.[17]

The use of excessive amounts of photoinitiator is prohibiting a full monomer conversion because all the light is absorbed near the surface by the photoinitiator. This behavior is described by the Beer-Lambert law, which describes the decrease in intensity with higher concentrations (see equation (1)). Hence, there is not sufficient penetration of light to deeper areas to cure the ink in depth. Another problem with too much photoinitiator content is the formation of too many radicals. This leads to polymer chains with low molecular weight and a less cross-linked polymer network creating softer coatings with reduced solvent fastness.[17]

$$\log\frac{I_0}{I} = \varepsilon(\lambda) \cdot c \cdot d \quad \textbf{(1)}$$

I is the intensity of transmitted light, ε(λ) the wavelength dependent molar attenuation coefficient, I_0 the intensity of the incoming light, c the molar concentration and d the thickness of the medium

An interesting approach is the utilization of different wavelengths to ensure a thorough surface and depth cure. Therein the influence of scattering and/or the utilization of the wavelength-dependent molar attenuation coefficient (equation (1)) are used. The molar attenuation coefficient is highly wavelength dependent and if a wavelength, where a low coefficient is prevalent, is used, a deeper cure can be achieved.[38] Furthermore, for suspensions (e.g. pigmented inks) due to the Rayleigh scattering of the light on the particles, the intensity of the scattered light is highly dependent on the wavelength (see equation (2)).[39] Consequently longer wavelengths are less affected by scattering than shorter wavelengths.

$$I \sim \frac{1}{\lambda^4} \quad \textbf{(2)}$$

The resulting varying depth of penetration of different wavelengths is used in pigmented UV curable compositions. Photoinitiators that absorb at low wavelengths (200-300 nm) are used to achieve a good surface cure, which helps to prevent oxygen to penetrate deeper into the coating. One typical photoinitiator for this purpose is 2-hydroxy-2-methyl-propiophenone (Figure 18).

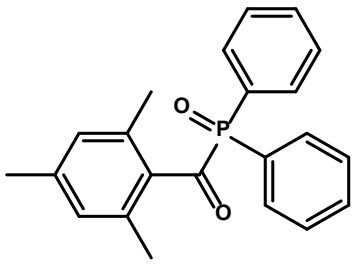

Figure 22: Diphenyl-(2,4,6-trimethylbenzoyl)-phosphine oxide

Photoinitators that absorb in the longer wavelengths are used to yield good depth cure as longer wavelengths are able to penetrate deeper into the coating. Especially photo-bleachable photoinitiators like phosphine oxides are suitable for this matter. These monomers change their absorption range upon photolysis. This can be seen in the color transformation of the originally yellow color of phosphine oxide. Upon photolysis it turns transparent, as neither of the cleavage products absorbs light above 400 nm. As a consequence, long wavelengths can penetrate deeper into the coating as the curing progresses. One example for such a phosphine oxide is diphenyl-(2,4,6-trimethylbenzoyl)-phosphine oxide (Figure 22).[17]

1.2.1.3. Monomers and oligomers of UV curable inks

The predominately used reactive species in UV curable inkjet inks are acrylates. A typical UV curable ink formulation contains several different acrylate monomers that in combination with the other ink components fulfill the desired requirements. The most important requirements are printability, adhesion to the desired substrate and resistance of the cured film. To achieve a printable ink especially the viscosity and surface tension of the ink have to meet the criteria of the used printhead. In general, inkjet inks need to be of low viscosity compared to other printing methods, such as offset or screen printing for example. This is obtained through the implementation of monofunctional and difunctional acrylates into the formulation. The use of suitable low-viscous monomers can be additionally used to promote adhesion to specific substrates. For example 2-phenoxyethyl acrylate and tetrahydrofurfuryl acrylate (Figure 23) are commonly used to promote the adhesion to polar surfaces like polycarbonates or poly(methyl methacrylate).[31,40]

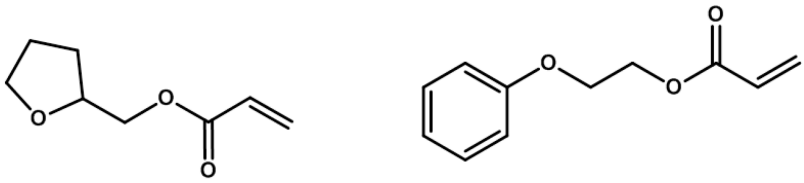

Figure 23: **Left**: tetrahydrofurfuryl acrylate; **right**: 2-phenoxyethyl acrylate

The introduction of multifunctional acrylates increases the curing speed and the crosslinking density and thus increases the hardness, brittleness and resistance of the cured film. One commonly used trifunctional acrylate is illustrated in Figure 24. Oligomers are also used in inkjet formulations albeit only in very low quantities as their viscosity is too high for comprehensive use. Altogether there are hundreds of commercially available acrylates to choose from. The properties of the ink and the cured film also depend largely on the non-

acrylic part of the monomer. For example linear monomers give more flexible films than cyclic ones. If aromatic monomers are used the films have a higher chemical resistance, but tend to have a higher yellowing (e.g. aromatic groups may extract light in the blue wavelengths through absorbance, which leads to an apparent yellowing of transmitted or reflected light). Ethoxylated or propoxylated monomers are more flexible and show lower skin irritancy compared to their non-alkoxylated counterparts.[31,40]

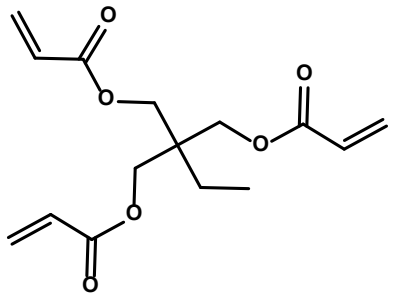

Figure 24: Trimethylolpropane triacrylate

1.2.1.4. Colorants

In the early stage of non-contact printing dyes were used. Dyes are colorants that are dissolved in the residual ink formulation. However, dyes do have unfavorable properties, like their poor light- and water fastness, which became insufficient for the increasing industrial requirements. The switch to pigments, which are insoluble dispersed particles, led to improved performances. Especially for black colors the difference was vast.[41]

For the use in inkjet inks pigments have to be dispersed into small particles in the range of 50 to 200 nm. Keeping these dispersions stable for an extended period of time is a challenging task. To obtain the desired shelf-life additives may be added.[41]

As the amount of nozzles in inkjet printing is limited, most printers work with a 4-color set that is called **CMYK**. It consists of cyan (**C**), magenta (**M**), yellow (**Y**) and black (**K**), while the medium (paper) serves as the white color (Figure 25). The color space is extended by the superposition of these colors. Nevertheless, if needed, additional colors have to be applied (e.g. white, if the used substrate is transparent).[41]

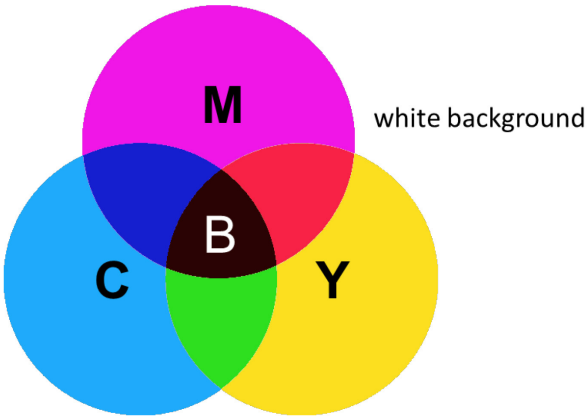

Figure 25: CMYK-colors

Black pigments have been in use for several thousand years. It is well known that incomplete combustion of hydrocarbons by the restriction of oxygen leads to their formation. Most of today's black pigments are still produced using this process, albeit it is precisely controlled and leads to pigments with clearly defined properties, which are called **Carbon Black**. Carbon Black is classified into two major categories, incomplete combustion or thermal decomposition of hydrocarbons, depending on the presence or absence of oxygen. More than 98% of the consumed Carbon Black worldwide is produced by the thermal-oxidative process (i.e. incomplete combustion). The thermal-oxidative decomposition may be classified into further detail, depending on the flow characteristics used. The most frequently used process is called Furnace Black Process. Its advantages are its flexibility and economy.[42]

Carbon Black is initially formed as roughly spherical Carbon Black particles, which are fused together to a discrete, rigid colloidal entity, namely a Carbon Black aggregate. Typically physical forces hold together a large number of those aggregates forming agglomerates. Particle sizes and aggregate sizes and shapes and its distribution vary.[43]

Carbon Blacks usually contain about 90 to 99% carbon. The rest is composed of oxygen and hydrogen. Small amounts of sulfur and nitrogen may be present as well, depending on the used process. This leads to a fairly complex surface chemistry as a wide spectrum of functional groups may be present. Investigations have shown that a mixture of carboxyl, phenol, lactones, aldehydes, ketones, quinones, hydrochinons, anhydrides and ethereal structures can be found on the surface of Carbon Blacks. The quantification of these groups is fairly complex and still an ongoing challenge.[44,45]

For the other colors a wide range of different pigments is available. The actual selected pigments depend on the desired properties (i.e. hue, weather fastness, etc.). Examples for the CMY colors can be found below (Figure 26). For **cyan** (C) the most common pigment is copper phthalocyanine (Figure 26, left). It exhibits a strong color with a very good light fastness and weatherability. For **magenta** (M) inks derivatives of quinacridone are frequently used (Figure 26, middle). Depending on the substitution the actual hue can be modified. They offer a good light fastness as well as a good weatherability. However, higher pigment loadings have to be used as they have poor color strength. A widely used **yellow** (Y) pigment is called Pigment Yellow 74 (Figure 26, right).[41]

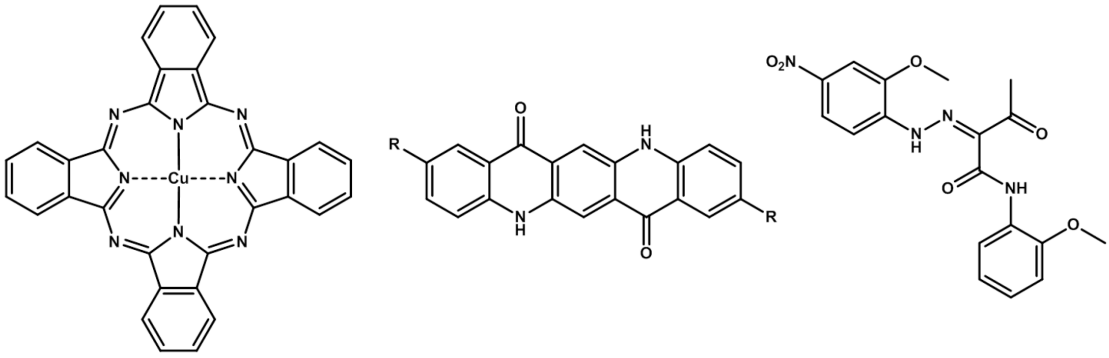

Figure 26: **Left**: copper phthalocyanine; **middle**: quinacridone; **right**: Pigment Yellow 74

1.2.1.5. Additives

Additives are substances that are added to ink formulations in small quantities to change the properties of the ink in the uncured and/or cured state into a desired direction.

One property in inkjet inks that is frequently altered is the surface tension as it is vital for a decent printing behavior. The surface tension must be high enough to hold the ink in the nozzles without dripping in the idle state but low enough to guarantee a controlled ejection of ink droplets.[46] Once ejected the surface tension of the ink plays a major role in the surface-substrate interaction as well.[47] To obtain an optimal wetting of the surface the surface tension of the ink has to be lower than the one of the substrate and existing contaminations on the surface. To reduce the surface tension of the ink surfactants, such as modified polysiloxanes for example, are commonly implemented into the formulation.

Another aspect of high importance in inkjet inks is the dispersion and wetting of pigments.[41] Agglomerates may accumulate or even clog the nozzles and channels completely and, hence, cause irreversible damage to the printhead. In the dispersion process agglomerates are being broken up and ideally being reduced to their primary particles. To prevent re-agglomeration over extended periods of time, wetting and dispersing additives are needed. Two different stabilization methods are being used. In the electrostatic stabilization the additive is introducing an electrochemical charge to the surface of the particles.[47] The repulsion of the charges keeps the particles from forming agglomerates. The second method is called steric stabilization.[47,48] Polymers that adsorb to the particles prevent particles to come close to each other. If they approach each other, the movement of the polymer chains is restricted. The result is the reduction of entropy that leads to the repulsion of the particles.

Several other additives may be used in inkjet inks as well. That includes stabilizers to enhance the shelf-life, like hindered amine light stabilizers (HALS), UV light absorbers, chelating agents, buffers, among others.[31,49]

1.2.2. Vinyl carbonates

In recent years intense research has been carried out on alternative monomer systems to the well-established (meth)acrylates, in particular by the group of Liska.[6,18] Special attention has been directed towards monomers based on vinyl carbonates and vinyl esters. Like the acrylates, those monomers may be polymerized by free radical initiation using photoinitiators or thermal initiators.[6,50–52] The huge interest in those monomers is especially owed to their low cytotoxicity and high stability in the uncured state and superior biocompatibility in the cured state, as well as their beneficial degradation behavior compared to acrylate-based systems.[19] Cross-linked acrylates form poly(acrylic acid) upon degradation, leading to a local decrease of pH, which may affect the surrounding cells negatively. In contrast, polymers obtained by vinyl carbonates degrade to poly(vinyl alcohol), which is well known and used in the drug-, cosmetic- and food industry due to its non-toxic behavior. These beneficial properties already led to the realization of medical implants like bone scaffolds from vinyl carbonate monomers.[6] *In vivo* testing already confirmed their biocompatibility.

To the present day there is no commercial source for the wide range of vinyl carbonate monomers needed for the formulation of inkjet inks. Vinyl carbonates, however, can be easily synthesized through different routes.[15] A straightforward and therefore the most frequently used method is the reaction of alcohols with vinyl chloroformate and pyridine as acid scavenger (Figure 27, 1).[53,54] Vinyl chloroformate is obtainable through the pyrolysis of ethyleneglycol bis(chloroformate),[55] or by the reaction of phosgene with bis(2-oxoethyl)mercury.[56,57] For the selective alkoxycarbonylation of secondary alcohols, vinyl chloroformate can be converted to acetone o-(vinyloxy)carbonyl oxime and then be reacted with the secondary alcohol under mild conditions (Figure 27, 2).[58] Another way to synthesize vinyl carbonates is the reaction of trimethylvinyloxysilane with fluoroformates in tetrahydrofuran (**THF**) with a catalytic amount of benzyltrimethylammonium fluoride (**BTAF**) (Figure 27, 3).[59] Moreover, acetaldehyde can be treated with chloro- or fluoroformates, potassium fluoride (KF) and 18-crown-6-ether or with fluoroformates and potassium fluoride in dimethyl sulfoxide (**DMSO**) without catalyst to yield vinyl carbonates (Figure 27, 4).[60] The most promising route for an industrial scale fabrication was patented in 2008 by BASF (Ludwigshafen am Rhein, Germany).[61] Herein the catalytic synthesis of vinyl carbonates through the reaction of the corresponding alcohol with carbon dioxide and acetylene is described (Figure 27, 5).

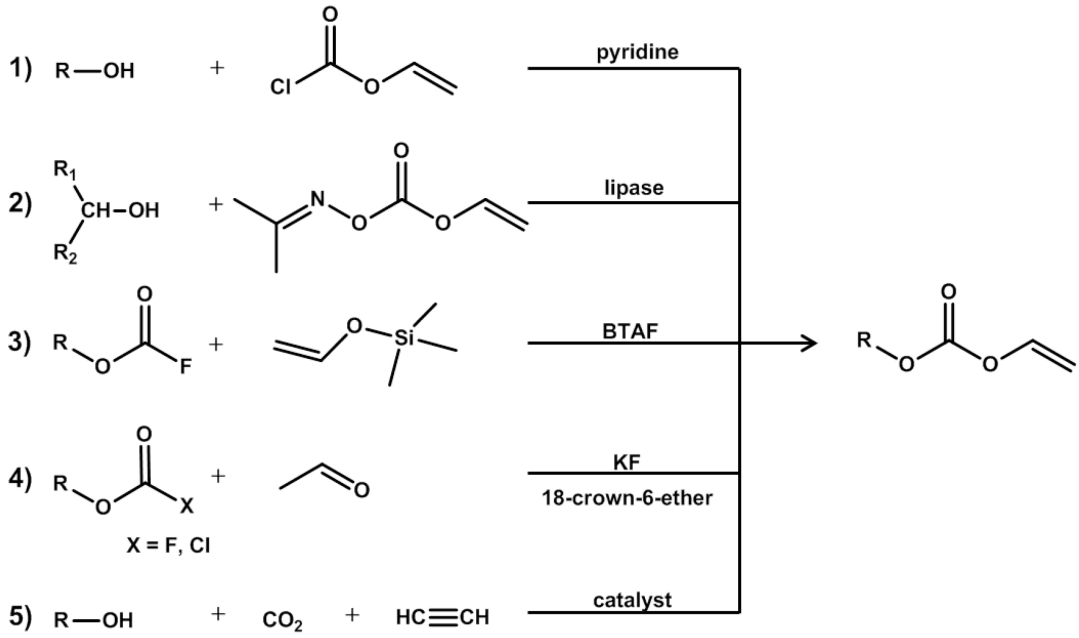

Figure 27: Vinyl carbonate synthesis routes[15]

One drawback of vinyl carbonates is that they offer only a low rate of polymerization. Ebdon et al.[62] showed that their reactivity after initiation is significantly slower than that of vinyl acetates. And the group of Liska showed that the curing speed of vinyl carbonates lies in between those of acrylates (fast) and methacrylates (rather slow).[6] This may be explained by the different reactivity of radicals formed by acrylates and vinyl carbonates. Radicals formed from acrylates offer good resonance stability, while the acrylate monomer is highly reactive. Therefore, homopolymerization is highly favored over side reactions, like hydrogen-abstraction (Figure 28).[7]

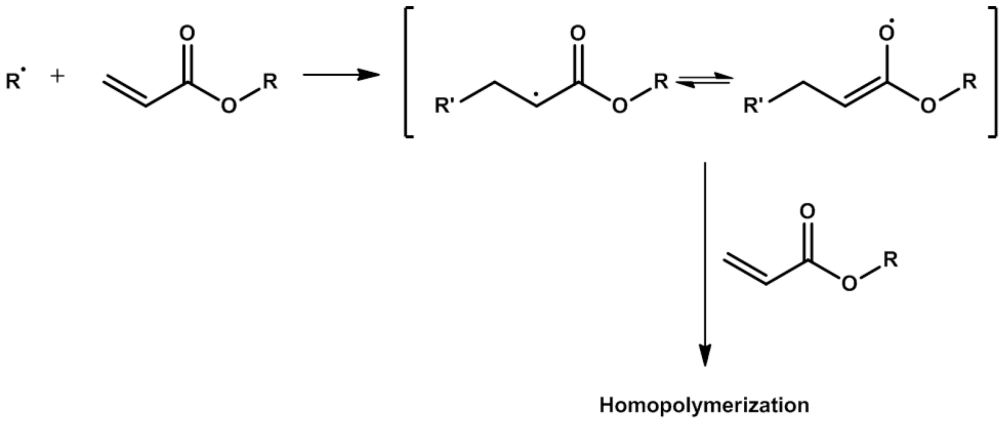

Figure 28: Acrylate polymerization[7]

The vinyl carbonate radicals, in contrast, offer no resonance stabilization and vinyl carbonate monomers show low reactivity. This leads to highly reactive radicals, which are prone to side reactions like hydrogen-abstraction. If this abstraction occurs from an ethylene glycol group, for example, this results in a radical of low reactivity, which essentially terminates the polymerization reaction as the monomer itself possesses low reactivity (Figure 29).[7]

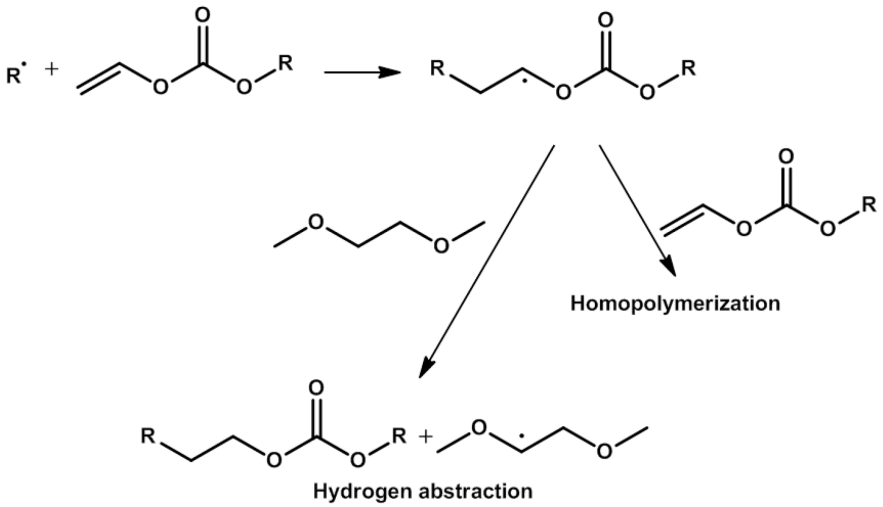

Figure 29: Vinyl carbonate polymerization, leading to homopolymerization (**right route**) and hydrogen-abstraction (**left route**)[7]

Mautner et al.[7] showed that the addition of multifunctional thiols to vinyl carbonate formulations enhance the curing speed up to values usually reserved for acrylates. Thiols are very susceptible to hydrogen abstraction under free radical conditions leading to the formation of highly reactive thiyl radicals, which propagate the polymerization. Consequently, the curing speed and the conversion of vinyl carbonates increase, leading to significant lower concentration of non-polymerized monomers in the cured polymer film.[7]

1.2.3. Thiol-ene reaction

The reaction of thiols with carbon-carbon double bonds (enes) has been known for several decades. It was discovered in 1905[63] and scientifically investigated in the 1970s.[64] But interest in its use has exploded only in the last few years, as a result of the search for alternatives to the widely-used, classical copper-catalyzed azide/alkyne click chemistry introduced by Sharpless in 2001.[65] “Click reactions” are defined as reactions that feature specific characteristics: (a) high yields, with easily removable by-products, (b) regio- and stereospecifity, (c) insensitivity to oxygen and water, (d) mild reaction conditions (in water or without solvent), (e) orthogonality with other common organic synthesis reactions and (f) an availability of a wide range of starting compounds.

Thiol-ene reactions possess most of these characteristics. They offer high yields, need only small amounts of catalysts, feature high reaction rates, operate in bulk or environmentally benign solvents, require essentially no clean up, are insensitive to water and oxygen, yield a single regioselective product and vast amounts of thiols and enes are commercially available. For that reason thiol-ene reactions are nowadays referred to as thiol click reactions in literature.[65]

In particular, two thiol reactions with enes emerged (Figure 30): **(1)** the free radical addition of thiols to electron rich and electron poor carbon-carbon double bonds and **(2)** the catalyzed reaction of thiol with electron-deficient carbon-carbon double bonds, which is called thiol-Michael addition.

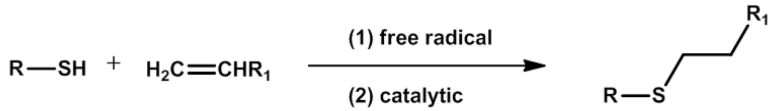

Figure 30: **(1)** Free radical thiol-ene and **(2)** catalytic thiol-Michael reaction[65]

1.2.3.1. Free radical thiol-ene reaction

The photoinitiation of a thiol-ene formulation starts a free radical addition of thiols to carbon-carbon double bonds by the formation of thiyl radicals (Figure 31). The initiation works with different kinds of photoinitiators[64,66,67] and even in the absence of any photoinitiator.[68] The formed thiyl radical reacts with the ene-monomer and forms a new radical, which can abstract a hydrogen atom from another thiol. The termination of the reaction occurs through the recombination of two radicals. Due to the step growth mechanism multifunctional thiols and enes have to be used to obtain a cross-linked network (i.e. polymerization).

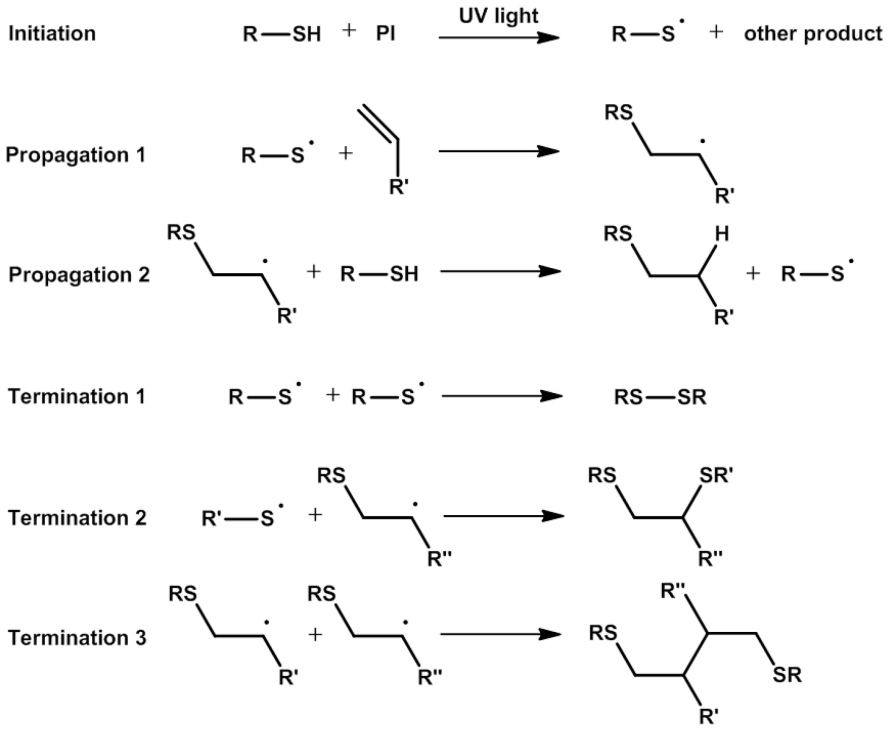

Figure 31: Free radical thiol-ene reaction[67]

The remarkable feature of the thiol-ene reaction is that almost any type of ene-monomer can be used. In general, the reactivity is related to the electron density of the ene, with electron-rich carbon-carbon double bonds reacting faster than electron poor ones.[64,67] The choice of ene-monomer influences the polymer structure as well.[66,68,69] In an ideal thiol-ene reaction, one thiol couples to one ene-monomer. Thus, the reaction follows a step growth mechanism with no homopolymerization occuring. This can be witnessed for norbornenes and vinyl ethers for example, whereas a strong homopolymerization can be found for acrylates and methacrylates.

One very beneficial property of thiol-ene reactions is the late onset of the gel-point compared to conventional radical acrylate polymerization.[67] This leads to a higher conversion and in less stress built into the network as the polymerization shrinkage occurs primarily in the liquid phase. This is especially advantageous for applications where a good adhesion to substrates is of great importance. Another advantage is that the thiol-ene reaction is fairly insensitive to oxygen inhibition compared to other free radical polymerization reactions.[67] This is based on the hydrogen-abstraction initiated by the peroxy radical (Figure 32). In thiol-ene formulations the peroxy radical forms a thiyl radical through the abstraction of hydrogen from a thiol group. The formed thiyl radical assures the continuation of the thiol-ene mechanism and consequently the chain propagation.

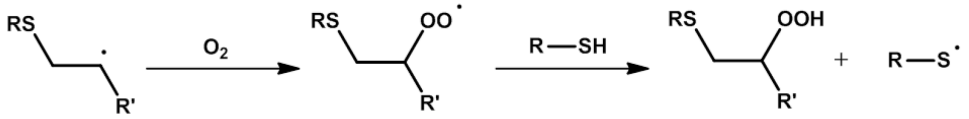

Figure 32: Oxygen-scavenging mechanism in a free radical thiol-ene polymerization[67]

One of the disadvantages of thiol-ene systems is the distinct odor that comes with the utilization of thiols. Although thiols with low molecular weights will never be odorless, it seems that for larger multifunctional molecules the smell largely stems from impurities, like thioglycolic acid or mercaptopropionic acid. A diligent clean-up after the synthesis improves the odor significantly.[67] Suppliers nowadays offer low odor versions of commercially available multifunctional thiols (e.g. low odor pentaerythritol tetra(3-mercaptopropionate (**PETMP l.o.**) from Bruno Bock).

The storage stability is another focal point that has to be considered when using thiol-ene formulations as they exhibit a dark reaction.[70] This means, that a premature polymerization takes place even in closed containers at room temperature without the incidence of light. Depending on the used monomers and the exact composition the storage stability of unstabilized formulations vary between a couple of hours to more than a month (at room temperature).[67] Acrylates and vinyl ethers are particularly unstable monomers in thiol-ene compositions. The instabilities may stem from a combination of different reasons, depending on the exact formulation: (1) a base catalyzed addition of thiol to the ene, (2) the decomposition of peroxide impurities and the subsequent initiation of a thermal free radical reaction, (3) the formation of thiyl radicals by hydroperoxide impurities and the following polymerization reaction, (4) the generation of radicals by a ground-state charge transfer complex formed by the thiols and the enes in the formulation.[67,71,72] Due to the importance of a prolonged shelf-life in industrial applications numerous groups have been searching for appropriate stabilizers. Subsequently multiple approaches have been patented. Stahly[73] described the use of free-radical scavenger-vinyl stabilizer in thiol-ene formulations. Another patent[74] describes the introduction of nitroso compounds as free radical scavenger in norbornene-thiol formulations. Furthermore, hydroquinone, catechol, 2,6-ditertiary-butyl-p-methylphenol, phenothiazine, n-phenyl-2-naphthylamine and phosphoric acids have been mentioned as stabilizers.[75] Klemm et al.[71] investigated the stabilizing effect of pyrogallol, hydroquinone and catechol in detail, with pyrogallol having the best stabilizing effect. Recently, a patent[70] has been published, describing the use of a combination of pyrogallol and phosphonic acid as stabilizers for thiol-(meth)acrylate systems, leading to far better results than for pyrogallol itself. An increase of methacrylate-thiol composition of only 15% after 79 days at 65°C has been reported. However, for formulations with the reactive

acrylates viscosity increases of about 100% after 76 days at 65°C are described. Unfortunately, already a viscosity increase of several percent can be problematic for inkjet inks as it may affect the printing properties (e.g. printing speed, drop formation) severely. Quite a few different stabilizers have been investigated, but unfortunately no general rule for the stabilization emerged. Depending on the used thiol-ene formulation the most effective stabilizer has to be evaluated on a case-by-case basis.[67]

1.2.3.2. Thiol-Michael reaction

The thiol-Michael reaction is described in detail in chapter 2.2.4.2.

1.2.3.3. Biocompatibility of thiol-ene compositions

Mautner et al.[7,76] investigated the use of vinyl carbonate and vinyl ester systems with ethoxylated trimethylolpropane trimercaptopropionate (**TMPMP**) and pentaerythritol tetra(3-mercaptopropionate (**PETMP**). They concluded that these thiol-ene systems offer superior cytotoxicity compared to acrylate formulations.

Due to the low toxicity of appropriate thiol-ene compositions several groups have investigated its use as biocompatible materials. A patent by Molenberg et al.[77] describes the use of compositions of high-functional acrylates with tetra(3-mercaptopropyl)silane for vertebroplasty procedures. Therein, the composition is injected into fractured vertebras to relieve back pain. A further patent describes several applications of thiol-ene compositions for the curative treatment of bone fractures, like its use as a stabilizing composition to reduce the necessity of screws to stabilize bone fractures.[78] Another group investigated compositions of TMPMP and multifunctional acrylates for the use as foam-like bone repair material and confirmed its biocompatibility.[79] Furthermore several patents describe the application of thiol-ene formulations as dental material.[80–82]

1.3. Experimental section

1.3.1. Materials

All chemicals were commercially available and obtained by Sigma-Aldrich or TCI Europe unless otherwise mentioned. The thiols trimethylolpropane trimercaptopropionate (TMPMP) and pentaerythritol tetra(3-mercaptopropionate) (PETMP) were obtained from Bruno Bock. (5-Ethyl-1,3-dioxane-5-yl)methanol acrylate was purchased at Sartomer. Lucirin TPO-L (ethyl phenyl(2,4,6-trimethylbenzoyl)phosphinate) and Irgastab 22 were obtained from BASF. 6-[2-[2-(2-Methoxy-ethoxy)-ethoxy]-ethoxy]hexylphosphonic acid was purchased at Sikemia.

1.3.2. Synthesis of vinyl carbonates

The general procedure for the synthesis of vinyl carbonates is depicted in Figure 33.[53,54]

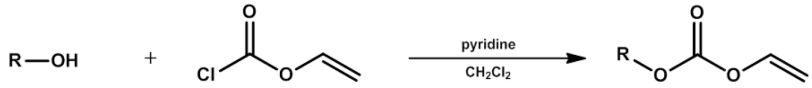

Figure 33: General procedure for the synthesis of vinyl carbonates

To a solution of the corresponding alcohol (1 Eq.) and pyridine (1 Eq.) in methylene chloride (20 mL per 10 mmol alcohol) vinyl chloroformate (1 Eq.) was added over a period of 10 min at 0°C under nitrogen atmosphere. The solution was stirred at 0°C for 30 min and at room temperature for additional 3 h. The solution was washed with HCl (1 M; 3 x 50 mL per 10 mmol of the added alcohol), $NaCO_3$ (saturated; 3 x 50 mL per 10 mmol of the added alcohol) and deionized water (3 x 100 mL per 10 mmol of the added alcohol). The organic layer was dried over Na_2SO_4 and the solvent was removed under reduced pressure. The crude product was purified by column chromatography on silica gel (cyclohexane (**Cy**) / ethyl acetate (**EA**)) and characterized by ^{1}H- and ^{13}C-NMR and FTIR. The synthesized vinyl carbonate monomers are illustrated in Figure 34.

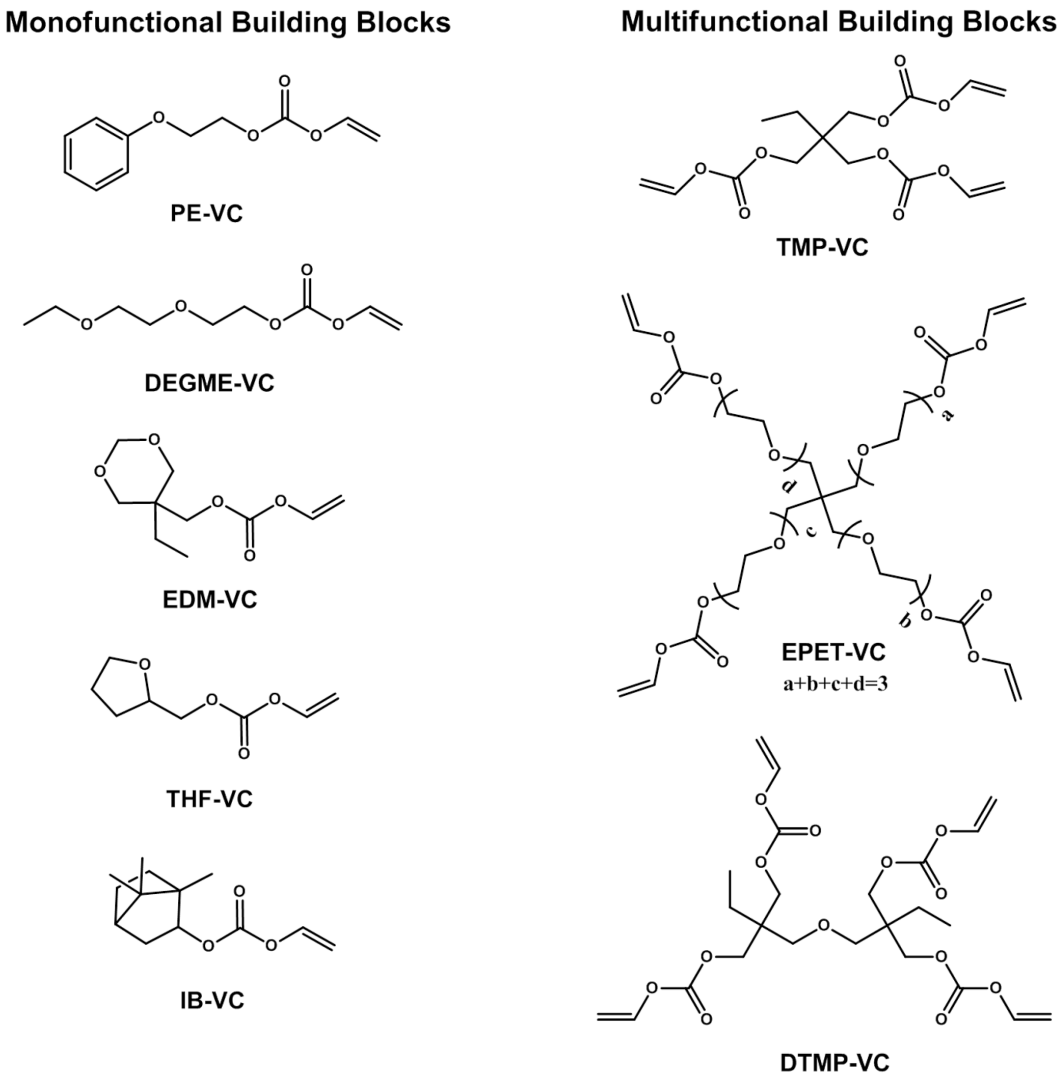

Figure 34: Synthesized vinyl carbonate monomers

2-Phenoxyethyl vinyl carbonate (PE-VC)

Yield: 16.1 g (66.3% of theoretical yield) of a colorless liquid (Cy/EA=7/1).

^{1}H-NMR (400 MHz, $CDCl_3$): 7.29 (m, 2H, $ph^{3,5}$); 7.08 (q, 1H, -CH=); 6.97 (t, 1H, ph^{4}); 6.92 (d, 2H, $ph^{2,6}$); 4.95 (dd, 1H, H_2C=); 4.59 (dd, 1H, H_2C=); 4.54 (t, 2H, CH_2); 4.22 (t, 2H, CH_2) ppm.

^{13}C-NMR (100 MHz, $CDCl_3$): 158.2 (1C, ph^{1}); 152.7 (1C, -C=O); 142.5 (1C, C=C-O); 129.6 (2C, $ph^{3,5}$); 121.3 (1C, ph^{4}); 114.6 (2C, $ph^{2,6}$); 98.2 (2C, C=C-O); 66.6 (1C, C-C); 65.4 (1C, C-C) ppm.

FTIR: 1755; 1651; 1600; 1495; 1300; 1260; 1227; 1157; 1085; 1065; 931; 878; 780; 754; 692 cm^{-1}.

(5-Ethyl-1,3-dioxan-5-yl)methyl vinyl carbonate (EDM-VC)

Yield: 17.1 g (67%) of a colorless liquid (Cy/EA=5/1).

^{1}H-NMR (400 MHz, $CDCl_3$): 7.06 (q, 1H, =CH-O); 4.95 (dd, 1H, H_2C=); 4.92 (dd, 1H, -CH_2); 4.63 (dd, 1H, H_2C=); 4.57 (dd, 1H, CH_2); 4.39 (s, 2H, CH_2); 3.85 (d, 2H, CH_2); 3.48 (d, 2H, CH_2); 1.31 (q, 2H, CH_2); 0.83 (t, 3H, CH_3) ppm.

^{13}C-NMR (100 MHz, $CDCl_3$): 152.7 (1C, C=O); 142.6 (1C, C=C); 97.8 (1C, C=C); 94.2 (1C, CH_2); 71.5 (2C, CH_2); 67.8 (1C, CH_2), 36.3 (1C, CH_2); 23.6 (1C, CH_2); 6.7 (1C, CH_3) ppm.

FTIR: 1755; 1650; 1300; 1248; 1161; 1105; 1085; 1031; 972; 924; 778 cm^{-1}.

2-(2-Ethoxyethoxy)ethyl vinyl carbonate (DEGME-VC)

Yield: 16.7 g (69.6%) of a colorless liquid (Cy/EA=3/1).

^{1}H-NMR (400 MHz, $CDCl_3$): 7.03 (q, 1H, =CH-O); 4.90 (dd, 1H, H_2C=); 4.55 (dd, 1H, H_2C=); 4.33 (t, 2H, CH_2); 3.73 (t, 2H, CH_2); 3.63 (t, 2H, CH_2); 3.56 (t, 2H, CH_2); 3.48 (q, 2H, CH_2); 1.17 (t, 3H, CH_3) ppm.

^{13}C-NMR (100 MHz, $CDCl_3$): 152.7 (1C, C=O); 142.5 (1C, =CH-O); 97.8 (1C, H_2C=); 70.7 (1C, CH_2); 69.8 (1C, CH_2); 68.7 (1C, CH_2); 67.5 (1C, CH_2); 66.6 (1C, CH_2); 15.1 (1C, CH_3) ppm.

FTIR: 1757; 1650; 1300; 1246; 1155; 1112; 1086; 1024; 946; 874; 782 cm^{-1}.

(Tetrahydrofuran-2-yl)methyl vinyl carbonate (THF-VC)

Yield: 18.8 g (78%) of a colorless liquid (Cy/EA=7/1).

^{1}H-NMR (400 MHz, $CDCl_3$): 7.05 (q, 1H, =CH-O); 4.90 (dd, 1H, H_2C=); 4.55 (dd, 1H, H_2C=); 4.17 (m, 3H, CH_2-O, fr^2); 3.85 (t, 2H, fr^5); 2.05-1.61 (m, 4H, fr^3, fr^4) ppm.

^{13}C-NMR (100 MHz, $CDCl_3$): 152.7 (1C, C=O); 142.5 (1C, C=C); 97.8 (1C, C=C); 75.9 (1C, fr^2); 70.2 (1C, CH_2); 68.4 (fr^5); 27.7 (1C, fr^3); 25.6 (1C, fr^4) ppm.

FTIR: 1756; 1650; 1300; 1240; 1158; 1078; 944; 876; 782 cm^{-1}.

1,7,7-Trimethylbicyclo[2.2.1]heptan-2-yl vinyl carbonate (IB-VC)

Yield: 24.5 g (82%) of a colorless liquid (Cy/EA=5/1).

^{1}H-NMR (400 MHz, $CDCl_3$): 7.05 (q, 1H, =CH-O); 4.89 (dd, 1H, H_2C=); 4.86 (q, 1H, nb); 4.59 (dd, 1H, H_2C=); 1.85 (m, 2H, nb); 1.75 (m, 2H, nb); 1.56 (m, 1H, nb); 1.09 (m, 2H, nb); 0.97 (t, 3H, -CH3); 0.89 (t, 3H, -CH3); 0.83 (t, 3H, -CH3) ppm.

^{13}C-NMR (100 MHz, $CDCl_3$): 152.7 (2C, -C=O); 142.5 (1C, C=C-O-); 98.2 (2C, C=C-O); 85.8 (1C, nb-O); 48.9 (1C, nb); 46.9 (1C, nb); 44.9 (1C, nb); 38.4 (1C, nb); 33.6 (1C, nb); 26.7 (1C, nb); 20.0 (1C, -CH3); 19.8 (1C, -CH3); 11.3.0 (1C, -CH3) ppm.

FTIR: 1755; 1650; 1297; 1249; 1156; 1046; 1000; 964; 946; 783 cm^{-1}.

Butane-1,4-diyl divinyl dicarbonate (BD-VC)

Yield: 15.2 g (56%) of a colorless liquid (Cy/EA=5/1).

^{1}H-NMR (400 MHz, $CDCl_3$): 7.04 (q, 2H, =CH-O), 4.90 (dd, 2H, H_2C=), 4.55 (dd, 2H, H_2C=); 4.22 (t, 4H, CH_2); 1.80 (t, 4H, CH_2) ppm.

^{13}C-NMR (100 MHz, $CDCl_3$): 152.7 (2C, C=O); 142.5 (2C, C=C); 97.8 (2C, C=); 67.8 (2C, CH_2); 24.9 (2C, CH_2) ppm.

FTIR: 1755; 1650; 1395; 1300; 1232; 1154; 1085; 941; 876; 783 cm^{-1}.

Oxybis(propane-2,1-diyl) divinyl dicarbonate (DPG-VC)

Yield: 16 g (66.6%) of a colorless liquid (Cy/EA=8/1).

^{1}H-NMR (400 MHz, $CDCl_3$): 7.04 (q, 2H, =CH-O); 4.91 (m, 2H, H_2C=); 4.55 (m, 2H, H_2C=); 4.13 (m, 2H, CH_2); 3.59 (m, 4H, CH_2); 1.30 (m, 3H, -CH_3); 1.17 (m, 3H, -CH_3) ppm.

^{13}C-NMR (100 MHz, $CDCl_3$): 152.7 (2C, C=O); 142.5 (2C, C=C); 97.8 (2C, C=C); 74.5-71.0 (4C, CH_2, CH); 16.32 (2C, CH_3) ppm.

FTIR: 1755; 1650; 1301; 142; 1155; 1084; 944; 876; 782 cm^{-1}.

2-(Methyl vinyl carbonate)-2-ethylpropane-1,3-diyl divinyl dicarbonate (TMP-VC)

Yield: 16 g (84.8%) of a colorless liquid (Cy/EA=8/1).

^{1}H-NMR (400 MHz, $CDCl_3$): 7.03 (q, 3H, =CH-O); 4.93 (dd, 3H, H_2C=); 4.58 (dd, 3H, H_2C=); 4.19 (s, 6H, CH_2); 1.54 (q, 2H, CH_2); 0.93 (t, 3H, CH_3) ppm.

^{13}C-NMR (100 MHz, $CDCl_3$): 152.4 (3C, C=O); 142.5 (3C, C=C); 98.2 (3C, C=C); 67.3 (3C, CH_2); 41.3 (1C, CH_2); 22.4 (1C, C); 7.2 (1C, CH_3) ppm.

FTIR: 1756; 1650; 1395; 1301; 1229; 1154; 1087; 944; 874; 780 cm^{-1}.

(Oxybis(methylene))bis(2-ethylpropane-3,2,1-triyl) tetravinyl tetracarbonate (DTMP-VC)

Yield: 23.4 g (80.7%) of a white solid (Cy/EA=8/1).

^{1}H-NMR (400 MHz, $CDCl_3$): 7.03 (q, 4H, =CH-O); 4.91 (dd, 4H, H_2C=); 4.56 (dd, 4H, H_2C=); 4.13 (s, 8H, C(O)-CH_2-O); 3.32 (s, 4H, CH_2-O); 1.46 (q, 4H, CH_2); 0.86 (t, 6H, -CH_3) ppm.

^{13}C-NMR (100 MHz, $CDCl_3$): 152.5 (4C, C=O); 142.5 (4C, C=C); 98.2 (4C, C=C); 70.2 (s, 4C, CH_2-O); 67.3 (4C, CH_2-O); 41.9 (2C, C); 22.7 (2C, CH_2); 7.2 (2C, -CH_3) ppm.

FTIR: 1755; 1650; 1299; 1229; 1155; 1088; 944; 873; 779 cm^{-1}.

Ethoxylated (3/4 EO/VC) 2,2-bis(methyl vinyl carbonate)1,3-propanediyl divinyl dicarbonate (EPET-VC)

Yield: 10.3 g (66.7%) of a colorless liquid (Cy/EA=7/1).

^{1}H-NMR (400 MHz, $CDCl_3$): 7.06 (q, 4H, =CH-O); 4.94 (dd, 4H; H_2C=); 4.58 (dd, 4H, H_2C=); 4.40-4.25 (m, 8H, CH_2); 3.75-3.45 (m, 12H, CH_2) ppm.

^{13}C-NMR (100 MHz, $CDCl_3$): 152.8 (4C, C=O); 142.6 (4C, C=C); 97.8 (4C, C=C); 71.0-66.8 (10C, CH_2); 44.0 (1C, C) ppm.

FTIR: 1755; 1650; 1393; 1300; 1231; 1155; 1085; 945; 872; 778 cm^{-1}.

1.3.3. Synthesis of tetra(3-mercaptopropyl)silane

The three synthesis steps of tetra(3-mercaptopropyl)silane are illustrated in Figure 35 through Figure 37.

Step 1: Tetraallylsilane:

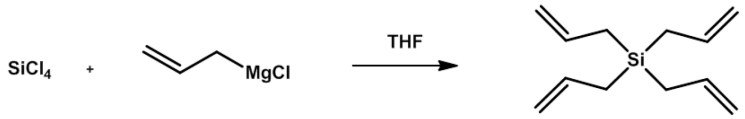

Figure 35: Synthesis of tetraallylsilane

Allylchloride (4 mL) was added to a suspension of magnesium (80 g, 3.29 mol) in 100 mL THF to start the reaction. Tetrachlorosilane (101.3 g, 596 mmol) and allylchloride (220 g, 2.876 mol) in 700 mL THF and 160 mL hexane was added drop wise over a 4 h period. The mixture was heated to 65°C for 3.5 h and then quenched with saturated ammonium chloride solution, which gave a strong exothermic reaction. The crude product was filtered and washed with hexane. The product was then extracted with cyclohexane, dried and afterwards purified by column chromatography on silica gel (cyclohexane) and characterized by ^{1}H- and ^{13}C-NMR.

Yield: 102 g (89 %) of a colorless liquid.

^{1}H-NMR (400 MHz, $CDCl_3$): 5.80 (m, 4H, $CH=CH_2$); 4.90 (m, 8H, $C=CH_2$); 1.60 (m, 8H, $Si-CH_2$) ppm.

^{13}C-NMR (100 MHz, $CDCl_3$): 134.0 (s, 4C, C=CH2); 113.9 (s, 4C, C=CH2); 19.2 (s, 4C, Si-C) ppm.

Step 2: Tetrakis(thioacetylpropyl)silane[77]

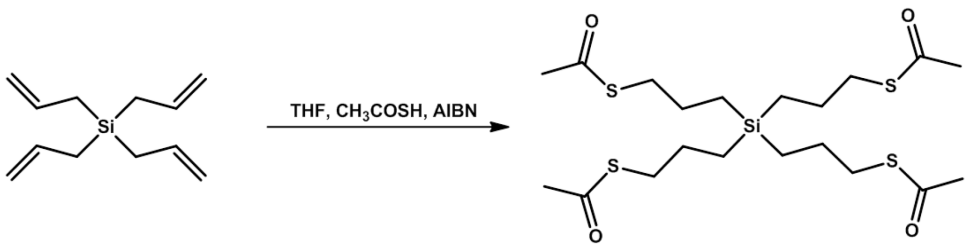

Figure 36: Synthesis of tetrakis(thioacetylpropyl)silane

Thioacetic acid (100 g; 1.314 mol) and tetraallylsilane (25.25 g, 131.3 mmol) were dissolved in 200 mL THF. Azobis(isobutyronitrile) (**AIBN**) (1.08 g, 6.6 mmol) was added and the mixture was heated to 65°C overnight. Afterwards the solvent was removed by vacuum. 200 mL ethyl acetate was added and the mixture was washed with 200 mL H_2O, 200 mL $NaHCO_3$ and 200 mL saturated NaCl solution. Afterwards the product was dried over vacuum and the residual water was removed by azeotropic drying with toluene.

Yield: 62.7 g (96%) of a yellow oil were obtained.

Step 3: Tetra(3-mercaptopropyl)silane[77]

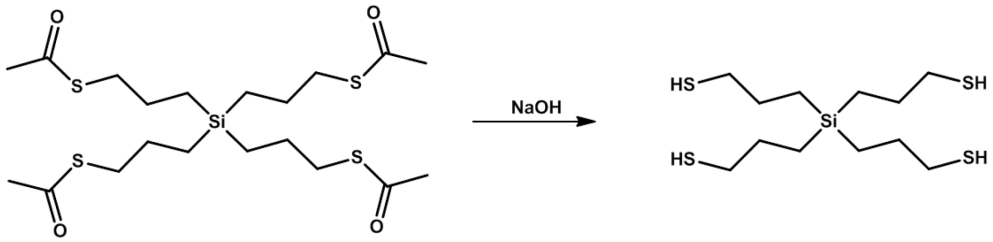

Figure 37: Synthesis of tetra(3-mercaptopropyl)silane

Tetrakis(thioacetylpropyl)silane (62.7 g, 126.2 mmol) was dissolved in 170 mL MeOH and cooled to 0°C. 32 mL of 25% NaOH solution was added drop wise and stirred over night until it was fully converted. Afterwards it was neutralized with 5% HCl and washed with 200 mL toluene once and three times with 200 mL H_2O. The product was dried with Na_2SO_4 and characterized by ^{1}H- and ^{13}C-NMR.

Yield: 30.6 g (73.8%) of a yellow oil.

^{1}H-NMR (400 MHz, $CDCl_3$): 2.51 (m, 8H, CH_2-SH); 1.58 (m, 8H, CH_2-C-SH); 0.63 (m, 8H, Si-CH_2) ppm.

^{13}C-NMR (100 MHz, $CDCl_3$): 28.7 (d, 4C, C-C-SH); 28.3(s, 4C, C-SH), 11.5 (s, 4C, Si-C) ppm.

1.3.4. Nuclear magnetic resonance spectroscopy (NMR)

For ^{1}H- and ^{13}C-NMR measurements 10 to 20 mg of the respective sample were dissolved in deuterated solvents. A 400 MR instrument from Varian (Palo Alto, California, USA) was used at 399.840 MHz for ^{1}H- and at 100.550 MHz for ^{13}C-measurements. Solvent residual peaks were used for referencing the NMR spectra to the corresponding values given in literature[83].

1.3.5. Density

The required densities of the vinyl carbonates and ink formulations were obtained with a pycnometer at 20°C.

1.3.6. Surface tension

The surface tension measurements were performed with a drop shape analyzer (DSA 100, Krüss, Hamburg, Germany) using the pendant drop method (see chapter V.iii).

1.3.7. Viscosity

The viscosity of the ink formulations was determined using a Brookfield viscometer (LVDV-III Ultra Digital Rheometer, Middleboro, USA) with a SC4-18 spindle at 23, 25, 30, 35 40, 45, 50 and 55°C respectively using the highest possible shear rate at 23°C. Individual components and stability experiments were measured using an Anton Paar rheometer (MCR-102, Graz, Austria) in a cone-plate system setup with an titanium cone with a diameter of 60 mm and an opening angle of 0.5° at a shear rate of 300 s^{-1}. Viscosities for the stabilization experiments were performed at 25°C.

1.3.8. Fourier transform infrared spectroscopy (FTIR)

The real-time-FTIR measurements were conducted on a VERTEX 70 (Bruker, Billerica, USA) with the measurement unit A513. 0.75 µL of the examined substance was applied in between two CaF_2-discs and put into the beam path. The specimen was illuminated using an Omnicure s1000 (Lumen Dynamics, Mississauga, USA) with an operating level of 10% and a 9 cm gap in between the light guide and the specimen (5.5 mW/cm^2). Two FTIR-measurements per second were taken.

1.3.9. Photo-differential scanning calorimetry (DSC)

The photo-DSC experiments were performed on a NETZSCH Photo-DSC 204 F1 Phoenix. All measurements were conducted at 50°C in aluminium crucibles under nitrogen atmosphere. The Omnicure s2000 was used as the light source at 1 W/cm^2 (0.5 W/cm^2 was used for the stabilization experiments). For the determination of the reaction enthalpy and the time to reach the maximum heat of polymerization (t_{max}) the sample (sample quantity: 8 mg) was illuminated twice for 10 min each. For the analysis the second run was substracted from the first one to give the reaction enthalpy curve. The double bond conversion was calculated by using literature values[6] for the reaction enthalpy of the respective functional group.

1.3.10. Cytotoxicity

Cytotoxicity tests were performed according to **ISO** 10993-5:2009. The cytotoxicity experiments were conducted by Cytox (Bayreuth, Germany). For these tests mouse fibroblast cells (L929) were used. Cells were cultured for 24 hours in Dulbecco's modified Eagle's medium (**DMEM**) with added antibiotics, supplemented with 10% fetal calf serum at 37°C in an incubator with 5% CO_2. Four different concentrations of the examined substance (solved in DMSO) were applied onto the cells and incubated for 48 hours at 37°C with 5% CO_2. The final concentration of DMSO in all cavities in the cell culture medium was 1% (v/v). Triton X 100 was used as toxic positive control (final concentration 1% (v/v)) and the cell culture medium was used as non-toxic negative control. All experiments were conducted four times simultaneously. After the incubation the L929-cells were washed with phosphate buffered saline (**PBS**), and after an alkaline lysis step the protein concentration was determined via the Bradford method.

1.3.11. Pigmentation for printing experiments

The pigmentation was conducted in a two-step process to exclude influences due to stability issues of pigmented thiol-ene systems. In a first step the pigment flakes (RKJ black ZE37J9, Flint Group, Luxembourg, Luxembourg) were added to the mixture of vinyl carbonates in small portions and dispersed with the Ultra Turrax T25 digital (IKA, Staufen, Germany) at 20000 rpm for 1 h. The obtained mixture was filtered three times (2 x 0.45 µm and 1 x 0.2 µm, **PTFE,** Pall Corp., Port Washington, NY, USA) and stored without the immediate introduction of the thiol component. Right before the printing experiments the thiol and, if included, pyrogallol (0.5 wt%) were added and stirred for 30 min and additionally dispersed for 1 min in an ultrasonic bath. The mixture was filtered (0.45 µm, PTFE, Pall Corp.) once more just before usage.

1.3.12. Preparation of the (pigmented) formulations for the stabilization experiments

The preparation of the thiol-vinyl carbonate systems was conducted in a two-step process due to the stability issues. In a first step the different stabilizers were added to the mixture of vinyl carbonates in small portions and stirred for 20 minutes. In a second step the thiol component was added and the formulation was homogenized for 20 minutes by stirring. For pigmented formulations the pigment flakes (RKJ black ZE37J9, Flint Group, Luxembourg) were added to the mixture of vinyl carbonates and stabilizing molecules in small portions and then dispersed with the Ultra Turrax T25 digital (IKA, Staufen, Germany) at 20000 rpm for 20 min. Finally, the thiol component was added.

1.3.13. Printer

The evaluation and optimization of the drop formation and the printing experiments were performed on a Dimatix Material Printer (**DMP**)-2831 (Fujifilm Dimatix, Santa Clara, USA). This printer features the possibility of exchangeable printheads/cartridges with integrated fillable reservoirs and heaters. DMC-11610 cartridges were used, which work in a bend-mode piezoelectric fashion. Each cartridge has 16 nozzles with a diameter of 21 µm. They are situated in a single row with a nozzle spacing (i.e. distance between the middle of two adjacent nozzles) of 254 µm. The voltage of each nozzle can be controlled individually. The optimum fluid for this printhead consists of a degassed, non-volatile fluid with a density higher than 1 g/cm^2, a surface tension in between 28 and 36 mN/m, particle sizes under 0.2 µm and a viscosity of 10 to 12 mPa*s at printing temperature, albeit higher viscosities up to 30 mPa*s can be jetted as well with some effect on the drop velocity.[84] The printing experiments were performed on Epson photo paper.

1.3.14. Cross hatch test

The Cross Hatch test was conducted according to ISO 2409. The polyethylene terephthalate (**PET**) substrate was coated with a 12 µm layer of the ink with a K-control-coater-system K 101 (RK print, Litlington, UK), which was cured with 1.34 J/cm^2 in an Aktiprint-L UV dryer (Technigraf, Grävenwiesbach-Hundstadt, Germany) with a medium pressure Hg-lamp.

1.3.15. Abrasion test

The abrasion was tested with an Elcometer 1720 using a paper towel soaked in the respective liquid (H_2O, isopropanol or acetone) attached to the universal material clamp (KT001720P207). The substrate was evaluated after 5, 50 and 500 cycles. The speed was set at 55 cycles per minute.

1.4. Results and Discussion

1.4.1. Synthesis

Several mono- and multifunctional vinyl carbonate monomers, analogous to commonly used acrylate monomers, were synthesized (Figure 34) using the well-known synthetic route[53,54] based on the reaction of vinyl chloroformate with alcohols illustrated in Figure 38. The vinyl carbonates were obtained in acceptable yields, ranging between 56.0 and 84.8% (Table 1). All synthesized monomers are liquids at room temperature, except DTMP-VC, which is a solid. NMR and IR spectra are all in good accordance with the expected structures.

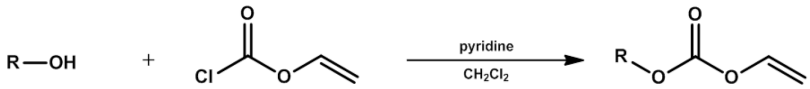

Figure 38: General procedure for the synthesis of vinyl carbonates

Table 1: Vinyl carbonate synthesis

Monomer	Yield / %	Molar mass / g/mol
PE-VC	66.3	208.2
EDM-VC	67.0	216.2
DEGME-VC	69.6	204.2
THF-VC	78.0	172.2
IB-VC	82.0	224.3
BD-VC	56.0	230.2
DPG-VC	66.6	274.3
TMP-VC	84.8	344.3
DTMP-VC	80.7	530.5
EPET-VC	66.7	~549

Tetra(3-mercaptopropyl)silane (Figure 39) was synthesized in a high overall yield (63%) via a multistep reaction starting from tetraallylsilane as described in a patent[77], where it is used as a biocompatible monomer for the vertebroplasty procedure in humans. In the first step the Grignard reaction was used to obtain tetraallylsilane in a yield of 89%. Thioacetic acid was coupled radically to the product of step 1 to yield tetrakis(thioacetylpropyl)silane (96%). In the final step tetra(3-mercaptopropyl)silane was obtained through the cleavage of the thioacetic acid ester group under alkaline conditions with a yield of 73.8%. NMR spectra are in good accordance with the calculated values.

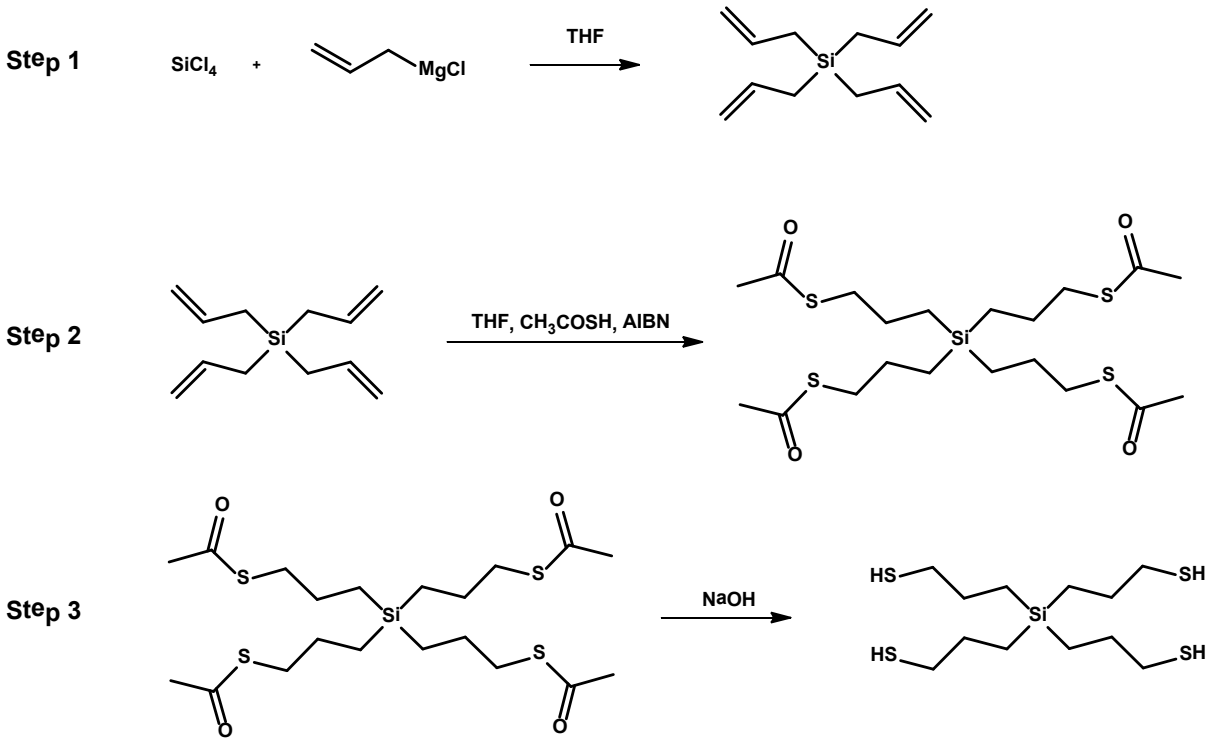

Figure 39: Multistep synthesis route for the synthesis of tetra(3-mercaptopropyl)silane

1.4.2. Physicochemical properties of the monomers

1.4.2.1. Density, surface tension and viscosity

The densities, surface tensions and viscosities of all vinyl carbonate monomers were determined and compared to their acrylate counterparts (Table 2). For the abbreviations of the monomers see page IX to XI and their illustration in Figure 34.

Table 2: Density (**ρ**), surface tension (**σ**), viscosity (**η**) and cell viability (**EC_{50}**) of vinyl carbonate monomers compared to corresponding acrylate monomers

Monomer	ρ / g/cm^3	σ / mN/m	η(25°C; 300 s^{-1}) / mPa*s	EC_{50} / mM
PE-VC	1.14 (1.11[a])	28.7 (39.4[a])	10.6 (7.8[a])	1.4 (<0.16[a])
EDM-VC	1.14 (1.09[a])	28.0 (35.9[a])	10.2 (12.5[a])	>11 (3[a])
DEGME-VC	1.05 (1.02[a])	27.0 (31.3[a])	3.7 (2.1[a])	2.2 (<0.16[a])
THF-VC	1.10 (1.06[a])	25.9 (35.8[a])	3.6 (2.5[a])	>11 (11[a])
IB-VC	1.03 (0.99[a])	28.8 (29.9[a])	11.3 (6.8[a])	0.7 (0.3[a])
BD-VC	1.13 (1.05[a])	28.1 (29.9[a])	7.2 (4.4)	10.5 (<0.16[a])
DPG-VC	1.11 (1.05[a])	28.4 (32.4[a])	12.5 (7.6[a])	3 (<0.16[a])
TMP-VC	1.18 (1.11[a])	32.2 (36.2[a])	378.2 (86.8[a])	0.3 (<0.16[a])
DTMP-VC	solid (1.10[a])	solid (36.1[a])	solid (611.2[a])	9 (<0.16[a])
EPET-VC[b]	1.20	34.3	271.1	0.5

[a] Value of the corresponding acrylate compound; [b] no corresponding acrylate commercially available; [c] thiol groups referred to carbon-carbon double bond (TMPMP)

The densities of vinyl carbonate monomers are uniformly higher than those of their acrylate analogues, albeit the difference is very small for most components (e.g. 1.14 g/cm^3 for PE-VC compared to 1.11 g/cm^3 for the corresponding acrylate). The surface tensions, however, differ significantly. Vinyl carbonates exhibit significantly lower surface tensions throughout compared to their acrylate counterparts (e.g. 28.7 mN/m for PE-VC to 39.4 mN/m for the acrylate monomer). Significant deviations have been detected for the viscosities as well. For vinyl carbonates, in general, higher viscosities were measured. However, this is not the case for EDM-VC (10.2 mPa*s for EDM-VC compared to 12.5 mPa*s for the corresponding acrylate).

1.4.2.2. Cytotoxicity

There are several considerable drawbacks in terms of health, safety and environmental compatibility when applying acrylate monomers.[1] They are known to have high irritancy levels in their uncured state and can cause sensitization after skin exposure.[2–5] This can be attributed to the reactivity of the acrylate double bond towards amino- or thiol-groups of proteins within the human body via Michael addition reactions.[85] Mautner et al.[7,76] investigated the use of thiol-vinyl carbonate systems and concluded that these systems offer less cytotoxicity compared to acrylate formulations.

To determine the improvement in toxicity for a monomer substitution in inkjet inks, the cytotoxicity of the vinyl carbonate monomers was compared to their respective acrylate counterpart (Table 2) via the assessment of the cell viability of mouse fibroblast cells (L929, ISO 10993-5:2009). L929 cells were incubated in a defined media with increasing concentrations of the monomers for 48 hours at 37°C with 5% CO_2. The concentration at which the half of the cells remained alive compared to the negative control (cell culture medium, see 1.3.10) was assessed as cell viability (**EC_{50}**). The results (Table 2) clearly reveal that the vinyl carbonate-based monomers are superior to the acrylate compounds in terms of cytotoxicity. The EC_{50} value of each investigated vinyl carbonate is higher than its acrylate analogue. This is in good accordance with previous findings.[6,7,76]

1.4.2.3. Photoreactivity

The reactivity of the synthesized monomers towards polymerization after photoinitiation has been investigated by means of photo-DSC and FTIR spectroscopy. While photo-DSC is a unique method for the fast and accurate evaluation of the curing behaviour of UV-polymerizable monomers, FTIR spectroscopy enables detailed information on changes in the molecular structure of the monomers during photo-curing.

Using photo-DSC, various important parameters can be obtained with one single measurement (Figure 40). The time to reach the maximum heat of polymerization (**t_{max}**) reveals information about the curing speed of the investigated system. Additionally, the reaction enthalpy (**ΔH**), which is proportional to the monomer conversion, can be determined through the integration of the curve (peak area).[6,86]

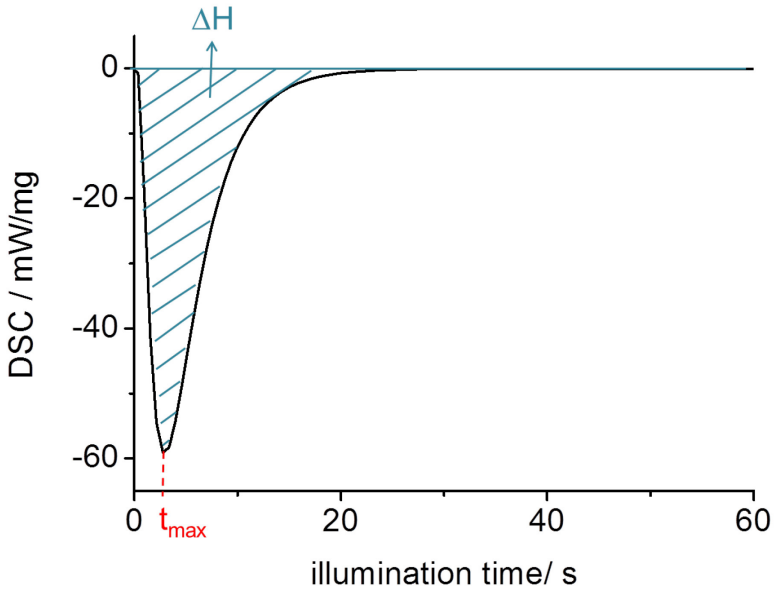

Figure 40: Determination of the reaction parameters ΔH (**cyan**) and t_{max} (**red**) of photo-DSC measurements on the example of the formulation of PE-VC with TMPMP (30 mol% thiol groups) and 5 wt% Lucirin TPO-L

The results of the photo-DSC measurements can be found in Table 4. Vinyl carbonates offer double bond conversions (DBC) that are similar to those of acrylates. However, the measurements reveal the inferiority of vinyl carbonates to acrylates regarding curing speed. For example, the time to reach its maximum heat of polymerization for PE-VC is almost three times as long as for the corresponding acrylate (7.3 s to 2.5 s) (Figure 41). This retardation can be observed for all synthesized monomers throughout. This demonstrates that, although vinyl carbonate monomers offer superior biocompatibility, its monomers are too slow for the implementation in high speed inkjet processes.

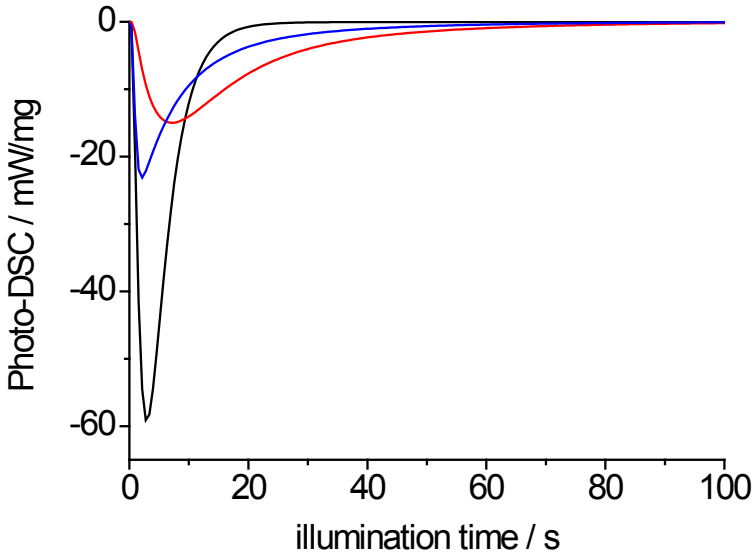

Figure 41: Photo-DSC measurements of PE-VC (**red**), PE-VC with TMPMP (30 mol% thiol groups) (**blue**) and the corresponding acrylate (**black**) with 5 wt% Lucirin TPO-L

This behavior can be explained by the poor resonance stabilization of the formed vinyl carbonate radicals leading to low monomer reactivity.[7] One possibility to overcome this limitation is the addition of multifunctional thiols to the monomer formulation causing a significant increase in curing speed. Two commercially available thiols are illustrated in Figure 42. In this case, the reaction mechanism changes from a radical-based chain growth towards a thiol-ene step growth mechanism.[67] This change in reaction mechanism can be observed through a decrease in the measured reaction enthalpy ΔH. In Table 3 the decrease of ΔH with increasing amounts of thiol groups on the example of THF-VC is depicted. FTIR measurements (*vide infra*) verified that the change in reaction enthalpy is not due to a lower conversion, but due to the change to the less exothermic thiol-ene reaction mechanism[7]. Furthermore, the significant increase of curing speed (observed through the decrease in the t_{max} value) upon the addition of thiol is illustrated. As can be seen in Table 4 and Figure 41 already the formulation with 30 mol% thiol groups of TMPMP increases the curing speed up to values typical for acrylates. Additionally, formulations with 30 mol% thiol of TMPMP, ethoxylated trimethylolpropane trimercaptopropionate (**ETTMP**) and 2,2'-thiodiethanethiol (**TDET**) were compared and no significant change in polymerization speed (t_{max}) could be observed.

Table 3: Heat of polymerization (ΔH) and the time to reach the maximum heat of polymerization (t_{max}) for THF-VC with the addition of different amounts of thiol; 5 wt% Lucirin TPO-L was used as photoinitiator for each formulation

Thiol groups / mol%	ΔH / J/g	t_{max} / s
0	429	9.1
10	356	8.0
20	239	6.7
30	187	2.7
40	153	2.8
50	114	2.2

Table 4: Heat of polymerization (ΔH), calculated double bond conversion (DBC, for the equation see chapter I.i.) and the time to reach the maximum heat of polymerization (t_{max}) of the vinyl carbonate monomers compared to acrylate monomers; 5 wt% Lucirin TPO-L was used as photoinitiator for each formulation; for the abbreviations of the monomers see page IX to XI and their illustration in Figure 34

Monomer	ΔH / J/g	DBC / %	t_{max} / s	$t_{max,\ (30\ mol\%\ thiol)}$ [c] / s
PE-VC	363 (384[a])	84 (92[a])	7.3 (2.5[a])	2.0
EDM-VC	344 (356[a])	83 (89[a])	5.0 (2.8[a])	5.3
DEGME-VC	385 (325[a])	88 (76[a])	17.4 (3.8[a])	5.5
THF-VC	429 (449[a])	83 (88[a])	9.1 (3.7[a])	2.7
IB-VC	290.4 (253.2[a])	73 (66[a])	5.5 (3.2[a])	3.0
BD-VC	573 (635[a])	74 (79[a])	3.7 (2.8[a])	3.5
DPG-VC	477 (478[a])	73 (72[a])	5.3 (2.7[a])	4.1
TMP-VC	394 (463[a])	51 (57[a])	6.6 (2.0[a])	4.1
DTMP-VC	solid (372[a])	solid (54[a])	solid (1.9[a])	2.0[d]
EPET-VC[b]	433	66	3.1	2.9

[a] Value of the corresponding acrylate compound; [b] no corresponding acrylate commercially available; [c] formulation of thiol groups of TMPMP to 70 mol% carbon-carbon double bonds; [d] due to solubility issues measured with 50 mol% thiol; the solid DTMP-VC was not evaluated without the addition of the thiol

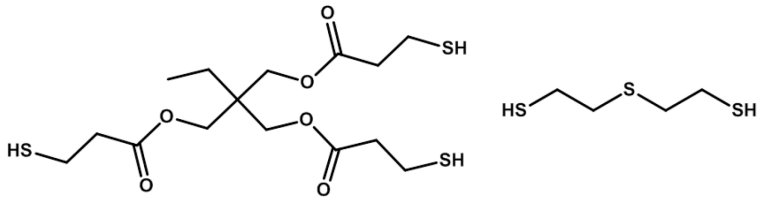

TMPMP **TDET**

Figure 42: **Left**: trimethylolpropane trimercaptopropionate (TMPMP); **right**: 2,2'-thiodiethanethiol (TDET)

The same photopolymerization behavior regarding curing speed was observed via FTIR measurements for THF-VC under ambient conditions. As can be seen in Figure 43 the decrease of the carbon-carbon double bond IR signal of the vinyl carbonate (1650 cm^{-1}; B, middle) is considerably slower compared to the acrylate signal (1635 cm^{-1}; A, top). However, already the formulation containing 30 mol% thiol groups of the commercially available thiol 2,2'-thiodiethanethiol (**TDET**) (1651 cm^{-1}, Figure 43, C, bottom) increases its reactivity to values similar to the corresponding acrylate. Furthermore, FTIR measurements revealed that the double bond conversion under ambient conditions increases through the addition of 30 mol% thiol groups of TDET. For THF-VC without thiols a double bond conversion of only 60% could be observed, whereas the value increases to 80% for the formulation with 30 mol% thiol (Figure 43). This is of paramount importance for the application in food packaging materials as non-polymerized monomers have to be assessed for the compliance with the overall and the specific migration limits (*vide supra*, 1.2.1.2). The observed acceleration of the polymerization reaction as well as the increase in conversion of the investigated vinyl carbonate monomers through the addition of thiol is in good agreement with the finding of Heller et al.[6].

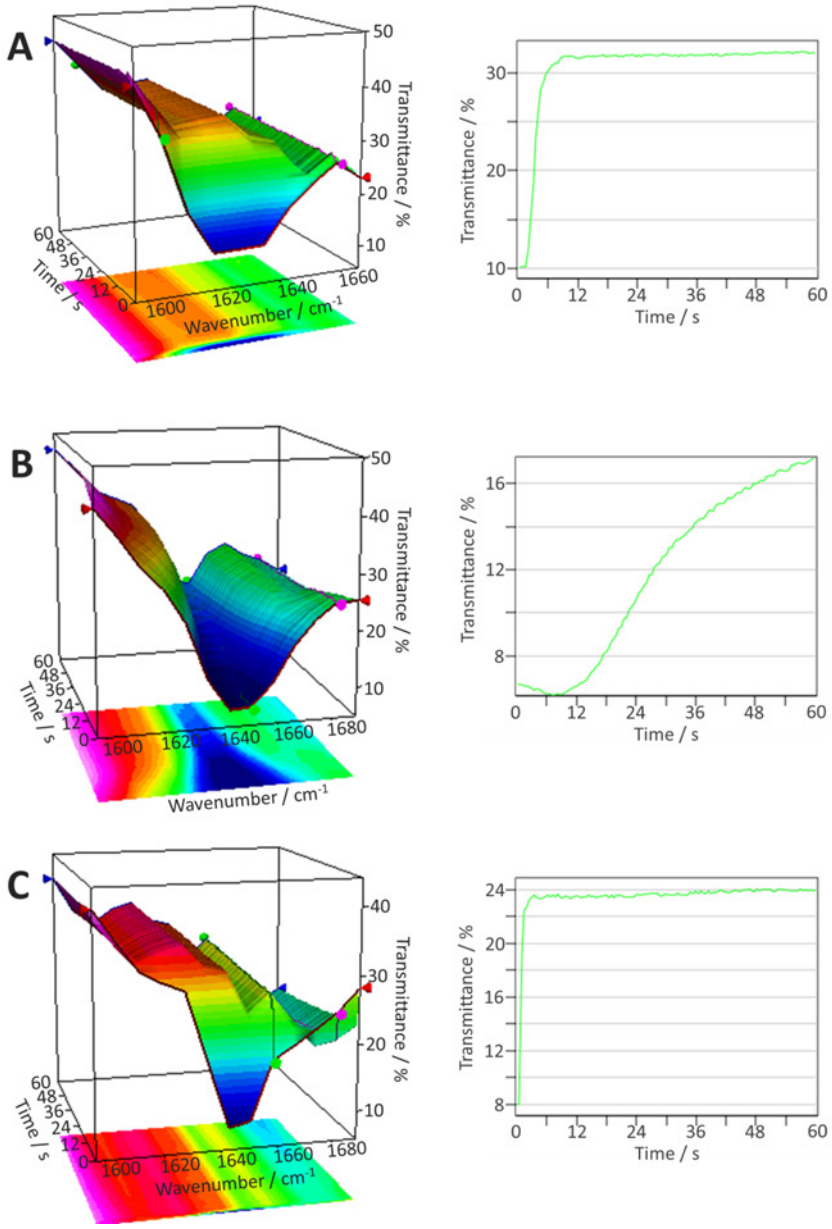

Figure 43: Real-time FTIR studies of the photopolymerization (5.5 mW/cm^2) of THF-AC (**A**), THF-VC (**B**) formulation of THF-VC with TDET (30 mol% thiol groups) (**C**); **left**: 3D-depiction of the carbon-carbon double bond peak; **right**: reduction of the carbon-carbon double peak over illumination time (at 1635 cm^{-1} for **A**, 1650 cm^{-1} for **B** and 1651 cm^{-1} for **C**); all formulations contain 5 mol% Lucirin TPO-L

1.4.2.4. Influence of the photoinitiator concentration

The influence of the photoinitiator (Lucirin TPO-L) concentration on the curing behavior was investigated by photo-DSC measurements (measured with 0.5 W/cm^2) (Figure 34). The reaction enthalpy of the photopolymerization correlates with the double bond conversion (see Analytic methods in chapter I.i.). For reason of comparison, the highest obtained reaction enthalpy for each monomer system was set as 100%. In Figure 44 it is apparent that the THF-VC formulation is significantly affected by a reduction of the photoinitiator concentration. A decrease of 38% of the relative enthalpy from 5 to 0.5 wt% photoinitiator was observed. This effect is clearly reduced by the addition of 30 mol% thiol (TMPMP). Only a decrease of about 7% is observed in this case. For reason of comparison the corresponding acrylate THF-AC was measured as well. The results in Figure 44 show that a lower relative enthalpy is prevalent in the acrylate formulation than for the thiol-ene formulation at low photoinitiator concentrations. The determined high conversion of thiol-ene compositions at low photoinitiator concentrations may be of special interest for applications where migration limits of photoinitiators have to be complied with.

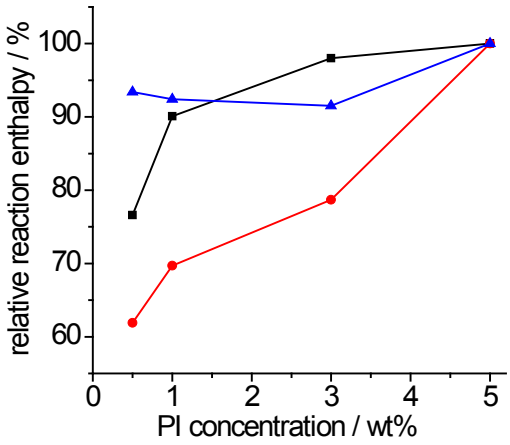

Figure 44: The influence of the photoinitiator concentration on the relative enthalpy determined by photo-DSC measurements in formulations of THF-AC (**black squares**), THF-VC (**red cycles**) and the formulation of THF-VC with TMPMP (30 mol% thiol groups) (**blue triangles**)

1.4.3. The formulation of inkjet inks

Printability is the foremost prerequisite for an inkjet ink. Through the choice of appropriate monomers, photoinitiators, pigments and additives the requirements for the used printhead have to be fulfilled. Thus, the viscosity, the surface tension and the pigment particle size distribution have to meet the criteria of the used printer. In this work a DMP-2831 (Fujifilm Dimatix Inc., Santa Clara, CA, USA) with DMC-11610 cartridges was used.

Other important requirements for inkjet inks are a suitable curing behavior, a good adhesion to the desired substrate and an appropriate shelf life. In principal, the formulation of inkjet inks is a time consuming process, which is mainly based on iterative development. Several formulations with varying monomers, pigments and additives have to be evaluated and individual concentrations have to be optimized to obtain the desired properties.

1.4.3.1. Non-pigmented ink formulation

At first, non-pigmented thiol-vinyl carbonate inks were formulated to investigate the general inkjet printing behavior. Equimolar thiol-ene formulations (i.e. equimolar ratio of thiol groups to VC groups) were chosen. Due to the strong odor of bifunctional thiols (like TDET) and furthermore to enable better crosslinking and thus better mechanical properties of the cured film, the commercially available trifunctional TMPMP was used as thiol component. To ensure an optimal surface and depth curing a blend of diphenyl(2,4,6-trimethylbenzoyl)-phosphine oxide and 2-hydroxy-2-methyl-propiophenone (**PI blend 50/50**) was used as photoinitiator for all ink compositions. A multitude of additives influencing the surface tension to improve the wetting behavior are commercially available. Most of the purchasable additives for this purpose are polyether siloxane copolymers. Already small differences in their composition can have a huge impact for the application. However, information about their exact formulation is scarce. A screening is generally necessary to find suitable additives for a given formulation. In Table 5 additives tested for the thiol-vinyl carbonate composition on PET substrates are listed.

Table 5: Additives investigated in the additive screening

Additives	Composition
Byk 307[a]	Polyether-modified polydimethylsiloxane
Byk 333[a]	Polyether-modified polydimethylsiloxane
Byk 377[a]	Polyether-modified, hydroxy-functional polydimethylsiloxane
Byk UV 3510[a]	Polyether-modified polydimethylsiloxane
Byk UV 3500[a]	Polyether-modified, acryl-functional polydimethylsiloxane
Byk UV 3535[a]	Modified, silicon-free polyether
Tego Glide 100[b]	Polyether siloxane copolymer
Tego Glide 130[b]	Polyether siloxane copolymer
Tego Glide 410[b]	Polyether siloxane copolymer
Tego Glide 432[b]	Polyether siloxane copolymer
Tego Glide 440[b]	Polyether siloxane copolymer
Tego Wet 270[b]	Polyether siloxane copolymer
Tego Wet 500[b]	Non-ionic organic surfactant

[a] Byk Chemie GmbH, Wesel, Germany; [b] Evonik Industries AG, Essen, Germany

The optimized formulations with the best wetting (no wetting defects) and adhesion (cross hatch test result 0) behavior on PET-substrates can be seen in Table 6.

Table 6: Composition of thiol-VC ink formulations

	Mass fraction / wt%	
Component	**Thiol-VC ink I**	**Thiol-VC ink II**
PE-VC	0.7	1.3
EDM-VC	0.7	1.4
THF-VC	2.3	1.4
DPG-VC	27.3	23.8
EPET-VC	18.5	21.8
TMPMP	46.8	46.7
Tego Glide 410	0.1	-
Byk 333	-	0.1
Pyrogallol	0.5	0.5
PI blend 50/50	3.0	3.0

Their physical properties are depicted in Table 7. Their densities and surface tensions are in the optimum range of the used printhead. The viscosities exceed the optimum specification due to the high content of TMPMP, however at 50°C the viscosities are in a manageable range. This can also be seen, when assessing the dimensionless Z number[87] through equation (3), which is an indicator for the printability of a fluid. A value in between 1 and 10 is assumed to be printable.[88] A Z value of 1.28 for thiol-VC ink I and 1.24 for thiol-VC ink II were calculated.

$$Z = \frac{\sqrt{d\rho\sigma}}{\eta} \quad \textbf{(3)}$$

d is the diameter of the orifice, ρ is the density, σ is the surface tension and η the viscosity of the ink

Table 7: Physical properties of the formulated thiol-VC inks

Formulation	Density / g/mL	Surface tension / mN/m	Viscosity (25°C) / mPa*s	Viscosity (50°C) / mPa*s
Thiol-VC ink I	1.17	28.9	73.1[a]	20.8[a]
Thiol-VC ink II	1.17	29.7	76.9[b]	21.7[b]

[a] measured at a shear rate of 48.8 s^{-1}; [b] measured at a shear rate of 46.2 s^{-1}

In general, these formulations showed an appropriate printability, although quite high voltages had to be used due to their comparably high viscosities. Thiol-VC ink I attains at drop ejection velocity of 7 m/s with an applied voltage of 28.2 V at 47°C and 2 kHz. Thiol-VC ink II achieves a lower drop speed of 6 m/s with a jetting voltage of 28.5 V at 50°C and 2 kHz, which was to be expected because of its higher viscosity. For both formulations a tailing behavior was observed (Figure 45). However, the tail recovers and a single droplet is formed. The droplet of thiol-VC ink I after 700 µm flightpath can be seen in Figure 45, bottom left. Due to camera constrains and the deviations in the cartridges, a clear image of the droplet of thiol-VC ink II after 700 µm was not obtainable. Instead an image after 360 µm flightpath is shown in Figure 45, bottom right. With a customary distance of about 1 mm from the nozzle plate to the substrate no adverse effect of the tailing on the printing results was to be expected, which was further confirmed by printing tests on PET-foils.

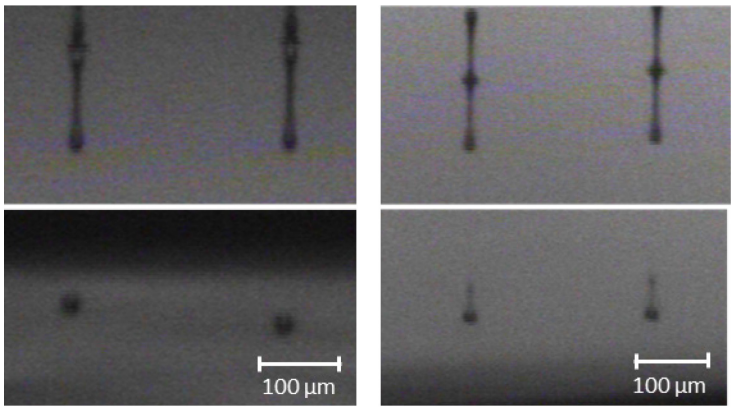

Figure 45: **Left**: images of the formed droplets of thiol-VC ink I; **top left**: ink droplets after 20 µs after actuation; **bottom left**: 100 µs after actuation; **right**: images of the formed droplets of thiol-VC ink II; **top right**: ink droplets after 20 µs after actuation; **bottom right**: 60 µs after actuation

1.4.3.2. Pigmented ink formulation

Pursuing the aim to make acrylate inks dispensable, pigmented inkjet formulations were developed using predispersed Carbon Black pigments. Due to the effect of pigments on the properties of the ink and the cured film, a separate iterative development had to be performed. These experiments unveiled that the addition of pigments increases the viscosities of formulations to values unsuitable for the used inkjet printer. A change of vinyl carbonate monomer composition to a higher content of low-viscous monomers turned out to be unfeasible as it reduced the crosslinking density and thus the mechanical properties of the cured film. Furthermore, a decrease in the pigment concentration is limited due to the requirement of a suitable color density. This leaves the thiol component as the only viable option for an adequate viscosity reduction as it is one of the main components in the ink. The replacement of the commercially available multifunctional thiols such as TMPMP or PETMP with commercially available thiols with lower viscosities (e.g. bifunctional thiols), though, has a negative effect on the crosslinking density (i.e. mechanical properties of the cured film) and leads to an objectionable odor.

Table 8: Viscosities of thiol components

Thiol	Viscosity[a] (25°C) / mPa*s	Viscosity[a] (50°C) / mPa*s
TMPMP	145.7	55.6
PETMP	186.7	46.4
Tetra(3-mercaptopropyl)silane	85.9	35.9

[a] *measured at a shear rate of 300 s^{-1}*

In order to overcome these issues tetra(3-mercaptopropyl)silane was synthesized. This tetrafunctional thiol provides a high crosslinking density, low odor and foremost a low viscosity. Table 8 shows the viscosity of the synthesized thiol compared to the commercially available TMPMP and PETMP. Additionally, photo-DSC measurements confirmed suitable reactivities of thiol-vinyl carbonate compositions comprising tetra(3-mercaptopropyl)silane. A composition of BD-VC with tetra(3-mercaptopropyl)silane (30 mol% thiol groups) revealed a t_{max} value of 3.4 s compared to 3.5 s for the formulation with TMPMP. The combination of a reduction of the thiol content to 30 mol% (thiol groups) and the utilization of tetra(3-mercaptopropyl)silane enabled the formulation of inks with appropriate viscosities.

Table 9: Composition of the pigmented ink formulation

Component	Mass fraction / wt%
	Pigmented ink
PE-VC	1.8
DEGME-VC	1.8
THF-VC	3.6
BD-VC	25.0
DPG-VC	17.8
TMP-VC	10.7
EPET-VC	10.7
Tetra(3-mercaptopropyl)silane	19.6
Pigment flakes	4.0
PI blend (50/50)	5.0

Table 10: Physical properties of the pigmented ink formulation

	Density / g/mL	Surface tension / mN/m	Viscosity (25°C)[a] / mPa*s	Viscosity (50°C)[a] / mPa*s
Pigmented ink	1.12	31.7	35.1	12.3

[a] *measured at a shear rate of 105.6 s^{-1}*

Using tetra(3-mercaptopropyl)silane together with vinyl carbonate monomers, an appropriate photoinitiator and predispersed Carbon Black pigments (Flint group ZE37J9) a basic inkjet ink was realized. The detailed composition is stated in Table 9. It provides the required physical and chemical properties requested for inkjet inks (Table 10). A Z value (equation (3)) of 2.22 was calculated. Consequently, an excellent printing behavior was observed. A drop speed of 7.8 m/s is attained with a jetting voltage of 19.5 V at 50°C and 2 kHz. Through drop watcher experiments a consistent drop flight with a tailing behavior was observed (Figure 46, left). However, as for the thiol-VC inks, the tail recovers and a single droplet is formed within 700 µm from the nozzles. Using a 1 mm gap between the nozzle plate and the substrate separated single droplets were ejected onto the substrate to prove the consistent printing behavior and that no satellites were being formed (Figure 46, right). Satellites are additional small droplets that develop, if the tail separates itself from the main droplet. If existent, small stains outside of the printed dots would be observable on the single droplet test. A printed pattern on photo paper can be seen in Figure 47.

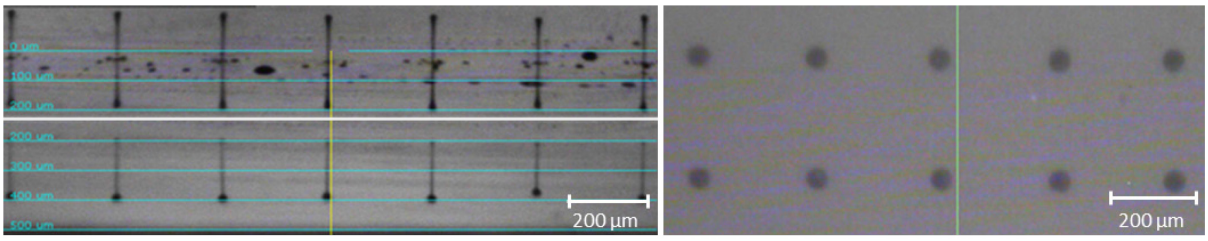

Figure 46: **Top left**: images of the formed droplets after 25 µs after actuation; **bottom left**: 50 µs after actuation; **right**: single droplet test

Figure 47: Print on photo paper (Epson photo paper glossy)

The adhesive properties of the cured film were investigated by means of a cross hatch test (ISO 2409). For that purpose a 12 µm thick film was deposited on the PET-substrate and cured with UV-light (energy dose = 1.34 J/cm^2). Figure 48 shows the scratched film after the detachment of the pressure-sensitive tape revealing an acceptable adhesion (result of 1 according to ISO 2409).

Furthermore, the solvent resistance was tested by means of the abrasion tests under the influence of different solvents. The test revealed a good solvent resistance against water (500 cycles without abrasion), a decent resistance against isopropanol (only a slight abrasion was observed after 500 cycles) and only a short-term resistance against acetone (no abrasion for 5 cycles and a slight abrasion after 50 cycles).

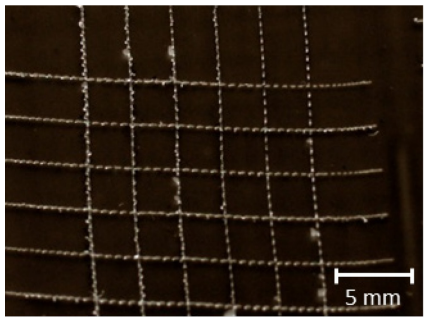

Figure 48: Cross hatch test of the pigmented ink on a PET-foil

1.4.1. Stability of the thiol-vinyl carbonate system

Due to industrial demands inkjet inks have to be storable for at least 9 months at room temperature without significant change in their physiochemical behavior. An increase in viscosity of a few mPa*s may already change the printing behavior (printing speed, drop volume) and compromise the printed image. Consequently, the storage stability under dark conditions of thiol-vinyl carbonate formulations was investigated. The influence of different stabilizer systems on the shelf life was evaluated by viscosity measurements. The applied concentrations of stabilizers were selected according to literature values[89,90] for other thiol-ene systems.

For an accurate shelf-life determination long term tests are preferential. Therein, the formulation is stored at recommended storage conditions such as room temperature. Due to the extensive time consumption of these tests accelerated heat stability tests are usually implemented to predict the actual shelf life. It has been shown that a storage time of 10 to 14 days at 50°C corresponds to a long term shelf life of about 6 month at room temperature.[91] Using this prediction model formulations have to stay stable for 3 weeks at 50°C to ensure a shelf life of approximately 9 months at room temperature.

Table 11: Composition of the vinyl carbonate formulation for the stabilization experiments

	Mass fraction / wt%
Component	**VC stabilization formulation**
PE-VC	5.0
THF-VC	10.0
DPG-VC	40.0
TMP-VC	45.0

Table 11 shows the vinyl carbonate formulation used for all stabilization experiments. For the initiation of each experiment the stabilizing additive was added to the vinyl carbonate formulation and subsequently the commercially available trifunctional thiol TMPMP was applied. Two different ratios of vinyl carbonate to thiol groups were investigated, the equimolar ratio of 1:1 and the ratio of 2:1. To each formulation 3 wt% of photoiniitator (PI blend 50/50) was added. Furthermore, different concentrations for one and bi-component stabilizers were applied. Subsequently, the effect of black pigments on the stability was assessed. The starting viscosity of the formulations was in the range of 70 mPa*s for 1:1 and 52 mPa*s for 2:1 formulations (slight deviations depending on the specific stabilizer system and concentration). The investigated pigmented formulations exhibit an initial viscosity of approximately 90 mPa*s. The stabilization efficiency was determined through their relative

viscosity increase upon storage at 50°C. The influence of the stabilizers on the reactivity of the prepared formulations towards photopolymerization has been investigated by means of photo-DSC.

As the instability of thiol-ene formulations may stem from different reasons (*vide supra*) and combinations thereof,[67,71,72] several different approaches were investigated. Phenolic radical stabilizers, like pyrogallol or monomethyl ether hydroquinone (**MEHQ**), can transfer a hydrogen atom to a radical and subsequently form a less reactive, stabilized radical themselves, preventing further polymerization.[92] A synergistic effect of these phenolic stabilizers is known in combination with oxygen.[92] Therein, the phenolic stabilizer is oxidized and consumed. In acrylate systems this consumption of the phenolic stabilizer is accelerated by a non-radical Michael reaction between carbon-carbon double bond and the stabilizer molecules.[93,94]

Single stabilizer system:

The tested formulations and their respective increases in viscosity are listed in Table 12. Although a stabilizing effect can be observed for each tested stabilizer, only the addition of pyrogallol or MEHQ limits the increase in viscosity to under 100% after 3 weeks at 50°C. The best stabilizing effect was observed for pyrogallol at a 90 mM concentration, while a less efficient stabilization was observed for the lowest concentration (9 mM). The addition of butylated hydroxytoluene, triphenylphosphite (**TPP**), Irgastab 22, propyl gallate or lauryl gallate has only a slight stabilizing effect leading to large increases in viscosity (over 100%) after 2 weeks at 50°C.

Photo-DSC measurements were performed to evaluate the reactivity of the stabilized formulations. As previously mentioned, the curing speed is of significant importance in the industrial inkjet process. Therefore, stabilizers have to be found, which enhance the shelf life, but do not significantly reduce the polymerization speed upon curing. The results of the photo-DSC measurements on the most promising single stabilizer systems can be found in Table 12 and Figure 49. Through the addition of pyrogallol or MEHQ the polymerization speed is reduced. Especially higher concentrations of pyrogallol are detrimental, as can be seen in the significantly higher t_{max} value and the lower recorded reaction enthalpy (ΔH).

Table 12: Relative increase in viscosity of a 1:1 thiol / vinyl carbonate mixture in the presence of different stabilizing systems after defined storage times at elevated temperature (50°C); parameters t_{max} and ΔH obtained through photo-DSC measurements on the unaged formulations

Stabilizer	Concentration / mM	Increase in viscosity after 1 day / %	Increase in viscosity after 1 week / %	Increase in viscosity after 3 weeks / %	t_{max} / s	ΔH / J/g
Reference	-	2700	-	-	2.0	298
Pyrogallol	9	13	50	-	2.4	298
	90	1	5	25	2.8	265
Butylated hydroxytoluene	9	570	2100	-	-	-
	90	57	225	-	-	-
TPP	9	2000	-	-	-	-
	90	980	2100	-	-	-
Irgastab 22	9	290	6000	-	-	-
	90	55	1400	-	-	-
MEHQ	9	180	1000	-	-	-
	90	22	30	90	2.5	270
Propyl gallate	9	190	550	-	-	-
Lauryl gallate	9	188	520	-	-	-

- formulations with an already measured increase of >50% in viscosity were not evaluated further

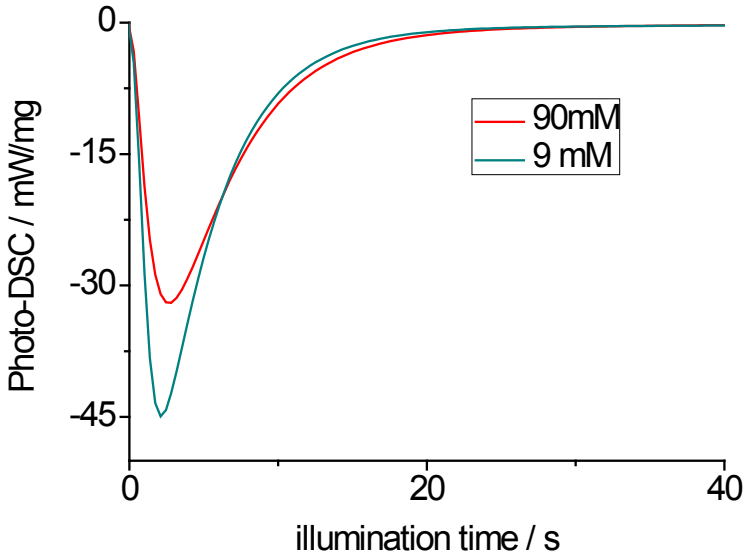

Figure 49: Photo-DSC measurements of VC-thiol formulation with the addition of varying amounts of pyrogallol; 90 mM (**red**) and 9 mM (**cyan**)

Co-stabilizing systems:

Two different synergistic effects can be applied to enhance the stability of thiol-ene formulations. The first strategy is a combination of stabilizers sharing the same stabilization mechanism. The second strategy is using a heterosynergetic effect using a blend of stabilizers featuring different stabilizing mechanisms.[95] The improvement of shelf life by the heterosynergetic effect was already described by several groups. A significant improvement was described by Belbakra using pyrogallol (a hydrogen donor) and TPP (a hydroxide decomposer).[89] In a patent by the group of Liska the synergetic effect of several acidic compounds based on phosphonic acids in combination with pyrogallol is reported.[70] Consequently, these concepts were investigated for their application in thiol-vinyl carbonate systems.

Table 13: Increase in viscosity of a 1:1 thiol / vinyl carbonate mixture in the presence of different stabilizing systems after defined storage times at elevated temperature (50°C); parameters t_{max} and ΔH obtained through photo-DSC measurements on the unaged formulations

Co-stabilizer	Concentration / mM	Pyrogallol / mM	Increase after 1 day / %	Increase after 1 week / %	Increase after 3 weeks / %	t_{max} / s	ΔH / J/g
Diisooctyl PA	90	9	0	3	25	2.3	350
Ethoxy PA	90	9	0	8	23	2.1	321
TPP	90	9	0	14	34	2.6	239
Irgastab 22	90	9	0	6	40	6.6	310

The different tested systems and the used concentration can be seen in Table 13. Diisooctylphosphinic acid (**Diisooctyl PA**), 6-[2-[2-(2-methoxyethoxy)ethoxy]ethoxy]-hexylphosphonic acid (**Ethoxy PA**), TPP and Irgastab 22 were investigated as co-stabilizer to Pyrogallol (9 mM). For all these stabilizing systems an improvement to the pure pyrogallol stabilizing system (9 mM) could be observed. The best results were obtained with pyrogallol (9 mM) and Ethoxy PA (90 mM) or Diisooctyl PA (90 mM), respectively, which only show an increase of about 25% after 3 weeks at 50°C. Unfortunately, the increase in viscosity for all tested formulations after storage at 50°C for 3 weeks is still too high to ensure a sufficiently stable printing behavior for industrial use.

Photo-DSC measurements on the non-aged co-stabilized systems revealed that the pyrogallol/TPP system leads to a significantly lower conversion (indicated by the lower reaction enthalpy), and the introduction of Irgastab 22 with pyrogallol significantly reduces the polymerization speed (6.6 s compared to 2.0 s for the non-stabilized formulation). The best results were obtained for the co-stabilization of pyrogallol and Ethoxy PA or Diisooctyl

PA, featuring the lowest increase in viscosity, a fast curing behavior (t_{max} of 2.1 s and 2.3 s, respectively) and a high reaction enthalpy indicating a high conversion.

While the aforementioned equimolar formulation (thiol groups / vinyl carbonate groups) can be stabilized for a week at 50°C, further experiments were conducted for a 1:2 (thiol groups / vinyl carbonate groups) formulation. This ratio was assumed to give more adequate results on the stabilization behavior of the ink formulations described above. Albeit the non-stabilized 1:2-formulation is more stable than the 1:1-formulation, no significant difference on the shelf life regarding its applicability as inkjet inks could be observed for the 1:2-formulations co-stabilized by Pyrogallol and respectively with Diisooctyl PA or TPP (Table 14).

Table 14: Increase in viscosity of a 1:2 thiol / vinyl carbonate formulation in the presence of different stabilizing systems after defined storage times at elevated temperature (50°C)

Co-stabilizer	mM	Pyrogallol / mM	Increase in viscosity after 1 day / %	Increase in viscosity after 1 week / %	Increase in viscosity after 3 weeks / %
-	-	9	3	43	423
Diisooctyl PA	90	9	0	4	16
TPP	90	9	0	8	35

Pigmented formulations:

Furthermore, the influence of Carbon Black pigments was assessed. For this matter 4 wt% of the commercially available, predispersed pigments (Flint group ZE37J9) used for the pigmented ink formulations was added to the formulation. The results of the viscosity measurements after one week at 50°C (Table 15) reveal the negative influence of these predispersed pigments on the shelf life of the thiol-vinyl carbonate system. This can be attributed to the complex surface composition of Carbon Blacks and the dispersants added. Carbon Blacks feature a wide range of functional groups on the surface due to their manufacturing process, like carboxyl, phenol, lactones, aldehydes, ketones, quinones, hydrochinons, and anhydrides, among others.[44,45] This leads to a catalytic effect on the thiol-vinyl carbonate formulation resulting in a significantly inferior shelf life.

Table 15: Increase in viscosity of a pigmented 1:1 thiol / vinyl carbonate formulation in the presence of different stabilizing systems after defined storage times at elevated temperature (50°C)

Co-stabilizer	mM	Pyrogallol / mM	Increase in viscosity after 1 week / %
Diisooctyl PA	90	9	113
Diisooctyl PA	90	90	55
Irgastab 22	9	9	72

1.5. Conclusion

In this work a variety of low-toxic vinyl carbonate monomers was synthesized and evaluated as replacement for acrylates in UV curable digital inks. Their cytotoxicity and reactivity was compared to their acrylate counterparts. The experiments revealed their superiority in cytotoxicity as well as their inferiority in curing speed. The curing of vinyl carbonates turned out to be too slow for the industrial inkjet process. To overcome this drawback thiol-vinyl carbonate formulations were prepared and investigated. The addition of thiol increased the curing speed to values typical for acrylates. Due to the viscosity increase through the addition of pigments for thiol-vinyl carbonate ink formulations, a low-viscous thiol alternative to the commercially available multifunctional thiols had to be found. Consequently, the tetrafunctional molecule tetra(3-mercaptopropyl)silane, offering low viscosity and low odor, was synthesized. Using this thiol in combination with the synthesized vinyl carbonate monomers a basic ink formulation was realized. This ink shows an excellent jetting behavior together with good film forming properties and adhesion on PET. However, a major challenge remains in the sufficient stabilization of thiol-ene systems due to premature dark polymerization. Especially for inkjet inks a constant viscosity over storage time is highly important as it significantly affects the printing quality. As shown in this work, a significant improvement on shelf life can be obtained through the addition of appropriate stabilizers. However, the stringent requirements regarding shelf life for industrial inkjet inks could not be satisfied. Still, thiol-vinyl carbonate inks are a promising alternative to the commercially available acrylate-based inks for applications, in which a separate storage of the thiol and the vinyl carbonate component is deemed to be acceptable. Especially due to the higher biocompatibility of the vinyl carbonates these UV curable inkjet formulations may open up new market niches.

2. Exploring thiol-based chemistry on surfaces

Parts of the work in this chapter have previously been published in Journal of Materials Chemistry B,[96] and have been the subject of oral presentations at conferences (see list of publications).

Dr. Simone Radl contributed with preliminary results on the polymer brush experiments. Polymer brush growth and photo-oxidation experiments were performed in close collaboration with Paul Rieger. Ellipsometry measurements were performed by Dr. Anna Maria Coclite, Technical University Graz. GPC measurements were performed by Ing. Josefine Hobisch at the Technical University in Graz. XPS measurements were conducted by Dr. Matthias Edler at the University of Leoben. Fluorescence imaging of the NeutrAvidin samples was conducted by Ing. Elfriede Zenzmaier, Technical University Graz. Confocal fluorescence microscope imaging was performed by Dr. Osama El Zubir and Sijing Xia (PhD student) at the University of Sheffield. Additionally, Dr. Osama El Zubir contributed to the non-specific protein patterns. Dr. Robert Ducker conducted the SIMS measurement at the University of Sheffield.

2.1. Introduction

The aim of the second part of my research was to explore different kinds of possibilities and derivatization strategies for thiol chemistry on surfaces beyond the classical radical thiol-ene reaction used in chapter 1. Thiol-based chemistry has blossomed in recent years due to the search for alternatives to the classic copper-catalyzed azide/alkyne “click” chemistry introduced by Sharpless in 2001.[69,97,98] Its attraction can mainly be attributed to its properties, which include most of the characteristics for a “click-chemistry” behavior.

Click-type reactions play an important role in the patterned immobilization of (bio)molecules on solid substrates. For this matter the application of self-assembled molecular layers is a convenient method to introduce reactive sites, e.g. thiol groups or carboxylic acid groups, on the surface. For the patterning of surface bound functional groups a wide range of strategies is feasible, such as scanning probe techniques[99–101], micro-contact printing (**μCP**)[102,103] and photolithography[104].

The engineering of controlled spatially defined patterns of proteins, genes and gene sequences on surfaces plays an important role in biotechnology. One relevant application is the fabrication of chips for biochemical analysis (i.e. DNA-chips and protein microarrays). DNA-chips consist of an array of probes, functionalized with DNA-sequences, on a carrier like glass or quartz. For the analysis the chip is flooded with the sample solution (the analytes). The higher the similarity between the analyte gene sequence and the immobilized

sequence the more hydrogen bonds are being formed between them. Thus, the higher is the strength of the non-covalent bond formed. Through a cleaning process, weakly bound and non-bound molecules are being washed off. Subsequently, the chips are being read out. The most widely used technique uses a laser to excite fluorophores on the analytes and the fluorescence response is being assessed.[8]

Another relevant application field is the imitation of cell behavior on surfaces. One important aspect therein is the nanoscale topography, which has an effect on cell adhesion, cell orientation, cell mobility, surface antigen display and modulation of intracellular signaling pathways, among others. To be able to fully imitate cell processes and investigate them small, dense nanometer scale features have to be fabricated.[9,10]

For protein patterning several criteria have to be met, as the goal is to construct complex protein patterns to investigate the interaction of different proteins. First, non-specific adsorption has to be inhibited, because proteins adhere to most surfaces, due to their complex compositions. Second, a selective introduction of protein-binding functional groups is required. Third, the protein should keep its native conformation upon binding to the surface. Fourth, the protein should be bound in a site-specific fashion. Fifth, substrates that facilitate the optical read-out, like glass, should preferably be used. Finally, the patterning of multiple components should be viable. For the successful realization of biological structures with dimensions in the sub µm range, lithographic techniques must be combined with appropriate chemical immobilization strategies.[11]

A variety of techniques exists for the nanopatterning of surfaces, e.g. dip-pen nanolithography[105–107] and nanoshaving/nanografting[108–110]. Alternatively, advanced photochemical methods such as interferometric[111] and scanning near-field lithography[112] enable chemical transformations with resolutions in the double-digit nanometer range. A significant advantage offered by the use of interferometric methods is that they facilitate patterning over large (square centimeter) areas, thus making them ideal for adaptation to biological applications. Moreover, this technique requires only limited resources, and its exploitation should be feasible for many laboratories not otherwise equipped with the infrastructure for nanofabrication.

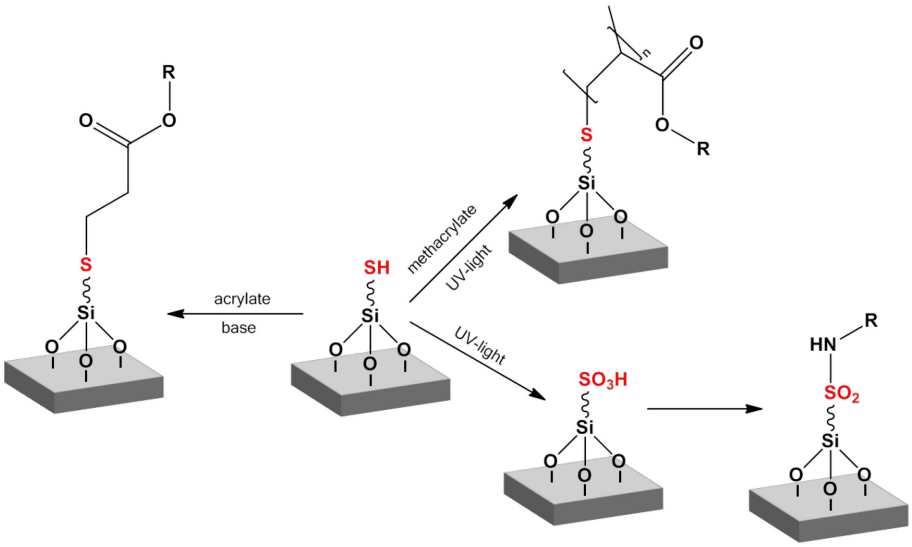

Figure 50: Overview of the applied thiol-based surface modification reactions

In the present work, mercaptopropyltrimethoxysilane (**MPTMS**) functionalized silicon oxide surfaces have been investigated for a new patterning strategy using the photo-oxidation of thiol groups (Figure 50). It is well known that surface bound thiol groups undergo oxidation to disulfides under ambient conditions. Subsequent oxidation to sulfinate and sulfonate derivatives occurs at a very slow rate,[113] although direct oxidation by means of electrochemistry or by a chemical treatment using a mixture of hydrogen peroxide and acetic acid is feasible.[114] Additionally, UV exposure provides a simple means to cause a spatially defined conversion of thiols to sulfonate groups.[115,116]

In this work, the application of the photo-oxidation of thiol groups to sulfonic acid groups for several patterning strategies has been assessed. It was investigated for the patterning of the surface induced polymer brush growth and for a selective thiol-Michael derivatization. Moreover, a selective derivatization of the formed sulfonic acid groups may enable new approaches for surface conjugation. A well reported approach for the activation of sulfonic acids is their conversion to the corresponding acid chlorides using thionyl chloride.[117] Nevertheless, this derivatization strategy requires relatively harsh conditions ($SOCl_2$ under reflux) limiting its applicability. In this work a mild and selective functionalization of photo-generated sulfonate groups is demonstrated, which enables the coupling of nitrilotriacetic acid (NTA), facilitating the site specific binding of green fluorescent protein (GFP). Furthermore the non-oxidized thiol groups are used for the growth of poly(oligoethylene glycol methacrylate) (POEGMA) brushes by a surface-induced polymerization reaction to inhibit non-specific adsorption of proteins in these regions. This novel route enlarges the toolbox for the realization of complex proteins patterns at the nanoscale.

2.2. Fundamentals

2.2.1. Molecular layers and the principle of self-assembly

In the last several decades molecular layers have gained considerable attraction, although its origins date back to the late 1910s, when Langmuir was the first to investigate the formation of oil films on water and their deposition onto surfaces.[118,119] Blodgett followed with experiments covering the deposition of long chain carboxylic acids.[120,121] In 1946 Zisman et al.[122] discovered that certain types of organic molecules form monomolecular layers on polished metal surfaces through adsorption. Many systems have been investigated since, for example alkanethiols on gold, silver and copper and alkyltrichlorosilanes or alkylphosphonic acids on hydroxylated surfaces,[123] just to name a few.

Nowadays organic molecular layers have a broad field of application. By applying appropriate molecular layers surface properties can be altered towards a desired direction. Albeit only of a thickness of a few nanometers, they can change the surface properties drastically without changing bulk material parameters. Different application methods are feasible. One of the most popular application works along the principle of self-assembly (Figure 51). Its distinct characteristic is that molecular layers applied by this principle feature chemisorbed molecules on the surface. The molecules consist of a head group and a tail group, which are linked by a spacer. Through the spontaneous reaction of the head group with the surface of the substrate the molecules are being strongly bound to the surface (either through an ionic or covalent bond).[123]

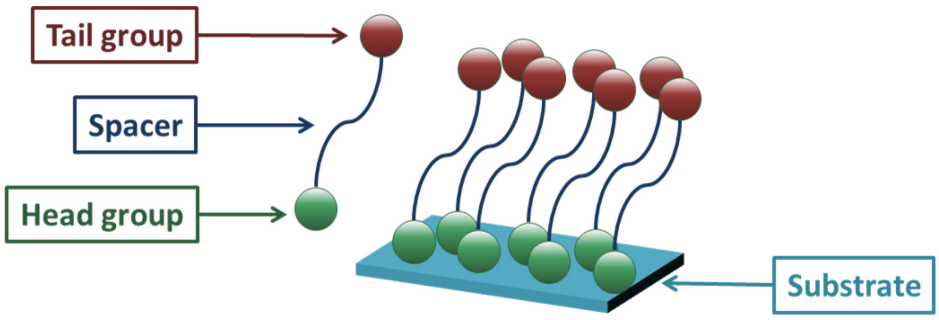

Figure 51: The principle of self-assembly

In this work the principle of self-assembly was used to immobilize thiol groups on silicon surfaces. Silicon surfaces have the advantage that they don't interact with thiols, as gold would for example, and feature smooth surfaces that allow an exact evaluation of chemical changes on the surface through analytical methods (i.e. atomic force microscopy, X-ray photoelectron spectroscopy, etc.).

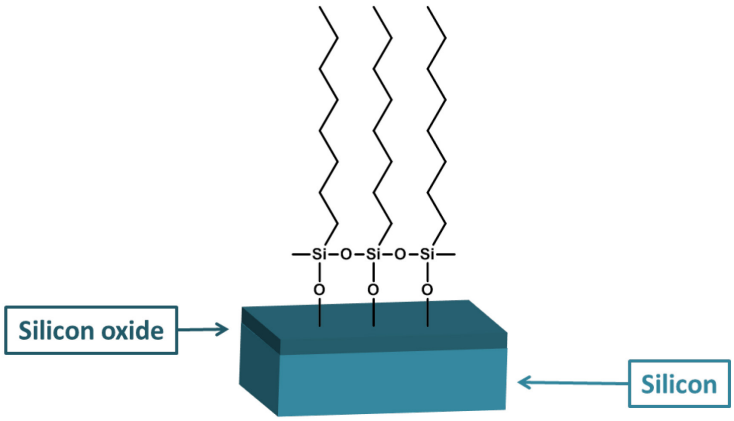

Figure 52: Schematic monolayer of an alkyltrichlorosilane on a silicon oxide surface

Due to its comprehensive use, the silanization process of trichlorosilanes is well investigated.[124] For the self-assembly on a substrate trichlorosilanes require a hydroxylated surface. The reaction is being driven by the formation of polysiloxane (Si-O-Si bonds) tethered to hydroxyl groups on the surface (Figure 52). Possible substrates include silicon oxide[125,126], quartz[127], glass[128] and mica[129], among others[124]. One of the disadvantages of alkyltrichlorosilanes is their sensitivity to water and its influence on the formed films.[124] In the absence of water only incomplete monolayers are being formed, while too much water leads to premature polymerization in solution and the deposition of polysiloxane onto the surface. Reaction conditions therefore play a crucial role. This circumstance can be seen in the various reaction times that have been reported to achieve fully covered monolayers by trichlorosilanes, which range from 2 min[130] to 24 h[125,130] depending on the respective conditions. Once the monolayer is adsorbed on the surface, further layers may build up and form multilayers.[124]

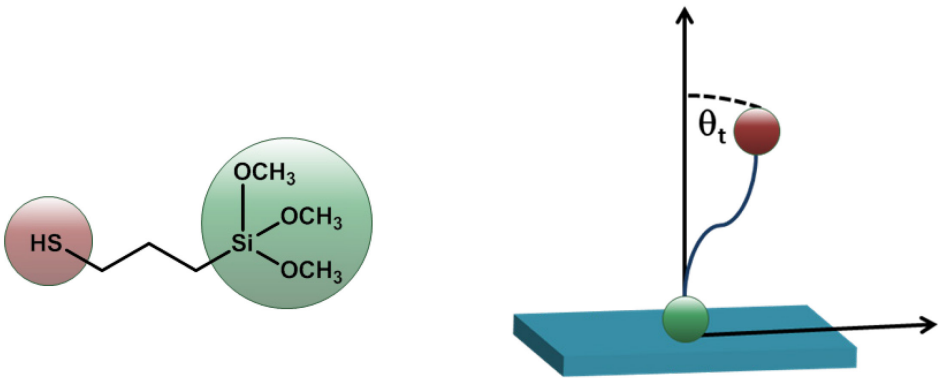

Figure 53: **Left**: the applied alkoxysilane (3-mercaptopropyl)trimethoxysilane (MPTMS) with the head group highlighted in green and the tail group highlighted in red; **right**: tilt angle (θ_t)

In this work an alkoxysilane (Figure 53, left) was used to introduce thiol groups onto the surface instead of a trichlorosilane as the synthesis of a trichlorosilane with a thiol tail group is not feasible.[131] An additional benefit of alkoxysilanes to trichlorosilanes relates to the purification step after synthesis. Trialkoxysilanes allow chromatographic purification, which facilitates the fabrication of uniform monolayers.[132] Bierbaum et al.[133] investigated the difference of the monolayer formation between trichloro- and trimethoxysilanes and assumed that they offer different reaction mechanisms. Trichlorosilanes form oligomers rapidly with traces of water in solution, followed by a physisorption to the surface and only then the chemisorption (formation of Si-O-Si bonds to the surface) takes place. In contrast, the lower reactivity of trimethoxysilanes restrains the hydrolysis and oligomerization reaction in solution. This results in primarily monomers reacting with the surface and a less packed surface. Even with longer reaction times, the lower reactivity will prevent the reaction with all surface sites on the substrate. This difference was observed through the measurement of the tilt angle (Figure 53, right) of the self-assembled layer. The tilt angle is an indicator for the density of the molecules on the surface (e.g. if there are rarely any molecules on the surface the spacer and tail of the molecule lie on the surface resulting in a high tilt angle). A tilt angle of $0 \pm 5°$ for octadecyltrichlorosilane and $20 \pm 5°$ for the less-closely packed octadecyltrimethoxysilane was observed, indicating the difference in reaction mechanisms.

For the self-assembling deposition of molecular layers two general methods are feasible, namely either solution or gas phase deposition.[123]

In the solution deposition process, the cleaned substrate is immersed into a solution of surface reactive molecules.[123] The molecules will self-assemble on the surface over a certain period of time and form a molecular layer. Subsequently, the substrate is withdrawn from the solution and thoroughly rinsed to remove excess molecules from the surface. The

convenience and low cost of this deposition method contribute to the popularity of molecular layers obtained through self-assembly. However, to obtain reproducible results special attention has to be paid to the cleanliness and purity of the used solution. Especially for silane-based molecular layers the water content plays a crucial role and has to be tightly controlled.

For the gas phase deposition method the substrate is placed in a high vacuum chamber. The surface reactive molecules are introduced at a controllable rate into the chamber, where they evaporate and subsequently attach to the surface. The chamber may be additionally heated to enhance the silane evaporation. In general, the gas phase deposition needs a longer period of time and sophisticated equipment and is, therefore, more cost-intensive, but yields more homogenous and reproducible results.[123,131] Pavlovic et al.[134] developed an alternative gas phase deposition method in which no high vacuum chamber is needed. In this approach an argon flow at room temperature is used to evaporate and transport the silane molecules for the silanization.

2.2.2. Polymer brushes

Polymer brushes are polymer chains that are attached to a surface or an interface with at least one anchor group. They feature a graft density, which is high enough that the polymer chains are forced to stretch away from the surface/interface.[135]

The interest in polymer brushes started in the 1950s, when it was discovered that polymer brushes can be used for steric stabilization of Carbon Black dispersions (see chapter 1.2.1.5).[136,137] Further research on polymer brushes increased their fields of applications, like their utilization as adhesives for rubber-rubber boundaries[138,139], as protein-resistant biosurfaces[140], as lubricants[141], and as polymer surfactant[142].

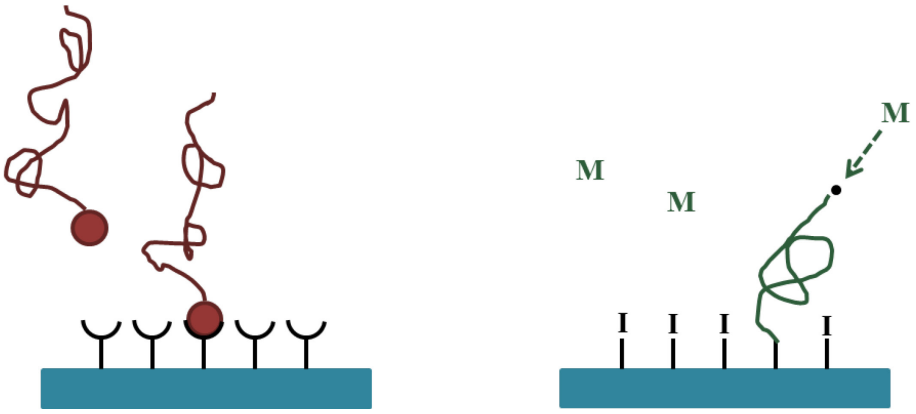

Figure 54**: Left**: grafting–to mechanism (polymer chains attach to the surface); **right**: grafting-from mechanism (surface initiated polymerization); M = monomer; I = initiator

Polymer brushes can be chemisorbed (irreversible process) or physisorbed (reversible process) to the surface.[143] They can further be categorized, depending on their synthesis mechanism, either into “grafting-to” or “grafting-from” (Figure 54).[102]

In the grafting-to process already formed end-functionalized polymers attach to the surface. This approach leads to low grafting densities and to low brush heights because reactive sites on the surface are being shielded by already attached polymer chains. In the grafting-from process monomers are directly polymerized through surface-initiated polymerization to form polymer brushes. This leads to higher grafting densities on the surface and thicker films.[102,143]

Although the immobilization of initiators on the surface is feasible through plasma or glow-discharge treatment, the use of self-assembled molecular layers for this purpose is beneficiary. Higher densities of initiators and self-defined initiation mechanics can be achieved and a well-controlled polymerization allows the adjustment of the polymer chain lengths.[143]

Great effort has been taken for the realization of grafting-from polymer brushes through free radical polymerization.[144–146] The immobilization of the radical initiators usually involves several synthesis steps, which may lead to lower grafting densities. However, the group of Rühe has worked on a strategy to overcome this problem and achieved the immobilization of the initiator in one single step.[147–151] In recent years, a further approach has been reported[152–154], wherein thiol groups on the surface are excited by UV-light and yield thiyl radicals[68]. In the presence of suitable monomers, like methacrylates, alkenes or allyl ethers, a surface initiated polymerization reaction sets in without the need for an additional initiator.

But polymer brush growth is not limited to free radical polymerization. Polymer brush growth through controlled radical[155,156], cationic[157], anionic[158] and ring-opening methathesis polymerization[159] has been reported among others[143].

2.2.3. Patterning strategies

Due to its importance extensive research has been conducted on the patterning of proteins and polymer brushes in the micro- and nanometer scale. Several techniques are feasible. As this work centers on photochemistry only photochemical patterning strategies will be described in further detail below. Other non-photochemical patterning strategies include scanning probe lithographic methods[102], like dip-pen nanolithography[160,161] and nanoshaving[99,100,162–165], although their applicability is restricted due to their limited throughput. A simple and efficient method, which has found its industrial application, is called micro contact printing (**μCP**).[102,103,128,166,167] μCP uses a relief pattern on a stamp to apply molecules to a surface upon contact. Further lithographic approaches, not based on the utilization of light, include, electron beam lithography, nanoimprint lithography, capillary force lithography, colloidal lithography and Langmuir-Blodgett lithography.[102]

Mask-based photolithography: One versatile possibility for a patterned illumination is by the irradiation through a mask. The theoretical resolution limit is dependent on the used wavelength,[168] as illustrated in equation (4) for hard contact printing.

$$b = \frac{3}{2}\sqrt{\frac{\lambda \cdot z}{2}} \qquad \textbf{(4)}$$

b is the minimal attained linewidth; z the thickness of the photoresist; λ the wavelength

Three different strategies have been reported for the use in polymer brush patterning (Figure 55).[104]

In the first technique, illustrated in Figure 55, left, polymer brushes are grown on the whole surface, followed by the patterning through UV ablation of already grown polymer brushes. The second method is the passivation of the already immobilized initiator on the surface by the means of UV illumination through a mask (Figure 55, middle). In a subsequent step the remaining intact initiators can be used for the thermal initiation of a radical polymerization. Figure 55, right, shows the third strategy using UV illumination through a mask to activate immobilized initiators on the surface. Thus, polymer brushes are grown in the regions not blocked by the mask.[104]

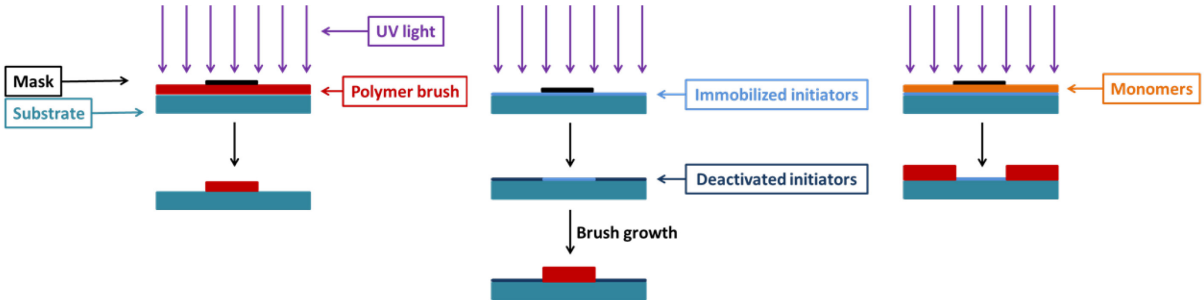

Figure 55**:** Photolithographic polymer brush structuring; **left**: structuring through UV ablation; **middle**: passivation of initiators through UV illumination; **right**: photoinitiated polymerization

The mask-based photolithographic process is a commonly used technique for protein patterning as well. Several different approaches have already been reported:

One possibility is the photodegradation of protein resistant self-assembled molecular layers. Tizazu et al.[169] and Reynolds et al.[170] used this technique and exploited aldehyde groups, which are being formed during the photodegradation process, for the site-specific binding of proteins in a subsequent step. Ahmad et al.[171] used photolithography to deactivate halogen photoinitiators in the illuminated areas. Atom transfer radical polymerization (**ATRP**) was used to grow protein resistant polymer brushes in the regions where the light was blocked by the mask. Carboxylic acid groups in the illuminated areas were used for the site-specific binding of proteins. In further works[172,173] protein patterning on gold is described. Through UV-illumination the thiol head groups of protein resistant self-assembled monolayers (**SAM**s) are oxidized to sulfonate groups, which are only weakly bound compared to the thiol groups. Protein patterns can be obtained through the removal of the oxidized molecules, which allows non-specific adsorption in these regions. Furthermore, a site-specific binding is enabled through an additional step. Carboxyl-terminated SAMs are deposited on the previously illuminated areas, which enables the immobilization of proteins.

In one particularly interesting case, which is in use in today's DNA-chip fabrication, photolithography is used to synthesize DNA-sequences in a multistep process using protective group chemistry directly on the substrate.[174] Using this technique feature sizes of 5 µm and arrays with millions of probes can be achieved, allowing the analysis of the whole genome on one single chip.[8]

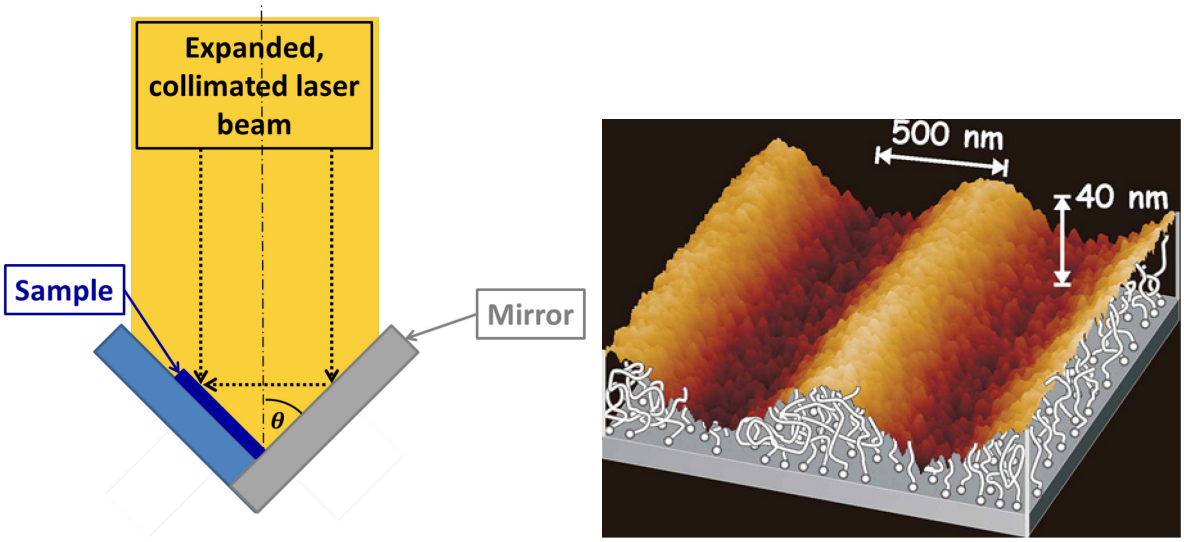

Figure 56**: Left**: IL Lloyd setup with the opening angle θ; **right**: AFM pattern of the sinusoidal polymer brush pattern obtained through IL by Schuh et al.[175] with an artist's view on the polymer brushes

Interference lithography (IL): A convenient way to obtain structures with features at the nanoscale is interference lithography. A big advantage of this system is that it's a mask free technique with the possibility to pattern nanoscale features over relatively large ares (square centimeter). One possible setup is called Lloyd setup[176] (Figure 56, left), where a laser beam partially illuminates the sample surface directly, while the other part is reflected by a mirror, which is placed at a 90° angle to the sample surface, onto the sample. Through the superposition of the light beams a sinusoidal intensity distribution is obtained. Schuh et al.[175] used this for the patterning of polymer brushes. Higher brushes were obtained in the regions with a higher light intensity, as more initiator groups were activated in these regions (Figure 56, right). Tizazu et al.[169] and Adams et al.[111] describe the use for IL for the photo-oxidation of SAMs and the exploitation of ensuing aldehyde groups for protein patterning. For Ahmad et al.[171] it was possible to use the deactivation of halogen photoinitiators by IL illumination. The same subsequent steps (ATRP and derivatization of carboxylic acids groups) as for the photolithographic micropatterns lead to protein nanopatterns.

Scanning near-field photolithography (SNP): In SNP a laser is coupled to a scanning near-field optical microscope (**SNOM**). In a typical setup a UV fiber coupled to a laser is scanned closely (5-10 nm) over the surface, which enables the writing of structures with resolutions below the far-field resolution limit.[177,178] Similar strategies to the ones used with photolithography have been applied to generate nanoscale protein patterns. The photodegradation of protein resistant self-assembled molecular layers on glass through SNP and the ensuing emergence of aldehyde groups was used to bind proteins and DNA molecules in a site-specific fashion to the surface yielding nanostructures.[170,179] Thiol head groups of a protein resistant SAM on gold were oxidized to sulfonate groups, which are only weakly bound. Protein nanopatterns through non-specific adsorption and site-specific binding were realized with the same strategies as for the photolithography patterns.[172,173,179] Several further works have been published describing the use of SNP for the nanopatterning of proteins on surfaces.[180–184]

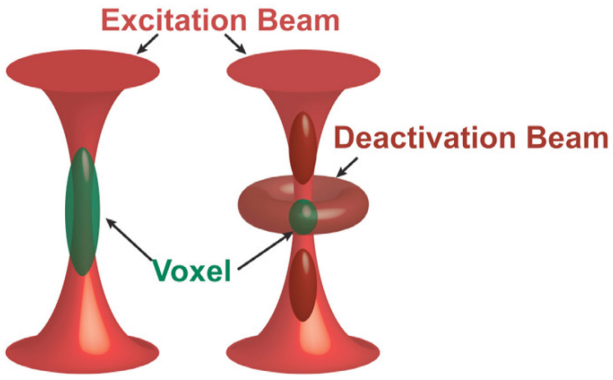

Figure 57**:** Stimulated emission depletion (**STED**) lithography using two-photon adsorption;[185] **left**: exited region (voxel, green) without the second depleting laser beam; **right**: reduced volume of the voxel due to the deactivating second beam

Stimulated emission depletion (STED) lithography: In optical STED lithography two lasers are used. One laser excites photoinitiators for radical polymerization, while the second donut-shaped laser beam is used to inhibit the starter molecules in these donut-shaped regions. The combination of the two lasers confines the exited volume and significantly reduces the spatial resolution (Figure 57). Feature sizes down to 55 nm have been reported.[186] Using STED-two-photon polymerization lithography the group of Klar was able to fabricate acrylate structures, which could be functionalized for the deposition of single proteins.[187,188]

2.2.4. Thiol toolbox

For the exploration of thiol chemistry in this work thiol groups were immobilized on silicon substrates. The spatially defined derivatization of thiol groups on surfaces is an important requisite for many applications. In Figure 58 an overview of known derivatization paths is illustrated. The different thiol reaction pathways are described in further detail below.

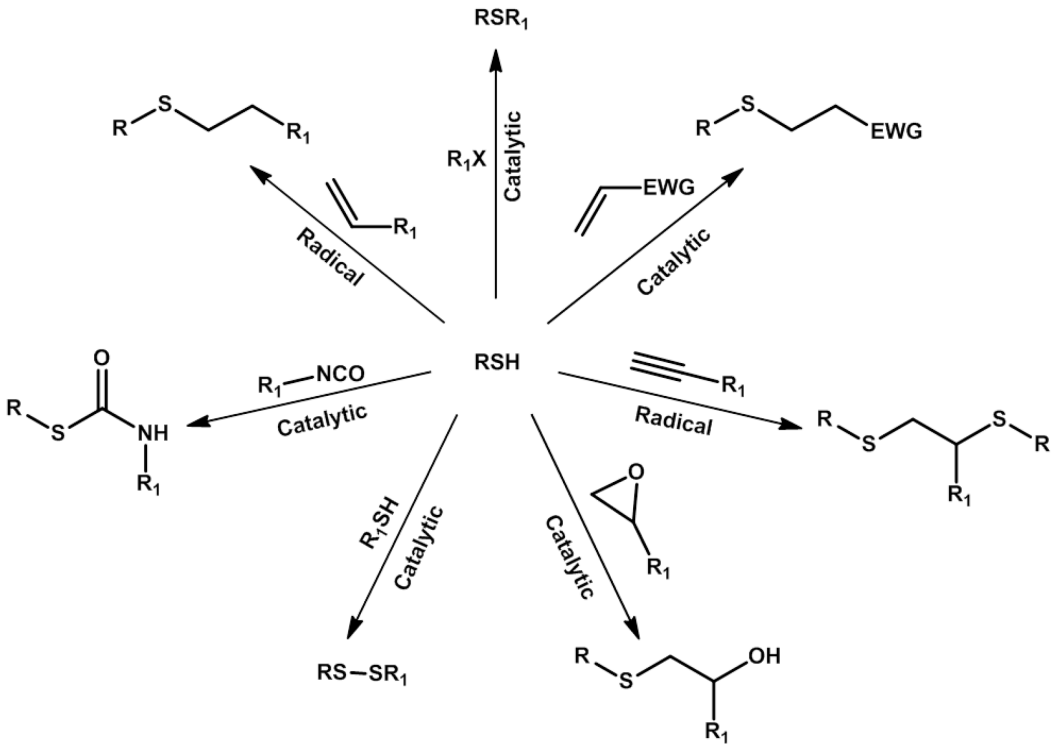

Figure 58**:** Thiol toolbox; X = Br,I; EWG = electron withdrawing group

2.2.4.1. Thiol-ene reaction

As already described in chapter 1.2.3 the thiol-ene reaction can be divided into two major pathways: (1) the free radical addition of thiols to electron rich and electron poor carbon-carbon double bonds and (2) the catalyzed reaction of thiols with electron-deficient carbon-carbon double bonds, which is called thiol-Michael addition. The thiol-Michael reaction is described in further detail below. For more information on the radical thiol-ene reaction see chapter 1.2.3.1.

2.2.4.2. Thiol-Michael reaction

Arthur Michael discovered the Michael addition reaction in 1886.[189] The Michael addition is the addition of a nucleophile, the so-called “Michael donor” to an activated electrophilic carbon-carbon multi bond, the “Michael acceptor”. Although the Michael addition is generally seen as the addition of enolate nucleophiles to activated olefins, other nucleophilic Michael donors, like amines, thiols and phosphines, can be used as well for the reaction. These are called “Michael-type additions”. As for possible Michael acceptors a wide range of carbon-carbon multibond groups are feasible. The prerequisite for its applicability is an electron withdrawing and resonance stabilizing activating group. Possible Michael acceptors include acrylate esters, acrylonitrile, acrylamide, maleimides, alkyl methacrylates and acetylene esters, among others.[190]

As this work centers on thiol chemistry only the Michael-type addition with thiols the “thiol-Michael reaction” will be elaborated on in further detail. The two predominant reaction pathways for the thiol-Michael addition can be categorized depending on the catalyst used, either in base-catalyzed or nucleophile-catalyzed thiol-Michael reaction. In Table 16 typical catalysts for the thiol-Michael addition are subsumed into their respective reaction pathways.

Table 16: Typical catalysts for the thiol-Michael addition[191]

Non-nucleophilic bases	N-centered nucleophiles	P-centered nucleophiles
Triethylamine	n-Alkylamine	Trialkylphosphine
1,8-Diazabicyclo[5.4.0]undec-7-ene **(DBU)**	4-Dimethylaminopyridine **(DMAP)**	Dimethylphenylphosphine **(DMPhPh)**
1,5-Diazabicyclo[4.3.0]non-5-ene **(DBN)**	Imidazole	Methyldiphenylphosphine **(MDPhPh)**

The base-catalyzed reaction involves the use of catalytic amounts of a Brønsted base, like triethylamine (**TEA**), which abstracts a proton from a thiol to generate a thiolate anion and a conjugate acid. The thiolate anion is a strong nucleophile that easily adds to an electron-deficient carbon-carbon double bond, yielding a carbon-centered anion, which abstracts the hydrogen from the conjugate acid forming the thioether product (Figure 59).[191,192]

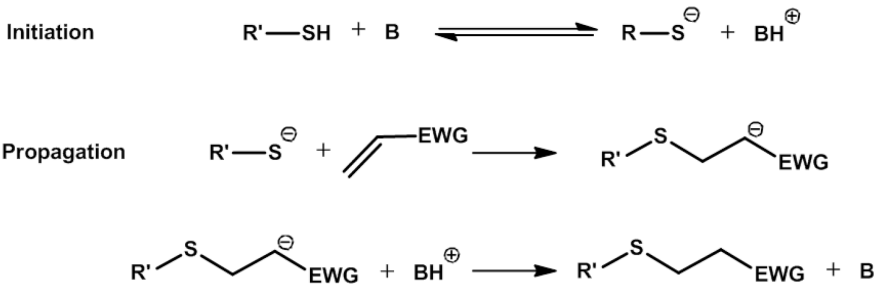

Figure 59: Base-catalyzed thiol-Michael reaction[191,192]; EWG stands for an electron withdrawing group and B for the base catalyst

As for the nucleophile-catalyzed reaction, recent studies[193,194] have shown that the nucleophile, although applied in catalytic amounts, is not a genuine catalyst. Instead, it adds to the electron-deficient carbon-carbon double bond forming a strong base, which starts an anionic chain-like mechanism (Figure 60).

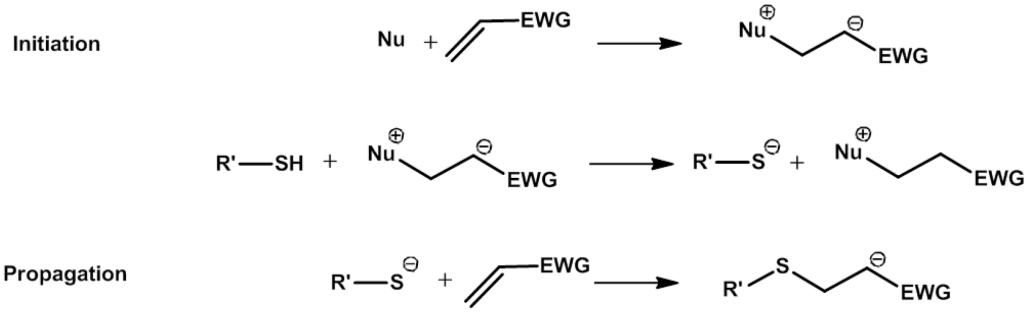

Figure 60: Nucleophile-catalyzed thiol-Michael reaction[191]; EWG stands for an electron withdrawing group and Nu for the nucleophile catalyst

2.2.4.3. Other thiol derivatization strategies

The thiol-yne reaction is the reaction of an yne (short for alkyne) with one or two thiols. In the first step a single thiol is added to yield the vinyl sulfide. Subsequently, a second thiol can be added to give the 1,2-disubstituted product.[195] The works of Fairbanks et al.[196,197] revealed, that the occurrence of the second step varies depending on the used alkyne. For 1-octyne, for example, the reactivity of the addition of the thiol to the vinyl sulfide significantly exceeds the reactivity of the addition of the first thiol to the alkyne. Thus, with at least two thiol groups prevalent per alkyne group, no vinyl sulfide product can be detected. In contrast, when ethyl propiolate is used as yne, for example, no addition of a second thiol can be observed.

Disulfide bridge formations are naturally occurring and essential in the folding and stabilization of proteins. Due to their importance a lot of research has been reported on how to form and break disulfide bond *in vitro* and *in vivo*.[198–204] Possible synthetic methods for the

disulfide formation are manifold. For the derivatization of thiols using the disulfide bridge formation the majority of the applied methods can be categorized into two major pathways, either in thiolysis-based methods or oxidative coupling methods. In the thiolysis-based methods the thiol or thiolate anion attacks a suitable leaving group in a nucleophilic substitution reaction. For the oxidative coupling of thiols different oxidizing agents, like metals or halogens, can be used. Other reaction pathways, like the disulfide formation via thiyl radicals or starting from other reactive groups, like alcohols or sulfonyl chloride, are feasible as well. More detailed information on disulfide bridge formations can be found in the review of Mandal et al.[204].

The catalyzed thiol-epoxy reactions can be conducted in water and solvent-free in high yields. Although the reaction mechanics of the based catalyzed reaction have not yet been completely resolved, it is assumed that a thiolate anion and a quaternary ammonium are formed by the reaction of the base catalyst and the thiol. The thiolate anion induces a nucleophilic ring-opening reaction of the epoxy group. Subsequently, the formed alcolate anion is protonated by the originally formed quaternary ammonium.[97] Several strong bases can be used as catalyst.[205–208] Thiol-epoxy reactions catalyzed by Lewis acids are also feasible. Lewis acids weaken the carbon oxygen bond and stabilize the alcolate anion upon the nucleophilic attack by the thiol.[97,208] One particular feature of interest of thiol-epoxy reactions is that they render polymer chains with free hydroxyl groups, which can easily be used for further derivatization.[205,206]

The base catalyzed addition of thiols to isocyanates yields thiourethanes without any byproducts. The polymerization of multifunctional monomers proceeds in a sequential anionic chain growth-step growth process.[97] Thiol-isocyanate polymers exhibit a high refractive index, which makes them suitable materials for optical materials.[209,210]

Moreover, thiols may participate in an efficient substitution reaction with halogens. Using a mild organic base the halogenated salt byproducts precipitate and can be easily removed.[211]

The electrochemical or photochemical oxidation of thiols is feasible as well and described in more detail in chapter 2.4.2.

2.3. Experimental section

2.3.1. Materials

All chemicals were commercially available and obtained from Sigma-Aldrich or TCI Europe unless otherwise mentioned. For the polymer brush growth experiments oligoethylene glycol methyl ether methacrylate (Mn~500 g/mol) and oligoethylene glycol methyl ether acrylate (Mn~480 g/mol) were used. Biotin-labeled fluorescence microspheres (0.2 µm; 505/515; 1% solids) were obtained from Thermo Fisher Scientific Inc., Austria. His-tagged green fluorescent protein (**GFP**) was synthesized using a protocol modified from the one previously reported[170] and provided by Michael Cartron and Neil Hunter of the Department of Molecular Biology and Biotechnology in Sheffield. Anti-Sheep IgG (whole molecule)–FITC antibody produced in donkey and Streptavidin−Cy3™ from Streptomyces avidinii were obtained from Sigma-Aldrich.

Single-side-polished p-type-doped (Boron) silicon wafers with a native silicon oxide layer of 6.9 nm (obtained from Infineon Technologies Austria AG, Villach, Austria) were used. Before utilization they were cleaned with piranha solution, a mixture of 30% H_2O_2 and sulfuric acid (98%) in the ratio 3:7 for 30 min. (Caution: Piranha solution is a strong oxidizing agent, that is known to detonate spontaneously upon contact with organic material. Handle with extreme care.) Subsequently they were rinsed 7 times with deionized water. In a second cleaning step the wafers were put into a mixture of ammonia solution (30%), hydrogen peroxide and deionized water (1:1:5) and heated to 70°C for 30 min. Afterwards they were again rinsed 7 times with deionized water and dried and stored like this in an oven at 100°C.

2.3.2. Silicon wafer preparation

A 5 cm^2 piece of cleaned silicon oxide substrate was immersed in a solution of mercaptopropyltrimethoxysilane (**MPTMS**, 100 µL) in 20 mL toluene (anhydrous, <0.001% water) for 30 min in nitrogen atmosphere in a glove box. Afterwards the sample was rinsed with toluene and subsequently with ethanol/toluene (1:1 mixture) and then ethanol. After rinsing, the sample was dried in an oven for 15 min at 100°C.

2.3.1. Ellipsometry

The film thicknesses were measured by *ex situ* variable angle spectroscopy ellipsometry (VASE, JA Woollam M-200, Lincoln, USA). The measurements were conducted at three different angles (65°, 70° and 75°) in the wavelength range of 200 – 1000 nm. The applied optical model consisted of three components, the silicon substrate, the native SiO_2 layer and the film layer. The film layer was modeled by Cauchy function adding the Urbach tail to model the absorption. The data was analyzed using the software COMPLETEASE.

2.3.2. Photo-oxidation

The samples were photo-oxidized by means of UV irradiation under ambient conditions using either a mask aligner (MJB4 SUSS, Germany) equipped with a 500 W HgXe lamp (power density of 21.3 mW/cm^2) or a coherent Innova 300C FreD frequency-doubled argon ion laser (244 nm, Coherent UK, Ely, UK) for static SIMS and IL experiments. (Caution: UV irradiation causes severe eye and skin burns. Precautions (UV protective goggles, gloves) must be taken!)

2.3.3. Interferometric lithography (IL)

Films formed by the adsorption of MPTMS were photo-patterned by IL using a Lloyd's mirror two-beam interferometer. A Coherent Innova 300C FreD frequency-doubled argon ion laser (Coherent UK, Ely, UK), emitting at 244 nm was used as a light source. The laser beam was focused using a lens through a spatial filter with aperture 5 μm to obtain a coherent beam. The edge of the coherent beam was cut by using a mask with an appropriate aperture. Half of the clean coherent beam was pointed directly onto the sample surface, and the other half of the beam was pointed onto the mirror, from which it was reflected onto the sample surface where it interfered with the other half of the beam to yield a sinusoidal pattern of intensity (Figure 56, left). Self-assembled molecular layers of MPTMS on silicon were exposed to 15-20 J/cm^2 through a Lloyd's mirror interferometer, with angle 2θ between the two half of the beam set to approximately 10°.

2.3.4. Sample derivatization

2.3.4.1. Thiol-Michael derivatization

For the thiol-Michael derivatization each 1 cm^2 piece of the silicon wafers covered with a MPTMS-layer was immersed into a solution of 100 µL heptadecafluorodecyl acrylate (**HDFDA**) and 1 µL 1,5-diazabicyclo[4.3.0]non-5-ene (**DBN**) in 1 mL dichloromethane for 3 h. Afterwards the samples were removed and thoroughly rinsed with dichloromethane. Additionally the samples were cleaned for 1 min in an US bath immersed in dichloromethane and ultimately rinsed once more with dichloromethane and dried with a stream of nitrogen.

2.3.4.2. Derivatization of sulfonic acid groups

The photo-oxidized samples were immersed in a mixture of pyridine and water (ratio 1:2) for 30 min to give the corresponding pyridinium sulfonate. Afterwards the samples were rinsed and then dried under vacuum. The activation of the sulfonate by triphenylphosphine ditriflate (**TPPDF**) and the subsequent reaction with the functional amine were performed under nitrogen atmosphere. Therefore, TPPDF was freshly prepared from triphenylphosphine oxide (0.019 mmol) and trifluoromethanesulfonic anhydride (0.009 mmol) in dichloromethane (6 mL). The samples were immersed in a freshly prepared TPPDF solution for 30 min. Subsequently, a solution of triethylamine (35 mmol) and the corresponding amine (35 mmol, heptadecafluoroundecylamine or poly(ethylene glycol) 2-aminoethyl ether biotin (M_n 2300)) in dichloromethane (6 mL) was added. For the derivatization with N_α,N_α-bis(carboxymethyl)-L-lysine hydrate DMSO was used as solvent, respectively. After 18 h the samples were removed from the solution and rinsed thoroughly with dichloromethane and ethanol abs.. Ultrasonic cleaning was performed in dichloromethane for 1 min and afterwards the samples were rinsed once more and dried with a stream of nitrogen.

2.3.4.3. Surface induced polymer brush growth

For the brush formation experiments, 4 µL of the monomer solution (oligoethylene glycol methacrylate (**OEGMA**) in 1,4-dioxane) were deposited onto a 1 cm^2 piece of a MPTMS modified silicon wafer and covered with a quartz chromium mask. Brush formation was accomplished after UV irradiation with a medium pressure Hg lamp (100 W, model 66990, Newport Corp., Irvine, California, USA) with a power density of 14.7 mW/cm^2 (measured with an EIT Power Puck II in the spectral range between 250-390 nm). Brush formation on the pre-oxidized samples was conducted with the same setup as described above using OEGMA solution and a quartz glass allowing flood illumination.

2.3.4.4. Protein immobilization

Non-specific adsorption: For the investigation of IL patterns using non-specific adsorption, the samples were first cleansed with deionized water (18.2 MΩ, Purelab ULTRA, Elgar Process water, Marlow, UK) and dried under a stream of nitrogen, and then immersed in 20 µg/mL solutions of the protein of choice in phosphate-buffered saline (0.01 M, pH 7.4) for 24 h at 2-4°C. Subsequently the samples were cleaned through rinsing with PBS and dried with nitrogen.

Site-specific immobilization: After the sulfonamide derivatization with poly(ethylene glycol) 2-aminoethyl ether biotin, the samples were immersed in a solution of fluorescent NeutrAvidin microspheres (400 µg/mL) in phosphate buffered saline (0.1 M PBS) for 3 h. Afterwards, the samples were rinsed with PBS and water and dried with a stream of nitrogen. For site-specific immobilisation of His-tagged green fluorescent protein (**GFP**), the samples, which were derivatized with N_{α},N_{α}-bis(carboxymethyl)-L-lysine hydrate, were immersed in a 100 mM aqueous solution of nickel (II) chloride for 30 min. The samples were washed with water, dried with nitrogen and immersed into a 20 µg/mL solution of His-tagged GFP in phosphate buffered saline (0.01 M PBS at pH 7.4) for 24 hours at 2-4˚C. The samples were then further rinsed with PBS and dried with a stream of nitrogen.

2.3.4.5. Contact angle measurements

The static contact angles were obtained by using the sessile drop method with a Drop Shape Analysis System DSA100 (Krüss GmbH, Hamburg, Germany). The data was analyzed using the software DSA1 1.92.0.1 (Krüss GmbH).

2.3.4.6. X-ray photoelectron spectroscopy (XPS)

XPS spectra were recorded using a Thermo Scientific instrument equipped with a monochromatic Al K_{α} X-ray source (1486.6 eV). High resolution scans of the C1s region were acquired at a pass energy of 20 eV and a step size (resolution) of 0.1 eV. Scans of the S2s region were performed at a pass energy of 100 eV and a step size of 0.1 eV. Wide scans were acquired with pass energy of 100 eV and a step size of 1.0 eV. All spectra have been normalized to the Au 4f7/2 peak. Charge compensation was performed with an argon flood gun. The average chemical composition was calculated from wide scan spectra in two different locations on each surface. The peaks were fitted using a Gaussian/Lorenzian mixed function employing Shirley background correction (Software Thermo Avantage v5.906). All analyses were performed at room temperature.

2.3.4.7. Secondary ion mass spectrometry (SIMS)

Static SIMS experiments were carried out using a time of flight (**TOF**)-SIMS V instrument (Ion-ToF GmbH, Münster, Germany) equipped with a Bismuth ion gun and a single-stage reflectron time-of-flight analyzer. During imaging charge neutralization was applied. A minimum of 3 images per sample was acquired and multiple samples were analyzed. High mass-resolution images were obtained by using high-current bunched mode, with $Bi3^{++}$ as the primary source and a target current of ca. 0.1 pA. To ensure the images were static SIMS, the primary ion dose was limited to $5*10^{12}$ ions/cm^2. All data was analyzed with SurfaceLab 6 software (Ion-ToF). Images of similar ions were grouped together (e.g. S^- and SH^-) and 4 pixels were binned together.

2.3.4.8. Atomic force microscopy (AFM)

AFM micrographs were recorded with a Nanosurf FlexAFM instrument. Silicon AFM probes with a resonance frequency of 190 kHz and a force constant of 48 N/m (Tap190AL-G, Budgetsensors) were used for tapping mode measurements, silicon AFM probes with a resonance frequency of 13 kHz and a force constant of 0.2 N/m (ContAL-G, Budgetsensors) for friction force measurements.

2.3.4.9. Gel permeation chromatography (GPC)

The average molecular weights (M_w and M_n) were determined by gel permeation chromatography with THF as a solvent, using the following arrangement: micro-volume double pistol pump, flow rate 1 mL/min, separation columns from Varian, particle size 5 µm, combined refractive index-viscosity detector. Polystyrene standards from Polymer Labs were used for calibration.

2.3.4.10. Fluorescence microscopy

For the samples with immobilized NeutrAvidin particles an Axiovert 35 AxioCam HRc (Carl Zeiss, Oberkochen, Germany) was used. For all other samples fluorescence images were acquired with a LSM 510 Meta laser scanning confocal microscope (Carl Zeiss, Welwyn Garden City, UK). Fluorescence images were analyzed using Zeiss LSM image browser software.

2.4. Results and Discussion

2.4.1. Silanization of silicon oxide surface

Mercaptopropyltrimethoxysilane (MPTMS) was immobilized on silicon oxide surfaces using the principle of self-assembly (Figure 61). This leads to thiol groups which are tethered to the surface and serve as the starting point for subsequent surface functionalization. By applying a strict methodology by working in inert atmosphere in a glove box and using an anhydrous solvent (toluene with <0.001% water content) a very low surface roughness of the obtained molecular layer was achieved. AFM measurements on at least 3 different sites per sample over a 1 μm^2 area revealed a calculated average R_{RMS} value of 0.12 nm and a R_a value of 0.10 nm. These are very low values for self-assembled molecular layers obtained through the solution deposition process coming close to values reserved for the gas phase deposition (R_{RMS} of 0.1 nm)[212]. Ellipsometry measurements revealed a thickness of 0.87 ± 0.03 nm. This is close to the reported theoretical value for a pure MPTMS monolayer of 0.77 nm,[213] and indicates that no multilayers were being formed.

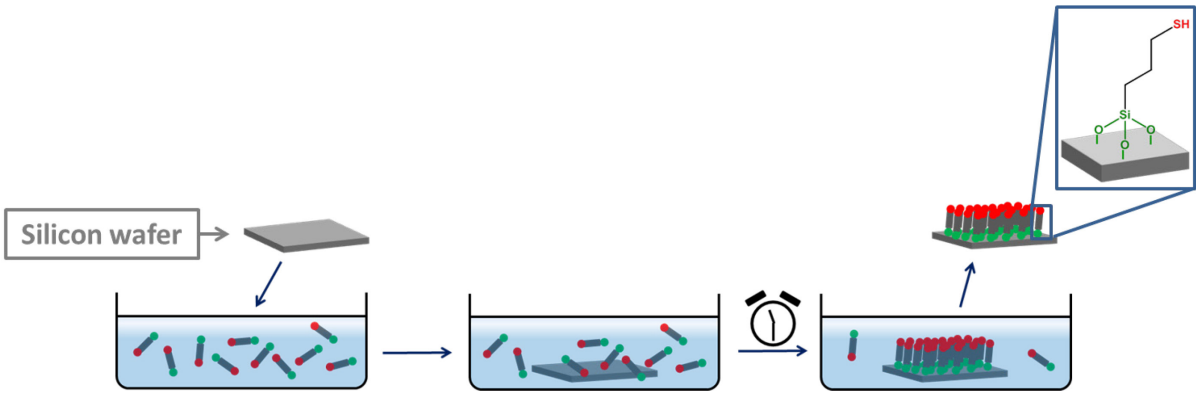

Figure 61: A simplified depiction of the solution phase deposition of MPTMS molecules on an silicon oxide surface through self-assembly

2.4.2. Photochemical oxidation of surface immobilized thiol groups

The oxidation of thiol groups to disulfide bridges is a naturally occurring process.[204] Further oxidation has been reported by Pavlovic[101,113,131]. She describes the patterned formation of thiolsulfinates and thiolsulfonates through an electrochemical oxidation process, where a voltage is applied between the AFM tip and thiol functionalities on the surface. The UV induced oxidation of surface bound thiol groups to sulfonate groups was already reported by Bhatia et al.[115] and by the group of Hlady[116,214]. Based on their findings, a detailed investigation on the photo-oxidation reaction of a MPTMS layer (Figure 62), i.e. the reaction kinetics of sulfonic acid formation and its influence on the surface polarity, was conducted by XPS and contact angle measurements.

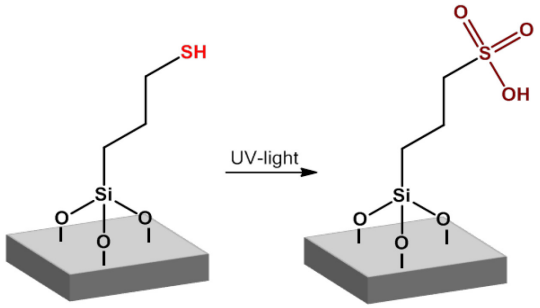

Figure 62: The photo-oxidation of thiol groups to sulfonic acid groups

In Figure 63, left, the S2s region of the XPS-analysis for the pristine MPTMS layer, the chemically (H_2O_2/acetic acid) oxidized MPTMS layer and MPTMS layer after UV illumination (E=44.4 J/cm^2) under ambient conditions is illustrated. The signal at 228 eV of the pristine molecular layer is typical for a mercapto group. The treatment with H_2O_2/acetic acid oxidizes the immobilized thiol groups to sulfonic acid groups, which has already been proven by Balachander et al.[114]. The oxidation using UV irradiation leads to the formation of a new peak at 233 eV, which is the same as for the oxidation using H_2O_2/acetic acid. Consequently, the new signal can be attributed to sulfonic acid groups. Figure 63, right, shows the variations of the signal intensity in the S2s region at both 228 eV and 233 eV as a function of UV exposure time. It was found that the SH species decreased in intensity following exposure to UV-light, while an increase in the sulfonic acid signal with a similar rate was observed. Both signals reached a limiting value after an illumination time of 20 min (44.4 J/cm^2).

Control experiments revealed that no photo-oxidation is occurring when light with wavelengths below 300 nm is blocked by a filter. No change in the S2s signal compared to the non-illuminated samples could be detected.

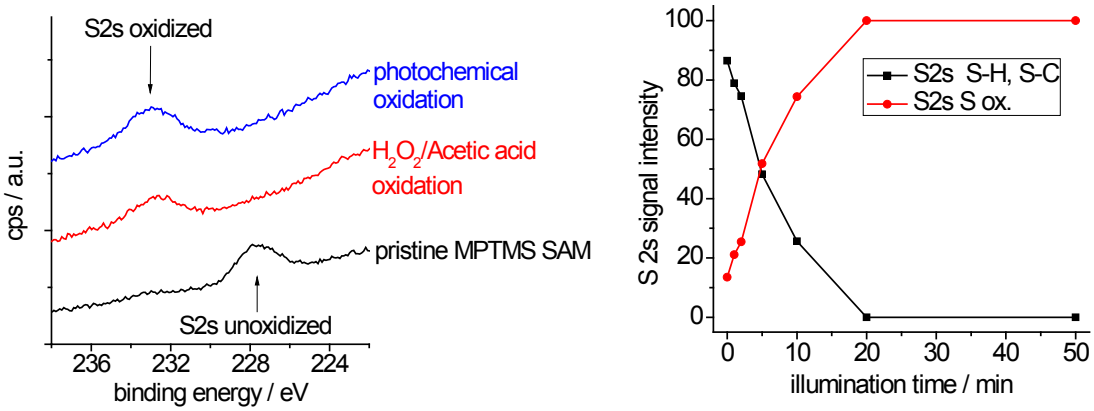

Figure 63: **Left**: XPS spectra of the sulfur 2s signal before (bottom, black line), after chemical oxidation using H_2O_2 and acetic acid (middle, red line) and after UV-illumination (top, blue line); **right**: variations of the signal intensity in the S2s region at 228 eV (S-H, S-C) and 233 eV (SO_3H) as a function of UV exposure time.

The change in surface chemistry was also followed by contact angle measurements. The pristine film exhibits a water contact angle of 38°, which is in accordance with literature values.[215] During UV exposure a decrease in the contact angle could be observed as shown in Figure 64. A value of 18° was reached after an exposure of 20 min, consistent with the formation of polar sulfonic acid groups, which is in accordance with values previously reported for self-assembled molecular layers with terminal sulfonic acid groups[114].

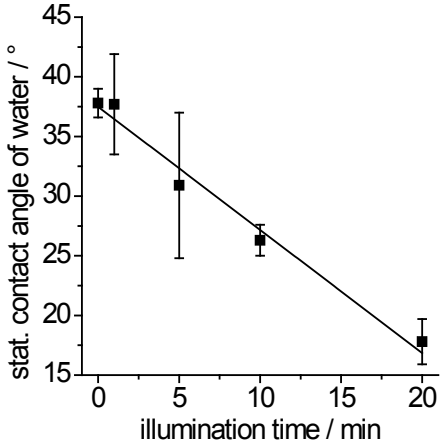

Figure 64: Static contact angle of water over the illumination time

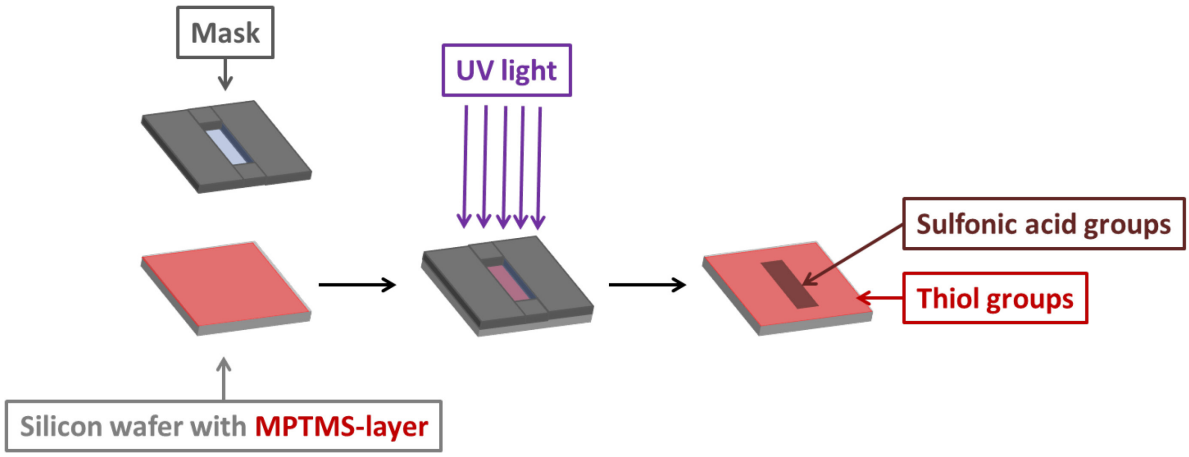

Figure 65: Patterned photo-oxidation using photolithography; the UV illumination yields sulfonic acid groups in the regions not shielded by the mask

In a further step micropatterns were realized using contact photolithography with appropriate chromium-quartz glass masks (Figure 65). To reveal a material contrast between illuminated and non-illuminated regions on the patterned samples friction force microscopy (**FFM**) was performed. In this mode a soft cantilever is scanned perpendicular to its long axis. Lateral forces resulting from the interaction of the tip with the substrate lead to a twist of the cantilever depending on the friction of the surface. Using this method changes in the chemical composition can be detected even if no height differences are present. A representative FFM image of a patterned surface is shown in Figure 66. The exposed regions, in which the mercapto groups have undergone the photo-induced oxidation reaction, yield bright contrast (high friction). Contrarily, the masked areas exhibit darker contrast (low friction) representing the unchanged thiol groups. The results demonstrate that a patterned oxidation of immobilized thiol groups is readily accessible.

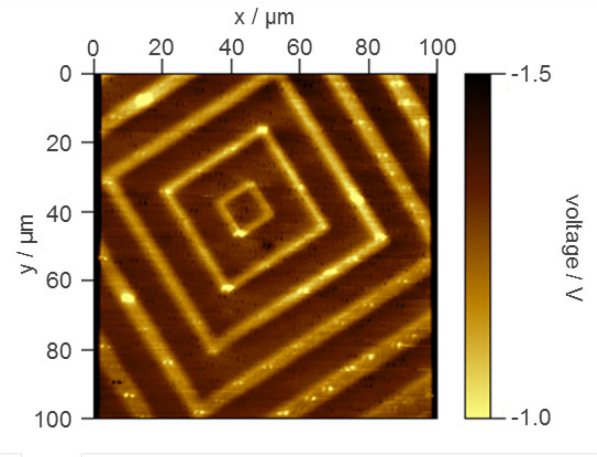

Figure 66: Friction force images after patterned UV-illumination. Bright contrast indicates high friction force (the SO_3H-terminated regions), while dark contrast indicates low friction (SH-terminated regions)

The oxidation by means of illumination with a 244 nm laser was followed by contact angle and SIMS measurements. A decrease of the contact angle to 18° was observed after 2 min (12 J/cm^2) of illumination. Micropatterned functionalized surfaces were prepared by contact lithography with appropriate chromium-quartz glass masks. Such samples were analyzed using SIMS imaging to confirm that photo-oxidation was occurring. Figure 67 shows the representative negative polarity SIMS images of a single region. The image on the left shows the combined image of the ions corresponding to the non-oxidized thiol groups (i.e. the S^- and the HS^- ions) and the right image shows the combined images of the ions corresponding to the oxidized thiol (i.e. the SO^{2-} and SO^{3-} ions). The left image shows bright regions in the areas that were protected by the mask (i.e. unexposed regions), and dark regions in the regions that are exposed to UV. This corresponds to a higher density of non-oxidized thiol species in the unexposed regions. The right image shows the opposite contrast to the left image, where the bright regions are the areas of the sample that have been exposed to UV light and the dark regions are the areas that were covered by the mask. This corresponds to a higher density of SO_2^- and SO_3^- groups in the areas of the sample that were exposed to UV light. This is consistent with the contact angle, XPS and AFM results of the samples oxidized with the HgXe lamp. The significant increase in oxidation speed (2 min for 244 nm laser compared to 20 min for HgXe lamp) can be explained by the higher UVC dose achieved by the laser. The increase of photo-oxidation speed by means of the 244 nm laser is of particular interest for applications where a higher throughput is needed.

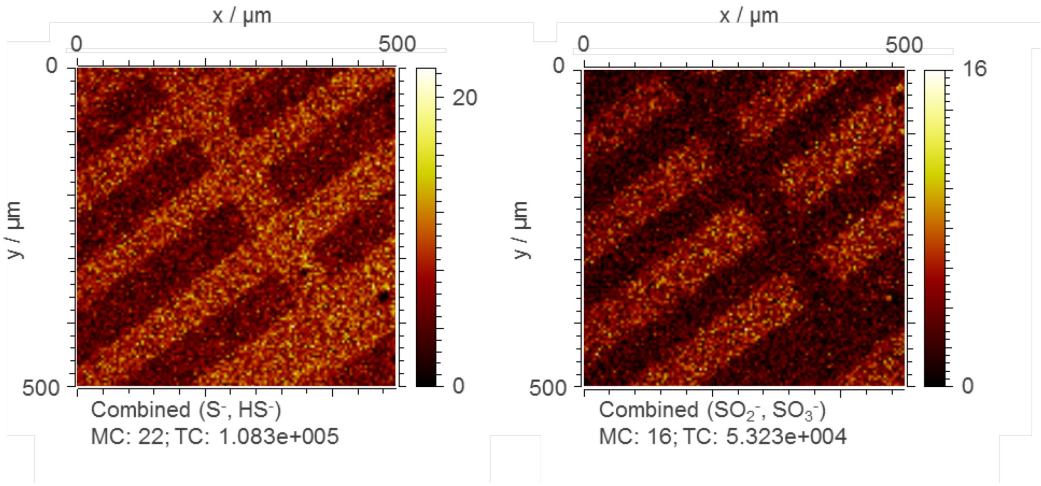

Figure 67: Negative polarity SIMS images of photo-oxidation patterns of a thiol surface; **left**: combined images of S^- and HS^- ions. **right**: combined images of SO_2^- and SO_3^- ion images

.

2.4.3. Thiol-Michael derivatization

The feasibility of the surface bound thiol groups for the thiol-Michael addition was investigated using contact angle and XPS measurements. Heptadecafluorodecyl acrylate (**HDFDA**) was used as the Michael acceptor as upon its immobilization the fluorine gives pronounced signals in the XPS spectra. Moreover, fluorinated chains are known for their high water contact angle yielding a significant contact angle change upon successful immobilization. Diazabicyclo[4.3.0]non-5-ene (**DBN**) was applied as base. The base-catalyzed thiol-Michael reaction (see chapter 2.2.4.2) abstracts a proton from the thiol to generate a thiolate anion. The thiolate anion adds to the electron-deficient carbon-carbon double bond. Using the base-catalyzed reaction ensures that only a single acrylate molecule binds to each thiol group on the surface, which is in contrast to the surface induced polymerization (*vide infra*, 2.4.4).

Table 17: Contact angle change with fluorinated thiol-Michael derivatization

Substrate	Static contact angle [H_2O] / °	Advancing angle [H_2O] / °	Receding angle [H_2O] / °
MPTMS-layer	38	49	27
After photo-oxidization	18	24	11
After HDFDA thiol-Michael derivatization	90	92	55

The change in contact angle is apparent in Table 17. Due to the attachment of the fluorinated acrylate to the surface the contact angle of water increases to 90°. However, for a fully fluorinated surface a higher contact angle would be expected.[216] The difference can be explained with an incomplete derivatization due to steric hindrance of the long chain fluorocarbon, which is visible in the high contact angle hysteresis (Table 17). The hysteresis is the difference between the advancing and receding angle. A high value is an indication for either a rough surface or a flat chemically heterogeneous surface.[217] Consequently, with a flat surface being prevalent in the silicon surface, the high hysteresis indicates the non-uniform chemical composition on the surface.

The immobilization of the fluorinated acrylate was observed by XPS investigations. The carbon C1s signal including the peak fits is illustrated in Figure 68. C-F_2, C-F_3 and C(O)-O peaks could be detected in significant amounts at higher binding energies compared to the standard carbon signal indicating that the thiol-Michael derivatization had taken place indeed. The wide scan spectrum (Figure 69 and Table 18) revealed a derivatization yield of 41% calculated from its F:S ratio (7:1). A higher C:F ratio was measured, as to be expected for this yield, which may be due to surface contaminations.

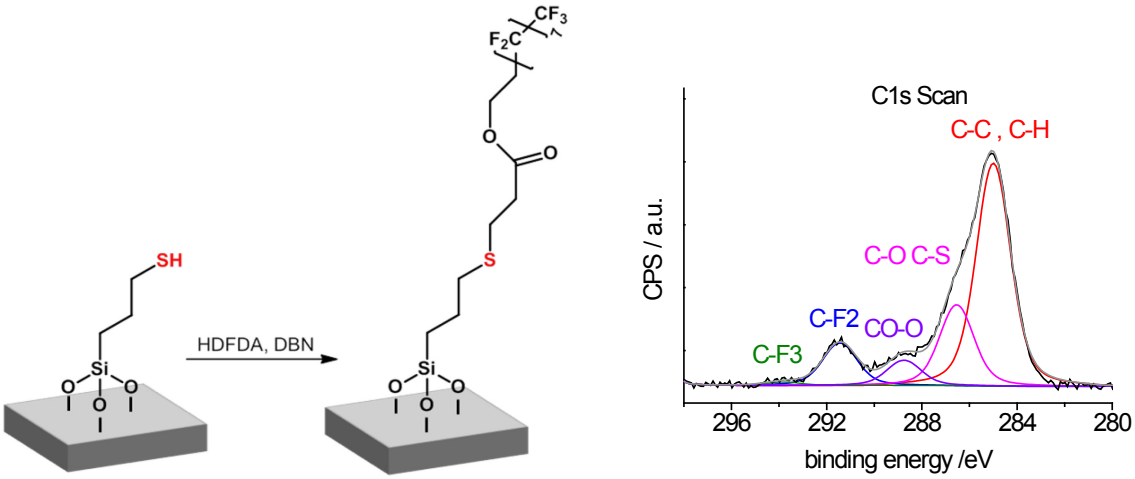

Figure 68: **Left**: reaction scheme of the thiol-Michael addition using heptadecafluorodecyl acrylate (**HDFDA**); **right**: XPS spectrum of the carbon C1s signal after thiol-Michael derivatization using HDFDA

Table 18: XPS wide scan spectrum of the surface after the thiol-Michael derivatization

Peaks	Elemental composition / atomic %
O1s	23.04
F1s	7.75
Si2p	49.32
S2s	1.10
C1s	17.45

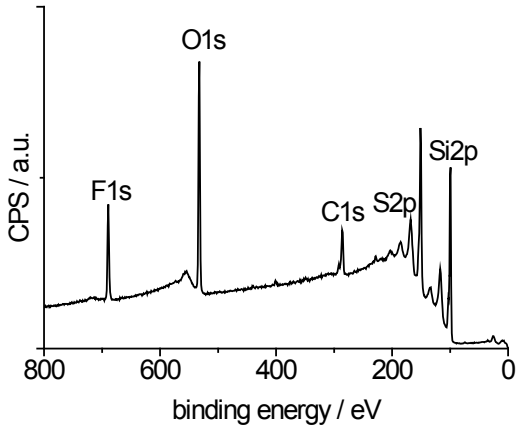

Figure 69: XPS wide scan spectrum after the thiol-Michael derivatization

As a proof of principle the possibility of the combination of the photo-oxidation and the thiol-Michael reaction was investigated. The reaction pathway is illustrated in Figure 68, left, and Figure 70. At first a silicon wafer was oxidized using a mask, yielding defined areas. The

areas, which are not shielded by the mask, are oxidized to sulfonic acid groups. These areas are consequently not susceptible for a thiol-Michael reaction, whereas areas, which were shielded by the mask, still feature pristine thiol groups on the surface. Treating this pre-structured substrate with a HDFDA solution with DBN, two areas with significantly different surface energy levels can be easily obtained. The oxidized hydrophilic areas promote wetting, whereas the fluorinated areas show a more hydrophobic behavior and repel water droplets. With this approach boundaries, e.g. for water droplets, can easily be drawn with the introduction of only minimal height differences (as only single molecules binds to each surface site) (Figure 70).

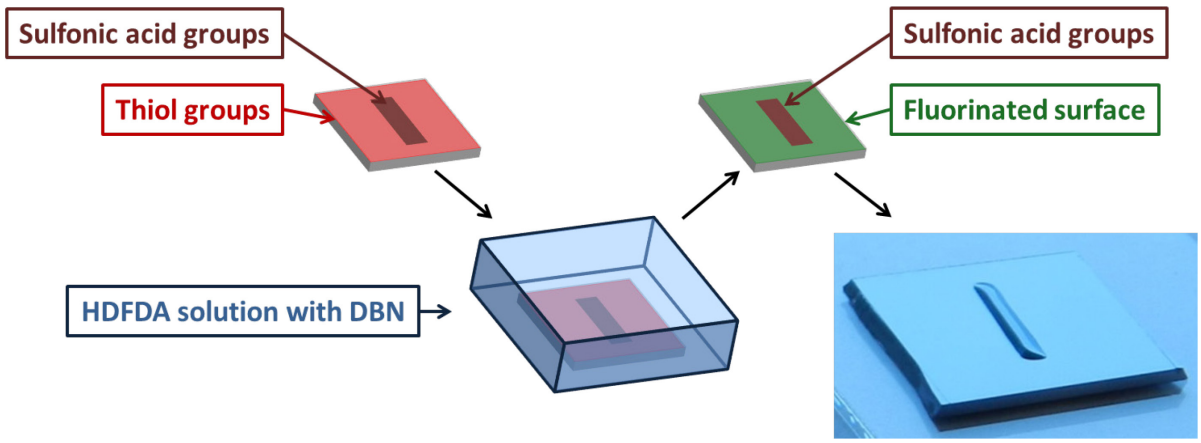

Figure 70: Thiol-Michael derivatization of a pre-patterned MPTMS-layer using HDFDA; the photo on the right shows a water droplet staying in the region containing sulfonic acid groups at the surface

2.4.4. Surface induced polymer brush formation

It has been widely reported that surface-bound thiyl radicals can initiate a polymerization reaction in presence of (meth)acrylate monomers resulting in the formation of polymer brushes (Figure 71).[152–154] In the reported procedures the substrates with thiol groups on the surface are placed in a degassed solution of methacrylate under inert conditions and subjected to UV flood illumination yielding polymer brush layers on the whole surface. However, to the author's knowledge no patterned brush formation has been previously reported using the principle of surface initiated polymerization starting from immobilized thiol groups.

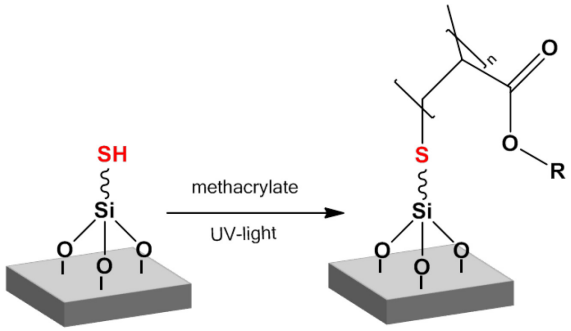

Figure 71: Surface induced polymer brush formation

For the investigation of patterned brush growth patterned photo-oxidized thiolated substrates were used. The surface covered with a film of monomer was exposed to UV illumination under ambient conditions (Figure 72). In this experiment, neat oligoethylene glycol methacrylate (**OEGMA**) was deposited on the pre-patterned MPTMS layers (Figure 66) and covered by quartz glass, before being exposed to UV irradiation (3.5 J/cm^2).

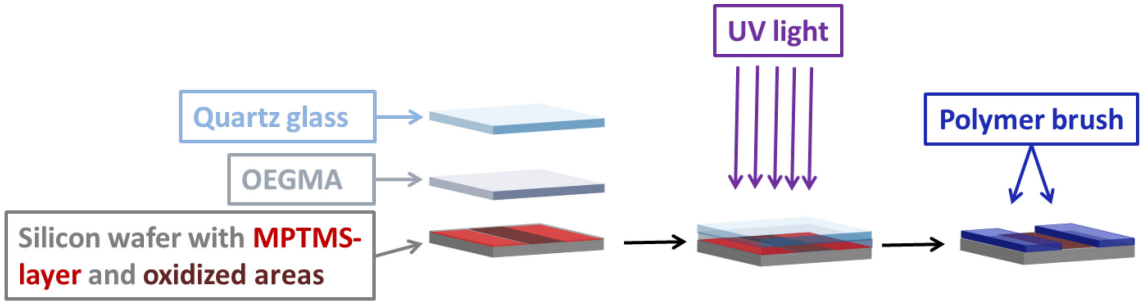

Figure 72: Setup for the patterned polymer brush growth using a pre-patterned thiolated surface

Surprisingly, this approach leads to polymer brush structures with well-defined dimensions, being uniform in all three spatial directions as shown in Figure 73. As displayed in the images

the intact thiol moieties initiated a polymerization reaction in the presence of OEGMA, while the photo-oxidized groups remained inactive.

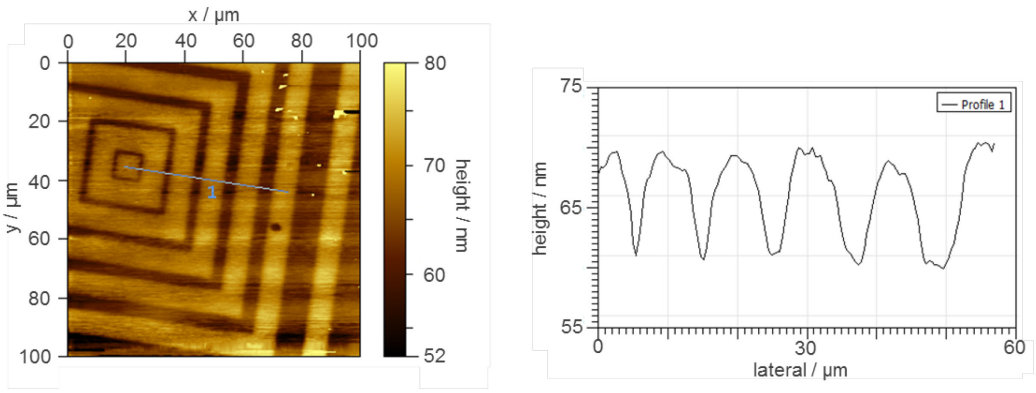

Figure 73: **Left**: Atomic force microscopy image of a pre-patterned MPTMS layer after surface induced polymerization; **right**: cross section of the obtained polymer brushes

In an alternative approach, polymer brush structures were obtained by patterned illumination using neat OEGMA on pristine MPTMS layers covered by a mask as illustrated in Figure 74. Figure 75 shows AFM images for micropatterned structures formed this way. Polymer structures grew selectively in the irradiated areas. Studies of individual samples at different UV irradiation times (0.5-6 minutes) revealed that a minimum dose of 2 J/cm^2 is required in order to obtain well-defined brushes. Using the threshold dose of 2 J/cm^2, it was observed that the OEGMA layer between the substrate and mask became highly viscous. This indicates significant polymer content in the monomer phase due to auto-initiated polymerization of methacrylate[218] under UV irradiation.

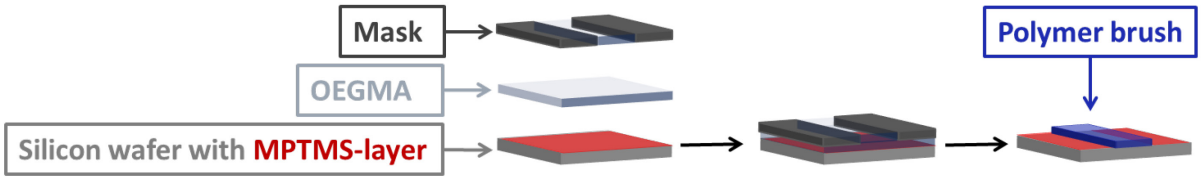

Figure 74: Setup for the patterned polymer brush growth using a mask

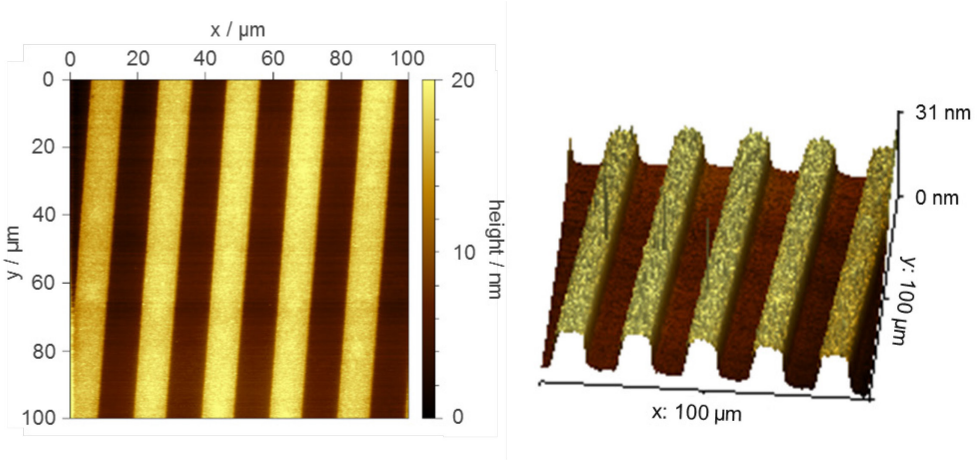

Figure 75: **Left**: atomic force microscopy image; **right**: three dimensionally reconstructed image of the obtained polymer brushes

Polymerization also occurred when a solution of OEGMA in 1,4-dioxane was used instead of neat OEGMA. Further experiments were conducted using a 100 µm line mask and varying OEGMA concentrations. The concentration of OEGMA in the used monomer solution significantly influenced the height of the obtained polymer brushes. By exposing the surface with an illumination dose of 5.3 J/cm^2 under ambient conditions the height of the polymer brush structures increased monotonically in the concentration range from 40 to 90 vol%, as shown in Figure 76. At 30 vol% and below no polymer brush structures could be observed. For neat OEGMA (i.e. 100 vol%) structures with heights of 51 ± 23 nm were measured. The structures obtained with OEGMA in solution featured a higher reproducibility (i.e. lower standard deviations) compared to samples prepared with neat OEGMA.

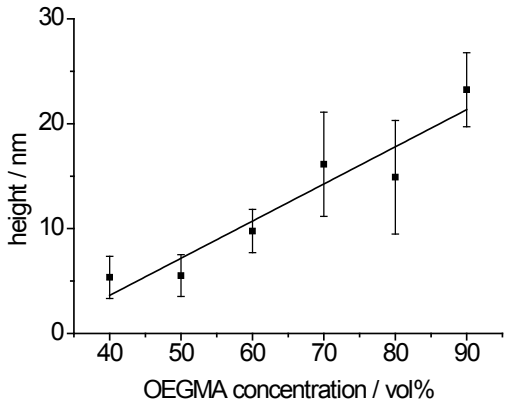

Figure 76: Height of the polymer brushes as a function of OEGMA concentration

In order to exclude a “grafting to” mechanism, which could be based on a coupling of self-polymerized macroradicals with surface bound thiyl radicals, control experiments were performed. Solutions with 50 vol%, 70 vol% and 100 vol% OEGMA in 1,4-dioxane were deposited on non-modified Si-wafers and were subsequently covered with a glass slide. UV illumination (E=5 J/cm^{-2}) leads to an increase in viscosity of the monomer solution indicating an auto-initiated polymerization reaction as already described (*vide supra*). GPC analysis, however, revealed only little variation in the molecular weight of the formed macromolecules in all three different solutions (Table 19 and Figure 77). As there are significant changes in the brush heights using these concentrations, the brush growth is not explainable with a “grafting to” mechanism, because in this case different molar weights would be expected, relating to the observed height variations.

Table 19: GPC-results of the investigation of the auto-initiated polymerization

OEGMA concentration in 1,4-dioxane / vol%	**Mn**	**M_w**
50	9110	10290
70	8260	10100
100	9230	10840

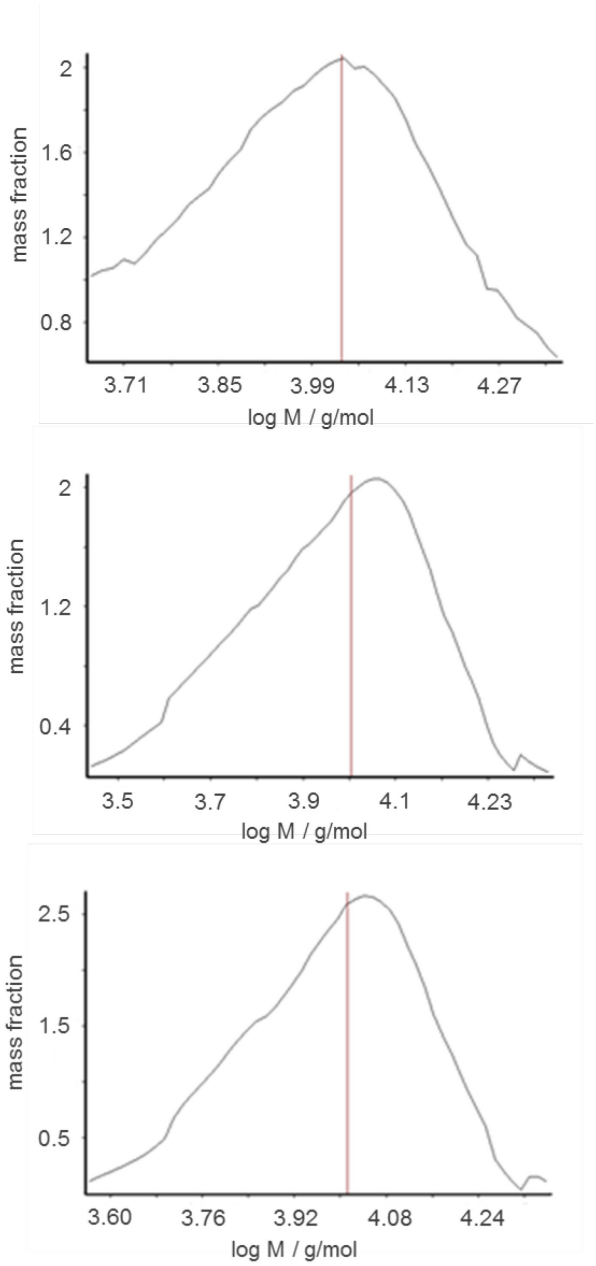

Figure 77: Differential molar mass distribution for the investigation of the auto-initiated polymerization of OEGMA at different concentrations in 1,4-dioxane; **top**: 100 vol% OEGMA; **middle**: 70 vol% OEGMA; **bottom**: 50 vol% OEGMA

In a further experiment the influence of the polymerizable group on the brush formation was investigated. The corresponding acrylate monomer, oligoethylene glycol acrylate (**OEGA**), was used for brush growth (E= 1.75 J/cm^2). It was found that the thiyl initiated polymerization of acrylates, although performed with a significantly lower UV dose, led to a film thickness of several microns as presented in Figure 78. This fact can be explained by the significantly higher rate of polymerization,[219] i.e. reactivity of acrylates compared to methacrylates.

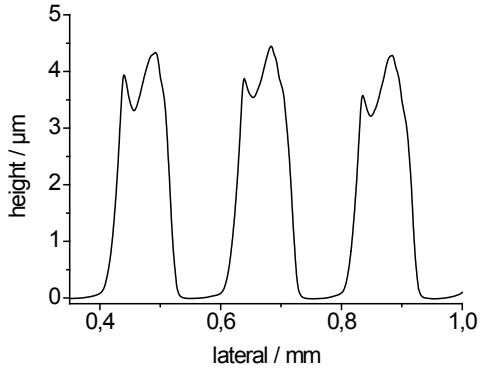

Figure 78: Surface profile of the polymer brushes obtained with acrylate (OEGA)

2.4.5. Derivatization of surface immobilized sulfonic acid groups

Sulfonic acid and sulfonate groups may be used for further derivatization with amines to give sulfonamides. Unfortunately, sulfonates are not accessible for carbodiimide chemistry, which is commonly used for selective modification of carboxylic acid groups.[220] A well reported approach for the activation of sulfonates is their conversion to the corresponding sulfonyl chloride using thionyl chloride.[117] Nevertheless, this derivatization strategy requires relatively harsh conditions ($SOCl_2$ under reflux) limiting its applicability. Several groups have reported new synthesis methods for aromatic and heteroaromatic sulfonamides,[221–225] but the most promising synthesis route has been reported by Caddick et al.[226]. Therein, the sulfonate groups are directly activated by triphenlyphoshine ditriflate (**TPPDTF**) (Figure 79). Their experiments revealed that the reaction is accessible for a variety of different molecules in high yields and features a good functional group tolerance.

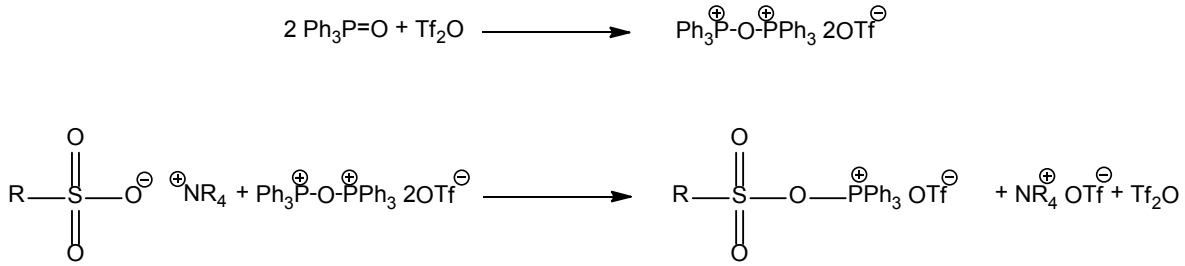

Figure 79: **Top**: generation of triphenylphosphine ditriflate;[226] **bottom**: The mechanism of the sulfonate group activation as proposed by Caddick et al.[226]

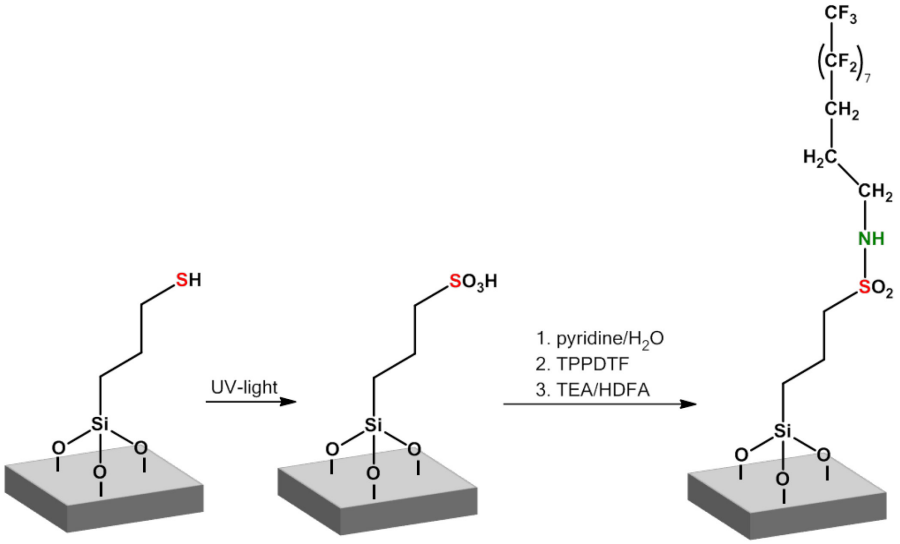

Figure 80: Scheme of the photo-oxidation and subsequent chemical modification

In order to expand the thiol-toolbox of reactions for surface modification together with the aforementioned oxidation of mercapto groups, a subsequent derivatization of the formed sulfonic acid groups was investigated. The procedure reported by Caddick et al.[226] for the direct activation of sulfonates by triphenylphosphine ditriflate (**TPPDTF**) for the coupling of nucleophiles was modified for its application in surface modification. The reaction scheme is shown in Figure 80. Following photo-oxidation to give the sulfonic acid groups the samples were treated with pyridine in water to yield the corresponding pyridinium sulfonate. Subsequently, they were immersed in a solution of triphenylphosphine ditriflate in dichloromethane. A solution of heptadecafluoroundecylamine (**HDFA**) and TEA in dichloromethane was added after 30 min. The reaction between the activated sulfonate group and the amine was expected to yield a sulfonamide bond. The fluorinated reagent was selected because it would yield characteristic peaks in XPS spectra if reaction occurred. XPS C1s spectrum exhibited additional CF_2 (292.0 eV) and CF_3 (293.8 eV) peaks, as shown in Figure 81, left, confirming that reaction had indeed taken place.

Table 20: Peaks fitted to the C1s high-resolution XPS spectra

Functional groups	Binding energy / eV
Si-C	283.5
C-C	285.0
C-F_2	292.0
C-F_3	293.8
C-N, C-S	286.7

Table 20 shows the peak assignments. The peak at 286.7 is composed of signals from the C-N bond of the formed sulfonamide group and from the C-S bond, respectively. The wide scan (see Figure 81, right, and Table 21) revealed elemental intensity ratios C:F of 1:1, which suggests a derivatization yield of 48%, and a F:S ratio of 9:1, which suggests a yield of 53%. The incomplete derivatization of the sulfonic acid groups is probably due to steric hindrance of the long chain fluorocarbon. However, perfluorinated organic molecules are also highly susceptible to X-ray-induced damage, and this may contribute to a reduction in the fluorine C1s signal of the wide scan spectrum.

Table 21: XPS wide scan spectrum of the sulfonamide derivatization

Peaks	Elemental composition / atomic %
O1s	24.2
F1s	14.2
Si2p	44.2
S2s	1.6
C1s	14.4
N1s	1.4

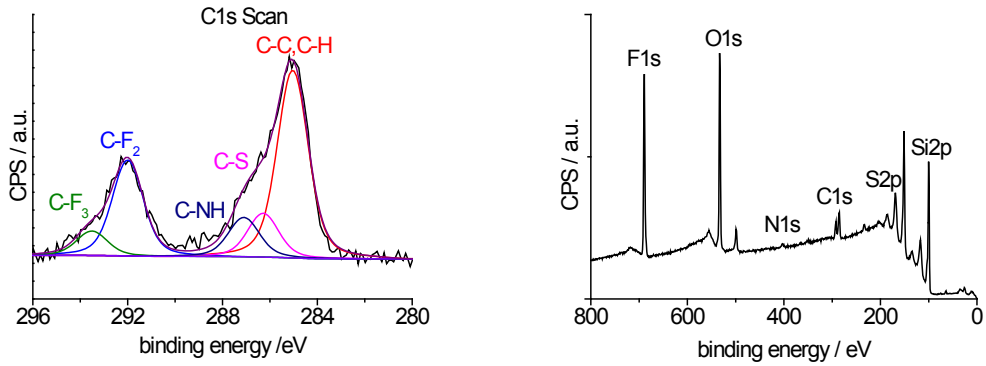

Figure 81: XPS scan spectrum of the sulfonamide derivatization; **left**: carbon 1s signal; **right**: wide scan spectrum

Besides XPS measurements the derivatized surfaces were also characterized by means of contact angle measurements (Table 22). Upon photo-oxidation to sulfonic acid groups the contact angle of water decreases to 18°. Using the sulfonamide derivatization with the fluorinated amine a significant increase of the static contact angle of water to 81° could be observed. However, the obtained value of 81° is lower than other studies[227] have revealed for fluoroalkyl derivatization of molecular layers, indicating the non-quantitative conversion of the highly polar sulfonic acid groups. Further evidence for the chemically heterogeneous surface consisting of highly polar sulfonic acid groups and hydrophobic fluorinated areas is provided by the significant contact angle hysteresis (difference between the advancing and receding angle) (Table 22).

Table 22: Contact angle change for the sulfonamide derivatization using heptadecafluoroundecyl amine (HDFA)

Substrate	Static contact angle [H_2O] / °	Advancing angle [H_2O] / °	Receding angle [H_2O] / °
MPTMS-layer	38	49	27
After photo-oxidation	18	24	11
After HDFA sulfonamide derivatization	81	86	35

2.4.6. Protein patterning

2.4.6.1. Protein patterning using non-specific adsorption

It has been previously reported that sulfonic acid groups exhibit protein resistant behavior, while thiol groups show a distinct affinity to proteins.[115,116] We investigated this behavior for its application for nanopatterns**.** MPTMS-layers on mica were oxidized via IL-lithography in a Lloyd's mirror setup, resulting in line patterns of oxidized areas. These pre-patterned samples were immersed in solutions of labelled proteins, and imaged by fluorescence microscopy. Clear fluorescence contrast was observed for the nanopatterns. The fabricated structures featured a period of 700 nm and a full width at half maximum (**FWHM**) of 350 nm, which could be imaged by confocal fluorescence microscopy. Figure 82 show samples that have been patterned using IL and were immersed in Streptavidin, anti-**IgG** or GFP solution respectively. While mercapto groups show strong non-specific protein adsorption, the oxidized areas remain dark due to their protein resistant behavior.

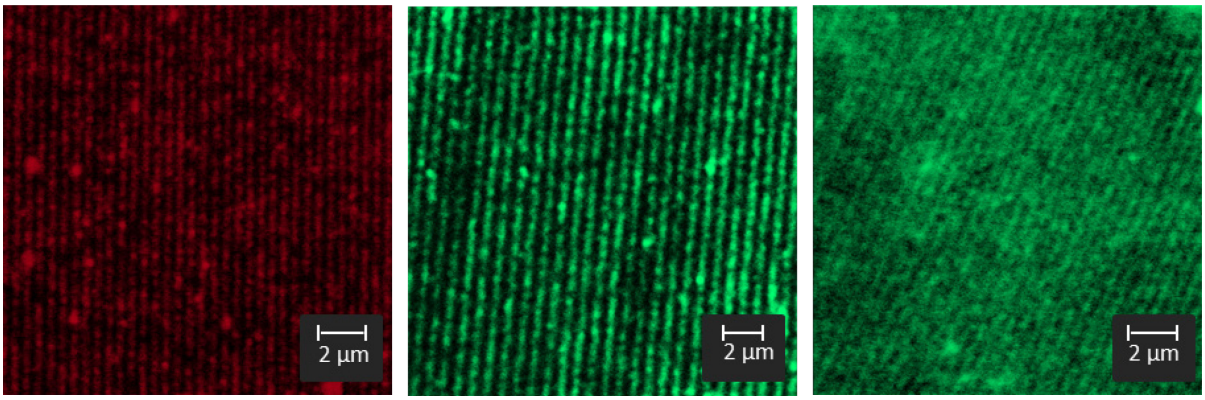

Figure 82: Fluorescence micrograph images of Streptavidin (**left**), Anti-IgG (**middle**) and GFP (**right**) nanopattern

2.4.6.1. Site-specific binding of proteins

As already mentioned in the introduction (chapter 2.1), the site-specific binding of proteins to the surface is desirable for the construction of complex protein patterns for the investigation of interactions of different proteins. The site-specific binding allows the controlled presentation of the protein to the medium above the surface.[11] For this matter the thiol induced polymerization reaction was combined with the derivatization of photo-generated sulfonates. First, the sample was photo-patterned and treated with pyridine in water to create sulfonate regions surrounded by areas with pristine thiol groups. Subsequently, a surface induced polymerization reaction of OEGMA monomers initiated by thiyl radicals was performed leading to polymer brush growth in the non-photo-oxidized regions. The protein resistant behavior of the oligoethylene glycol group has been already described as early as 1991.[228] It's especially effective properties of decreasing the adsorption of proteins due to its extreme hydrophilicity has led to a multitude of applications.[19,128,140,172,173,229,230] For the investigation of site-specific protein patterning the sulfonic acid groups were derivatized with poly(ethylene glycol) 2-aminoethyl ether biotin to the corresponding sulfonamide. In a subsequent step, the substrate with the immobilized biotin groups on the surface is immersed in a solution of green fluorescent microspheres labeled with NeutrAvidin groups. Through the well-known biotin-NeutrAvidin interaction the fluorescent particles attach to the surface only in the predefined areas. A fluorescence micrograph image of such obtained microstructures can be seen in Figure 83. The reduced fluorescence response in the image, compared to all the other fluorescence images in this work, can be explained by the use of the non-confocal fluorescence microscope.

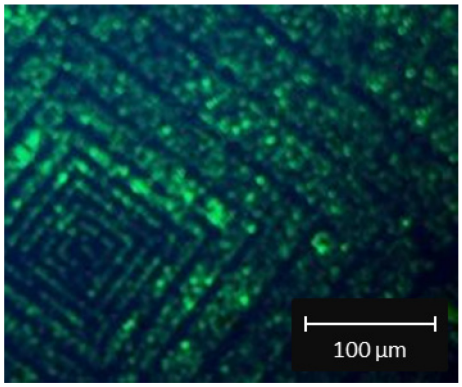

Figure 83: Fluorescence micrograph images of patterned MPTMS layer using contact lithography, brush growth and subsequent biotin-NeutrAvidin immobilization

As the aim of this work was to evaluate this protein immobilization strategy at the sub-micrometer scale, changes on the used protein and the fluorescence microscope were conducted after these preliminary results. With the change from the microspheres with a diameter of 200 nm to the His-tagged GFP and the switch to a confocal fluorescence microscope a higher resolution was anticipated. Thus, after the patterned oxidation and the subsequent brush growth, N_{α},N_{α}-bis(carboxymethyl)-L-lysine hydrate (a derivate of NTA) was coupled to the sulfonate functionalized areas using TPPDF activation, to enable the selective immobilization of His-tagged GFP through a Ni-complex.

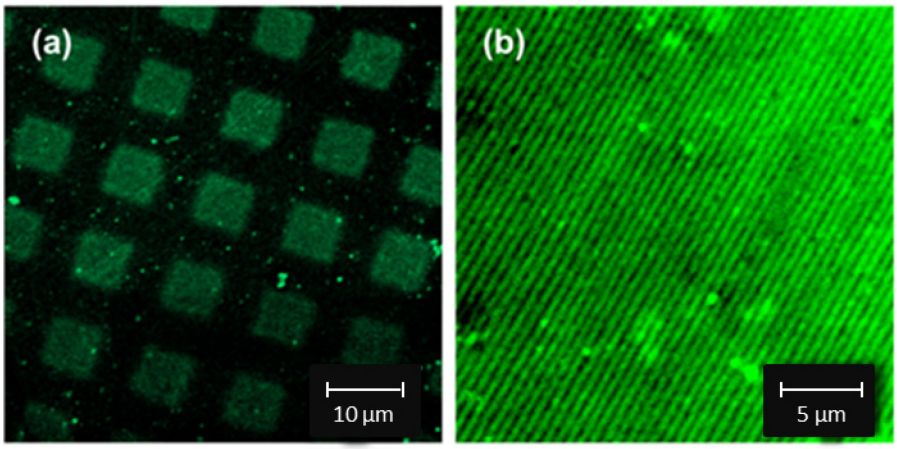

Figure 84: Fluorescence micrograph images of patterned MPTMS layer using (**a**) contact lithography and (**b**) interference lithography (**IL**), subsequent brush growth and GFP immobilization

Figure 84 shows samples patterned this way. MPTMS films were patterned using both mask-based and interferometric exposure. OEGMA solution was deposited onto the samples, and illuminated with UV light, yielding polymer brushes in the non-oxidized areas. The oxidized areas were functionalized by NTA molecules attached to amino terminated linkers using TPPDF activation. Highly fluorescent GFP was coupled to the patterns via the specific interaction between Ni-NTA and His-tagged proteins, and the samples were imaged using confocal fluorescence microscopy (Figure 84). Bright fluorescence was observed in the oxidized and subsequently derivatized areas, while the regions with OEGMA brushes remained dark.

In control experiments, pre-oxidized samples were immersed directly in GFP solutions after OEGMA brush formation. In this case, the whole surface is covered by protein resistant layers, either by OEGMA brushes or by sulfonic acid groups, respectively. Thus only dark images were obtained indicating a very poor coverage of GFP. Immersion of patterned samples in a solution of imidazole (100 mM of imidazole in water for 4 hours) also led to the disappearance of the fluorescence signal. This is an indication of the displacement of the His-tagged protein by imidazole and evidence for the site-specific immobilization in the patterned regions in Figure 84.

2.5. Conclusion

In the second part of my work surface bound thiol groups were explored for derivatization strategies towards the realization of (bio)nanostructures. Mercaptosilane layers on silicon were patterned by utilizing UV-induced photo-oxidation of the thiol to yield sulfonic acid groups. Micrometer-scale patterns were generated in a mask-based process. Remaining thiol groups were investigated for a thiol-induced polymerization and a thiol-Michael reaction for the selective modification of surface properties. Protein-resistant polymer brushes containing oligoethylene glycol groups were grown from the intact thiol groups by a surface-induced polymerization reaction. Depending on both, the concentration and the choice of the used polymerizable group, i.e. methacrylate or acrylate, brushes with nanometer heights (methacrylates) and micrometer heights (acrylates) were realized. The sulfonic acid groups were used for a selective immobilization of amino-functionalized molecules after activation with triphenylphosphine ditriflate. Through the combination of the polymer brush growth and the sulfonic acid derivatization it is possible to couple amino-labelled nitrilotriacetic acid (NH_2-NTA) to sulfonate-functionalized regions, facilitating the site-specific binding of green fluorescence protein (GFP) and to realize protein-resistant polymer brushes by exploiting remaining thiol groups. Control experiments revealed the antifouling behavior of the obtained POEGMA brushes as well as the immobilization of the GFP via Ni-NTA and His-tag interaction. Interference lithography (IL) using a Lloyd's mirror dual-beam interferometer also yielded photo-oxidation of mercapto groups and enabled the nanopatterning of GFP. Although the results were obtained on silicon, which exhibits a significant fluorescence quenching,[231] distinct fluorescence images of the micro- and submicropatterns were obtained. With the results on silicon being easily transferable to glass and mica, this patterning strategy facilitates (bio)molecule structuring for relevant application. The extended versatility of thiol group chemistry paves the way towards novel strategies for surface conjugation enabling the fabrication of complex protein nanopatterns beyond thiol-ene chemistry.

Analytical methods

I. Differential scanning calorimetry (DSC)

Differential scanning calorimetry (DSC) is a thermoanalytical technique, wherein the change of the difference in the heat flow rate to the sample is compared to a reference sample while being subjected to a controlled temperature program. Different designs and measurement principles for DSC measurements are feasible. They can be categorized into two basic types, either heat flux DSC or power compensation DSC.[232]

In the case of this work a heat flux DSC was used. The sample and the reference are subjected to the same temperature and same heat flows in the furnace. If a difference in heat capacities is existent, or if the sample is experiencing a physical transformation (e.g. phase transition) or chemical reaction, a different heat flow causes temperature gradients at the thermal resistances of the sensor, which are being recorded (Figure 85).[233] Possible applications are the determination of heat capacity, fusion temperature, crystallization state and glass transition temperature of polymers, among others.[232]

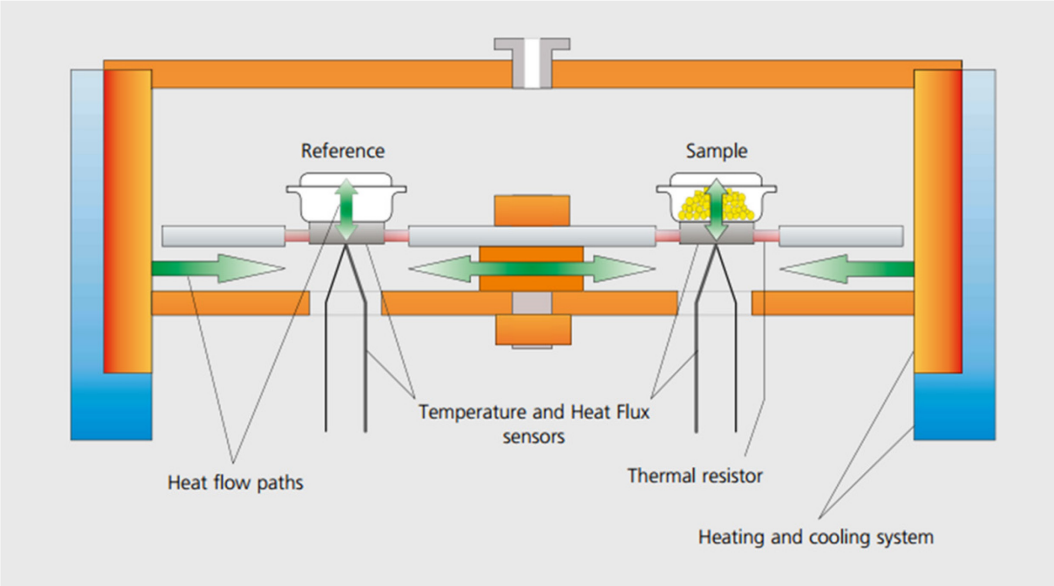

Figure 85: Heat flux DSC setup[233]

i. Photo-DSC

In a photo-DSC measurement both the sample and the reference (e.g. empty) crucible are irradiated with UV light at a constant temperature until the photo-reaction is completed. Afterwards a second irradiation run (same time, same UV dose and same temperature) is performed. The subtraction of the second from the first run is calculated and yields the heat of reaction curve (see Figure 86). Hence, photo-DSC measurements are a fast and accurate method for obtaining information on the polymerization with one single measurement.[234] The reaction enthalpy can be calculated through the integration of the curve (peak area). Consequently, the double bond conversion (DBC) can be calculated, if the theoretical enthalpy for the used monomer system is known (equation (5)). Additionally, the time to reach the maximum heat of polymerization (t_{max}) yields information about the reaction speed.

$$\mathrm{DBC} = \frac{\Delta \mathrm{H}}{\Delta \mathrm{H_{th}}} \qquad \textbf{(5)}$$

ΔH is the measured enthalpy; ΔH_{th} is the theoretical value for 100% conversion

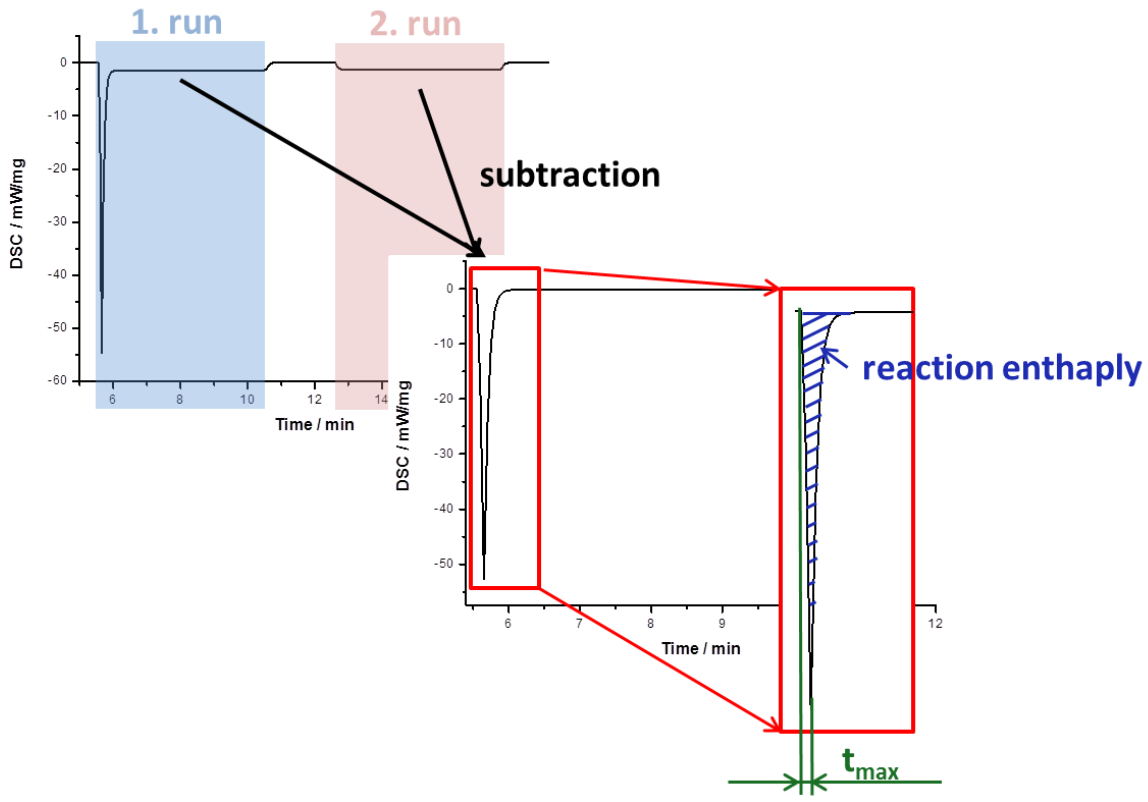

Figure 86: Photo-DSC measurement evaluation

II. X-ray photoelectron spectroscopy (XPS)

XPS is a technique for surface analysis. It enables the quantitative determination of all elements except for hydrogen and helium on a surface. Furthermore it is possible to determine the chemical states of the elements due to its high sensitivity.[235]

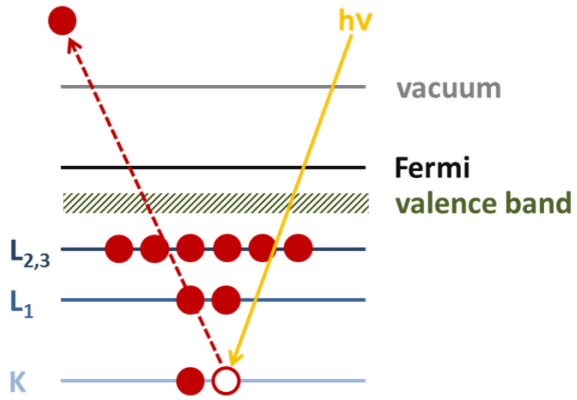

Figure 87: The principle of the XPS

XPS was invented in the 1960s by the group of Siegbahn at the University of Uppsala, Sweden, which eventually earned him the Nobel Prize for Physics in 1981. Measurements are based on the photoelectric effect. The sample is irradiated by soft X-rays. Mg Kα (1253.6 eV) or Al Kα (1486.6 eV) x-rays are most commonly used. The photons penetrate into the surface of the sample (maximum depth of 1-10 microns) and interact with the atoms. This leads to electrons being emitted by the photoelectric effect (Figure 87). Although ionization occurs to deeper regions, only electrons from a few nanometers within the surface are emitted due to the interaction of the electrons with matter. Leaving electrons, which are not subjected to an energy loss, produce the spectrum, while electrons that loose energy due to inelastic scattering form the background. The electrons are detected by an electron analyzer according to their respective kinetic energy (equation (6). The kinetic energies of the spectra can be calculated using equation (6). XPS can be used to identify elements and its concentration on the surface, as each element has a unique set of binding energies. Variations in the binding energies, called chemical shifts, yield information about the chemical state of the analyzed materials.[236]

$$E_{kin} = h\nu - E_b - \Phi_S \quad \textbf{(6)}$$

E_{kin} is the kinetic energy; hv is the photon energy; E_b is the binding energy of atomic orbital from which the electron originates; Φ_s is the spectrometer work function

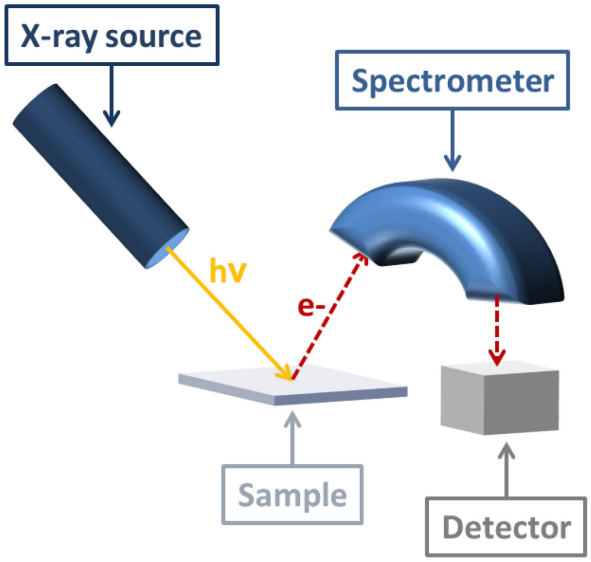

Figure 88: Schematic XPS setup

III. Scanning probe microscopy (SPM)

In SPM techniques a physical probe is used to scan the sample surface. The interactions of the probe with the sample surface are utilized to obtain images of physical quantities of the surface. The first SPM technique, the scanning tunneling microscopy (**STM**), was invented in 1981 by Binnig and Rohrer,[237] which earned them the Nobel prize only 5 years later. Nowadays a multitude of different modes is feasible. The two modes used in this work will be discussed in further detail.

i. Atomic force microscopy (AFM)

Only five years after inventing the STM, Binnig invented the AFM.[238] Instead of measuring the tunneling current, as in the case of the STM, the force interaction between a small tip and the surface is used to investigate the sample surface. A small sharp tip is approximated to the surface. Interactions between the tip and the surface cause a deflection, either through attractive or repulsive forces. To measure the existing deflection a laser beam is reflected from the back of the cantilever into an array of photo diodes allowing the imaging of the surface (see Figure 89).

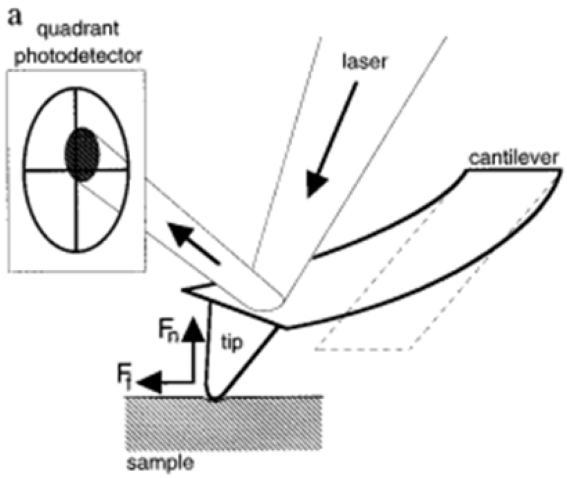

Figure 89: AFM setup[239]

Different modes, which vary in the spacing between the tip and the surface, are feasible (see Figure 90).

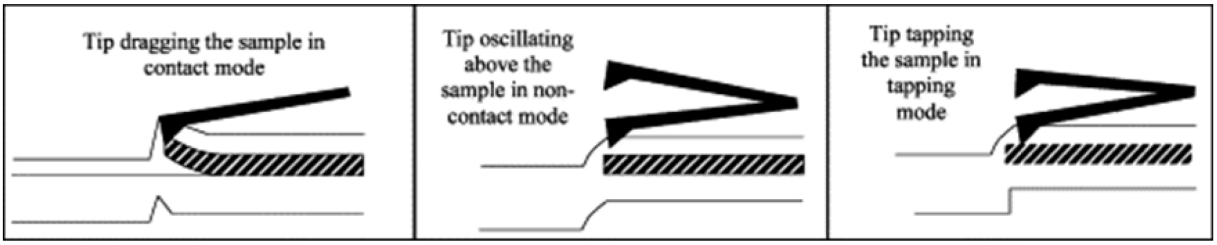

Figure 90: Different AFM modes;[240] **left**: contact mode; **middle**: non-contact mode; **right**: tapping mode

Contact mode: As the name suggests, in contact mode the tip is in contact with the sample surface. Two different methods are possible: Constant height and constant force. When using constant height, the scanner is kept at a fixed height and the cantilever deflects more or less depending on the scanned sample surface height. In constant force mode, a feedback circuit is used to keep the applied force constant while regulating the height of the tip.[240]

Tapping mode: In tapping mode the cantilever is oscillated close to its resonance frequency with the tip striking the surface once each cycle. Each time the tip approaches the surface interactions between the tip and the surface cause the amplitude to change. Large amplitudes of up to 100 nm ensure that the tip overcomes the adhesion forces. A feedback circuit adjusts the height of the cantilever to keep the amplitude constant as it is scanned over the surface allowing for the imaging of the surface. With this method differences in local sample elasticity and adhesion can be revealed as a change in damping (soft areas exhibit a higher damping) generate a different phase shift between the actuation and the response signal. The tapping mode leads to a reduced damage to the sample compared to contact mode, which makes it particularly compelling for soft materials like plastics.[241]

Non-contact mode: In non-contact mode the tip oscillates above the sample and the van der Waals forces are being detected. The advantage is a non-destructive measurement, however, only lower resolution can be obtained.[240]

Friction force microscopy (FFM): In FFM the tip of an AFM is slid over the surface, which results in a twisting of the cantilever. Differences in friction between the tip and the substrate can be used to detect material differences simultaneously with topography changes. For this purpose a trace and retrace have to be recorded.[242]

IV. Secondary ion mass spectrometry (SIMS)

Secondary ion mass spectrometry is a surface and thin film analysis technique. A focused ion beam (oxygen or heavier) is directed at the sample surface. The impact of these ions yields the ejection of surface material (sputtering), typically one to several atoms per incident ion. A small proportion of these ejected parts is being ionized during the ejection process. The ejected ions can be detected and classified by mass spectrometry analysis. All elements can be detected, even hydrogen and helium, which is not the case in XPS.[243,244]

In this work a time-of-flight mass spectrometer was used. Therein an ion is accelerated by an electric field. The obtained speed is dependent on its mass-to-charge ratio. Consequently, the time to reach the detector varies with its mass-to-charge ratio.[244]

V. Contact angle and surface tension measurements

i. Static contact angle

The measurement of the contact angle is a simple and very sensitive method for surface analysis. For the determination of the static contact angle in this work the sessile drop technique was used. Therein drops with a defined volume of a liquid are deposited on a surface. After reaching equilibrium the angle θ_c is measured (see Figure 91). The interaction between the three phases (gas, liquid, solid) is described by the Young equation (equation (7)).[245]

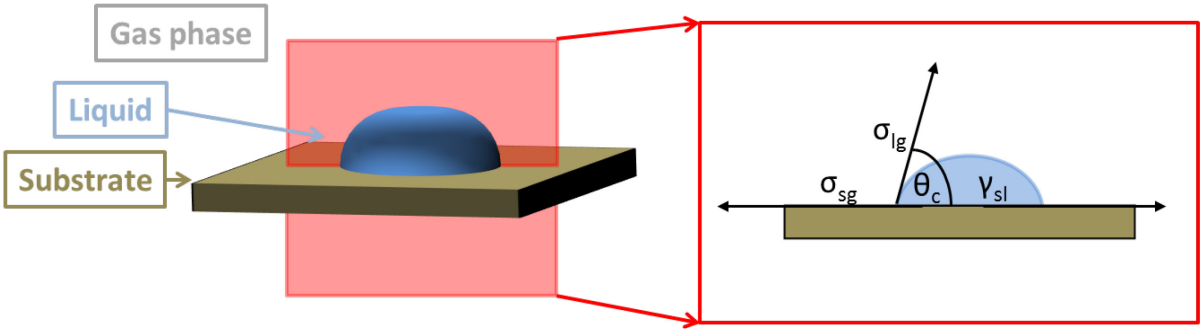

Figure 91: Contact lines between the 3 phases (gas, liquid, solid); γ_{sl} is the interfacial tension between solid and liquid, σ_{lg} is the surface tension between the liquid and the gas phase, σ_{sg} is the surface tension between the solid and the gas phase, θ_c is the angle between the vectors of σ_{lg} and γ_{sl}

$$\sigma_{lg} \cdot \cos\theta_c = \sigma_{sg} - \gamma_{sl} \qquad (7)$$

γ_{sl} is the interfacial tension between solid and liquid, σ_{lg} is the surface tension between the liquid and the gas phase, σ_{sg} is the surface tension between the solid and the gas phase, θ_c is the angle between the vectors of σ_{lg} and γ_{sl}

ii. Dynamic contact angle

According to the Young equation (equation (7)) only one static contact angle θ_c should be prevalent. However, it has been shown, that this is not the case as a whole spectrum of contact angles exists. These contact angles may range from the so-called advancing contact angle (the maximum) to the receding contact angle (the minimum).[245]

The advancing contact angle is determined by continuously increasing the volume of the drop while measuring the contact angle at the same time. When the drop becomes larger and consequently the influence of the needle, which stays in the liquid, becomes negligible, the advancing contact angle stays constant. The receding angle is measured while reducing the volume.[246]

The difference between the advancing and receding angle is called hysteresis. A pronounced hysteresis is an indication for a rough surface or a flat chemically heterogeneous surface.[217]

iii. Pendant drop method

In the pendant drop method a liquid drop is pending from the needle. If the density difference between the liquid and the surrounding phase (usually air) is known, the surface tension can be calculated from the shape of the drop using the Young-Laplace equation (equation (8)).[247]

$$\Delta p = \sigma \cdot \left(\frac{1}{r_1} + \frac{1}{r_2}\right) \quad \textbf{(8)}$$

Δp is the pressure difference across the fluid interface, σ is the surface tension and r_1 and r_2 are the radii of the curvature

VI. Spectroscopic ellipsometry

Ellipsometry is technique in material science, which is used to determine optical properties of transparent films or thin layers. Therein a change in polarization upon reflection or transmission is measured, specifically the amplitude ratio ψ and the phase difference Δ between light waves in p- and s- polarization direction (see Figure 92). The s-component is perpendicular to the plane of incidence parallel to the sample surface, while the p-component is parallel to the plane of incidence. Using equation (9) the complex reflectance ration ρ_s can be calculated. By measuring at different wavelengths and applying a theoretical model the thickness, the refractive index and the roughness can be assessed.[248]

$$\rho_s = \tan(\Psi)\, e^{i\Delta} \qquad \textbf{(9)}$$

ψ is the amplitude ratio between p- and s-direction, Δ is the phase difference of the light in p- and s-direction

Two general restrictions apply for spectroscopy ellipsometry: 1.) The surface roughness has to be quite low, typically below 30% of the wavelength. 2.) The measurement has to be performed at oblique incidence, as the s and p polarizations have to be distinguished. Typical applications are semiconductor thin films, dielectric gates, characterization of photoresists, polymer thin films, SAMs, among others.[248]

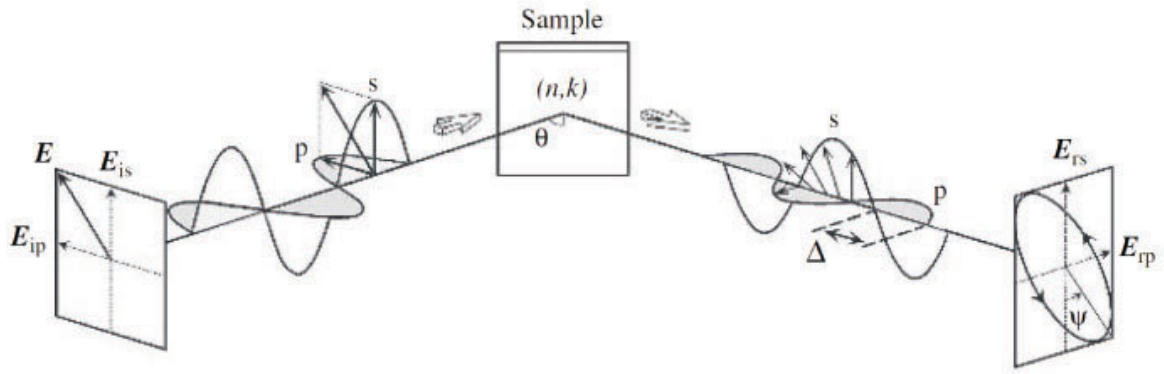

Figure 92: Measurement principle of ellipsometry[249]

List of Figures

List of Tables

List of publications

Patents:

Roth, M.; Mostegel, F. H.; Grießer, T.; Edler, M.; Oesterreicher, A.; Gassner, M.; Billiani, J., WO 2015031927, *Photoinitiator* 12. Mar. **2015**

Roth, M.; Mostegel, F. H.; Grießer, T.; Edler, M.; Oesterreicher, A.; Gassner, M.; Billiani, J., Patent Application GB 1406683.1, *Resin Composition Suitable for Printing and Printing Method Utilizing the Same*

Papers:

Mostegel, F. H.; Ducker, Robert E.; Rieger, Paul H.; el Zubir, Osama; Xia, Sijing; Radl, Simone V.; Edler, M.; Cartron, M. L.; Hunter, C. N.; Leggett, G. J.; Griesser, T.: *Versatile thiol-based reactions for micrometer- and nanometer-scale photopatterning of polymers and biomolecules*, Journal of Material Chemistry B **2015**, 3, 4431

Mostegel, F. H.; Roth, M.; Gassner, M.; Oesterreicher, A.; Piock, R.; Edler, M.; Griesser, T.: *Vinylcarbonates as Low-Toxic Monomers for Digital Ink-Jet Inks: Promising Alternatives to Acrylate Based Systems, Progress in Organic Coatings*, submitted 16. Jan. **2015**

Maver, T.; Maver, U.; Mostegel, F.; Grießer, T.; Spirk, S.; Smrke, D. M.; Stana-Kleinschek, K.: *Cellulose based thin films as a platform for drug release studies to mimick wound dressing materials*, Cellulose **2015**, 22, 749

Roth, M.; Oesterreicher, A.; Mostegel, F. H.; Moser, A.; Pinter, G.; Edler, M.; Piock, R.; Griesser, T.: *Silicon Based Mercaptans: High-performance Monomers for Thiol-Ene Photopolymerization*, Journal of Polymer Science Part A: Polymer Chemistry, published online 17. Aug. **2015**

Oral presentations:

Mostegel, F. H.; Ducker, E. D.; Rieger, P. H.; El Zubir, O.; Xia, S.; Radl, S. V.; Edler, M.; Cartron, M. L.; Hunter, C. N.; Leggett, G. J.; Griesser, T.: *Photochemical Patterning of Green Fluorescent Protein on Molecular Layers*, Smart Materials **2015**, Busan, Republic of Korea

Mostegel, F. H.; Rieger, P. H.; Edler, M.; Griesser T.: *Photochemical Patterning of Proteins on Thiol-terminated Monolayers*, ESPS **2014**, Vienna, Austria

Mostegel, F. H.; Rieger, P. H.; Edler, M.; Griesser T.: *Photo-Induced Polymer Brush Growth on Thiol Terminated Self-Assembled Monolayers,* Macro **2014**, Chiang Mai, Thailand

Poster:

Mostegel, F. H.; Roth, M.; Gassner, M.; Oesterreicher, A.; Piock, R.; Edler, M.; Griesser, T.: *Digital Inkjet Inks Based on Biocompatible Vinylcarbonates: An Alternatives to Acrylate Based Systems*, Smart Materials **2014**, Busan, Republic of Korea

Curriculum vitae

Personal Information

Name:	Florian Hermann Mostegel
Date of birth:	27.11.1985
Place of birth:	Graz, Austria

Education

02/2012-present	PhD studies, Chair of Chemistry of Polymeric Materials, Montanuniversität Leoben, Austria
03/2005-12/2011	Studies at the Montanuniversität Leoben, Austria, with a MSc degree with distinction in Polymer Engineering and Science
09/1996-06/2004	BG Dreihackengasse, Graz, Austria

Work Experience

01/2012-present	Research Associate, Christian Doppler Laboratory for functional polymer based inkjet inks, Leoben, Austria
07/2010-12/2010	Junior Researcher, Polymer Competence Center Leoben GmbH, Leoben, Austria
07/2008-09/2008	Internship R&D, Isovolta AG, Werndorf, Austria
08/2007-09/2007	Internship, SKF Economos, Judenburg, Austria
07/2006-09/2006	Internship, Magna Steyr, Graz, Austria
07/2004-03/2005	Military Service, Graz, Austria
06/2002-07/2002	Internship, Magna Steyr, Graz, Austria

Literature

[1] Andrews, L. S; Clary, J. J. *Journal of Toxicology and Environmental Health* **1986**, *19*, 149.

[2] Nethercott, J. R. *British Journal of Dermatology* **1978**, *98*, 541.

[3] Nethercott, J. R; Nosal, R. *Contact Dermatitis* **1986**, *14*, 280.

[4] Emmett, E. A. *Contact Dermatitis* **1977**, *3*, 245.

[5] Surakka, J; Lindh, T; Rosen, G; Fischer, T. *The Annals of Occupational Hygiene* **2000**, *44*, 635.

[6] Heller, C; Schwentenwein, M; Russmüller, G; Koch, T; Moser, D; Schopper, C; Varga, F; Stampfl, J; Liska, R. *Journal of Polymer Science Part A: Polymer Chemistry* **2011**, *49*, 650.

[7] Mautner, A; Qin, X; Kapeller, G; Russmüller, G; Koch, T; Stampfl, J; Liska, R. *Macromolecules Rapid Communications* **2012**, *33*, 2046.

[8] Pasquarelli, A. *Materials Science and Engineering: C* **2008**, *28*, 495.

[9] Flemming, R; Murphy, C; Abrams, G; Goodman, S; Nealey, P. *Biomaterials* **1999**, *20*, 573.

[10] Stevens, M. M; George, J. H. *Science* **2005**, *310*, 1135.

[11] Leggett, G. J. *Nanoscale* **2012**, *4*, 1840.

[12] Le, H. P. *Journal of Imaging Science and Technology* **1998**, *42*, 49.

[13] Holmström, M; Granstrand, P; Nylander-French, L. A; Rosén, G. *American Journal of Industrial Medicine* **1995**, *28*, 207.

[14] Nylander-French, L. A; Fischer, T; Hultengren, M; Lewné, M; Rosén, G. *Applied Occupational and Environmental Hygiene* **1994**, *9*, 962.

[15] Husar, B; Liska, R; Husár, B. *Chemical Society Reviews* **2012**, *41*, 2395.

[16] Scherzer, T; Müller, S; Mehnert, R; Volland, A; Lucht, H. *Polymer* **2005**, *46*, 7072.

[17] Green, W. A., *Industrial photoinitiators: A technical guide*, CRC Press, Boca Raton **2010**.

[18] Heller, C; Schwentenwein, M; Russmueller, G; Varga, F; Stampfl, J; Liska, R. *Journal of Polymer Science Part A: Polymer Chemistry* **2009**, *47*, 6941.

[19] Liska, R; Schuster, M., *Basics and applications of photopolymerization reactions*, Vol. 3: *Biocompatible photopolymers.* Fouassier, J.-P; Allonas, X. (Eds.), Research Signpost, Kerala, India **2010**.

[20] Elmquist, R. US 2566443, *Measuring Instrument of the Recording Type* 4. Sept. **1951**.

[21] Rayleigh, J. W. S. *Proceedings of the London Mathematical Society* **1878**, *10*, 4.

[22] Sweet, R. G. *Review of Scientific Instruments* **1965**, *36*, 131.

[23] Sweet, R. G. US 3596275, *Fluid Droplet Recorder* 27. Jul. **1971**.

[24] Hudd, A., *The chemistry of inkjet jets: Inkjet Printing Technologies.* Magdassi, S. (Ed.), World scientific **2009**.

[25] Kyser, E. L; Sears, S. B. US 3946398, *Method and Apparatus for Recording with Writing Fluids and Drop Projection Means Therfor* 23. Mar. **1976**.

[26] Zoltan, S. I. US 3683212, *Pulsed Droplet Ejecting System* 8. Aug. **1972**.

[27] Endo, I; Sato, Y; Saito, S; Nakagiri, T; Ohno, S. GB 2007162, *Liquid jet recording process and apparatus therefor* 16. May. **1979**.

[28] Brünahl, J; Grishin, A. M. *Sensors and Actuators A: Physical* **2002**, *101*, 371.

[29] Lima-Marques, L. WO 1993011866, *Method and Apparatus for the Production of Discrete Agglomerations of Particulate Matter* 24. Jun. **1993**.

[30] Hadimioglu, B; Elrod, S; Steinmetz, D; Lim, M; Zesch, J; Khuri-Yakub, B; Rawson, E; Quate, C., in *IEEE 1992 Ultrasonics Symposium Proceedings: Acoustic Ink Printing*, IEEE **1992**, p. 929.

[31] Edison, S. E., *The chemistry of inkjet jets: Formulating UV Curable Inkjet Inks.* Magdassi, S. (Ed.), World scientific **2009**.

[32] Gupta, M. K; Singh, R. P., *Basics and applications of photopolymerization reactions*, Vol. 1: *Cationic initiators in photocuring applications.* Fouassier, J. P; Allonas, X. (Eds.), Research Signpost, Kerala, India **2010**.

[33] Rabek, J. F., *Mechanisms of photophysical processes and photochemical reactions in polymers: Theory and applications*, Wiley, Chichester [West Sussex], New York **1987**.

[34] Crivello, J. V; Dietliker, K; Bradley, G., *Chemistry & technology of UV & EB formulation for coatings, inks & paints* **1998**.

[35] Sagratini, G; Caprioli, G; Cristalli, G; Giardiná, D; Ricciutelli, M; Volpini, R; Zuo, Y; Vittori, S. *Journal of Chromatography A* **2008**, *1194*, 213.

[36] Anadon, A; Bell, D; Binderup, M.-L; Bursch, W; Castle, L; Crebelli, R; Engel, K.-H; Franz, R; Gontard, N; Haertle, T; Husoy, T; Jany, K.-D; Leclercq, C; Lhuguenot, J.-C; Mennes, W; Milana, M. R; Pfaff, K; Svensson, K; Toldra, F; Waring, R; Wölfle, D. *The EFSA Journal* **2009**, *1104*, 1.

[37] Lalevee, J; Fouassier, J. P; Allonas, X., *Basics and applications of photopolymerization reactions*, Vol. 2: *New highly reactive acrylate monomers: The importance of the hydrogen abstraction reaction.* Fouassier, J. P; Allonas, X. (Eds.), Research Signpost, Kerala, India **2010**.

[38] Lecamp, L; Lebaudy, P; Youssef, B; Bunel, C. *Polymer* **2001**, *42*, 8541.

[39] Seinfeld, J. H; Pandis, S. N., *Atmospheric chemistry and physics: From air pollution to climate change*, J. Wiley, Hoboken, N.J **2006**.

[40] Hutchinson, I., *The chemistry of inkjet jets: Raw Materials for UV Curable Inks.* Magdassi, S. (Ed.), World scientific **2009**.

[41] Magdassi, S., *The chemistry of inkjet jets: Pigments for Inkjet Applications.* Shakhnovich, A; Belmont, J. (Eds.), World scientific **2009**.

[42] Donnet, J.-B; Bansal, R. C; Wang, M.-J., *Carbon black - Science and technology: Manufacture of Carbon Black.* Voll, M; Kühner, G. (Eds.), Dekker, New York **1993**.

[43] Donnet, J.-B; Bansal, R. C; Wang, M.-J., *Carbon black - Science and technology: Microstructure, Morphology and General Physical Properties.* Hess, W. M; Herd, C. R. (Eds.), Dekker, New York **1993**.

[44] Donnet, J.-B; Bansal, R. C; Wang, M.-J., *Carbon black - Science and technology: Surface Groups on Carbon Blacks.* Donnet, J.-B; Bansal, R. C. (Eds.), Dekker, New York **1993**.

[45] Boehm, H. *Carbon* **2002**, *40*, 145.

[46] Macfaul, P., *Ink technologies for ink jet printing, Digital Printing - 2003 Onwards*, Enfield, London **2003**.

[47] Müller, B., *Additive kompakt*, Vincentz Network, Hannover **2009**.

[48] Clayfield, E; Lumb, E. *Journal of Colloid and Interface Science* **1966**, *22*, 269.

[49] Fink, J. K., *The Chemistry of Printing Inks and Their Electronics and Medical Applications*, Wiley **2014**.

[50] Meunier, G; Hemery, P; Senet, J.-P; Boileau, S. *Polymer Bulletin* **1981**, *4*, 705.

[51] Meunier, G; Hémery, P; Boileau, S; Senet, J.-P; Chéradame, H. *Polymer* **1982**, *23*, 849.

[52] Gomes Freire, M. T; Danicher, L; Lambla, M. *Die Makromolekulare Chemie* **1988**, *189*, 67.

[53] Olofson, R. A; Schnur, R. C; Olofson, R; Schnur, R. C. *Tetrahedron Letters* **1977**, *18*, 1571.

[54] Ebdon, J; Aukrust, I; Redford, K; Solberg, J; Ebdon, J. R; Aukrust, I. R. F; Redford, K; Solberg, J. *Polymer* **1994**, *35*, 4819.

[55] Küng, F. E. US 2377085, *Unsatured Chlorocarbonates and Method of Preparation 29. May.***1945**.

[56] Malfroot, T. FR 2381739, *Procede de Synthese Industrielle du Chloroformiate de Vinyle 28. Nov.* **1980**.

[57] Olofson, R. A; Bauman, B. A; Wancowicz, D. J. *The Journal of Organic Chemistry* **1978**, *43*, 752.

[58] Moris, F; Gotor, V. *The Journal of Organic Chemistry* **1992**, *57*, 2490.

[59] Olofson, R; Cuomo, J. *Tetrahedron Letters* **1980**, *21*, 819.

[60] Olofson, R. A; Dang Vu Anh; Morrison, D. S; Cusati, P. F. de *The Journal of Organic Chemistry* **1990**, *55*, 1.

[61] Henkelmann, J; Kessinger, R; Staffel, W. WO 2008084086, *Method for the Production of O-vinylcarbamates and Vinylcarbonates* 17. Jul. **2008**.

[62] Ebdon, J. R; Aukrust, I. R. F; Redford, K; Solberg, J. *Polymer* **1994**, *35*, 4819.

[63] Posner, T. *Berichte der deutschen chemischen Gesellschaft* **1905**, *38*, 646.

[64] Morgan, C. R; Magnotta, F; Ketley, A. D. *Journal of Polymer Science: Polymer Chemistry Edition* **1977**, *15*, 627.

[65] Kolb, H. C.; Finn, M. G.; Sharpless, K. B. *Angewandte Chemie* **2001**.

[66] Cramer, N. B; Bowman, C. N. *Journal of Polymer Science Part A: Polymer Chemistry* **2001**, *39*, 3311.

[67] Hoyle, C. E; Lee, T. Y; Roper, T. *Journal of Polymer Science Part A: Polymer Chemistry* **2004**, *42*, 5301.

[68] Cramer, N. B; Scott, J. P; Bowman, C. N. *Macromolecules* **2002**, *35*, 5361.

[69] Hoyle, C. E; Bowman, C. N. *Angewandte Chemie International Edition* **2010**, *49*, 1540.

[70] Cherkaoui, Z; Esfandiari, P; Frantz, R; Lagref, J.-J; Liska, R. WO 2012126695, *Stable Curable Thiol-Ene Composition* 27. Sep. **2012**.

[71] Klemm, E; Sensfuß, S; Holfter, U; Flammersheim, J. J. *Angew. Makromolekulare Chemie* **1993**.

[72] Kühne, G; Diesen, J. S; Klemm, E. *Angewandte Makromolekulare Chemie* **1996**, *242*, 139.

[73] Stahly, E. E. US 3619393, *Process for the Preperation of Shelf-Stable, Photocurable Polythiols* 9. Nov. **1971**.

[74] Dowling, J. P; Richardson, S. C; Quigley, K. US 5358976, *Stable Thiol-ene compositions* 25. Oct. **1994**.

[75] Guthrie, J; Rendulic, F. US 3855093, *Radiation Curable Polyene-Polythiol Coating Compositions* 17. Dec. **1974**.

[76] Mautner, A; Qin, X; Wutzel, H; Ligon, S. C; Kapeller, B; Moser, D; Russmueller, G; Stampfl, J; Liska, R. *Journal of Polymer Science Part A: Polymer Chemistry* **2013**, *51*, 203.

[77] Molenberg, A; R; Zamparo, E; Rapillard, L; Cerritelli, S. WO 2011004255, *Compositions for Tissue Augmentation* 21. Apr. **2011**.

[78] Hult, A; Malkoch, M; Von, H. H; Nordberg, A. WO 2011048077, *Composition for the Treatment of a Bone Fracture* 22. Sep. **2011**.

[79] Garber, L; Chen, C; Kilchrist, K. V; Bounds, C; Pojman, J. A; Hayes, D. *Journal of Biomedical Materials Research Part A* **2013**, *101*, 3531.

[80] Rheinberger, V; Moszner, N; Salz, U. DE 19619046, *Verwendung einer Zusammensetzung als Dentalmaterial und Dentamaterial* 6. Nov. **1997**.

[81] Eckhardt, G; Luchterhandt, T; Klettke, T. DE 19919581, *Dentalmaterialien, Verfahren zu Ihrer Aushärtung und Deren Verwendung* 2. Nov. **2000**.

[82] Bowman, C. N; Carioscia, J; Lu, H; Stansbury, J. W. WO 2005086911, *Reactive Oligomeric Thiol and Ene Materials as Dental Restorative Mixtures* 22. Sep. **2005**.

[83] Gottlieb, H. E; Kotlyar, V; Nudelman, A. *The Journal of Organic Chemistry* **1997**, *62*, 7512.

[84] FUJIFILM Dimatix, I., *Jettable Fluid Formulation Guidelines* **2013**.

[85] Friedman, M; Cavins, J. F; Wall, J. S. *Journal of the American Chemical Society* **1965**, *87*, 3672.

[86] Dworak, C; Kopeinig, S; Hoffmann, H; Liska, R. *Journal of Polymer Science Part A: Polymer Chemistry* **2009**, *47*, 392.

[87] Fromm, J. E. *IBM Journal of Research and Development* **1984**, *28*, 322.

[88] Reis, N; Ainsley, C; Derby, B. *Journal of Applied Physics* **2005**, *97*, 94903.

[89] Belbakra, Z; Cherkaoui, Z. M; Allonas, X. *Polymer Degradation and Stability* **2014**, *110*, 298.

[90] Esfandiari, P; Ligon, S. C; Lagref, J. J; Frantz, R; Cherkaoui, Z; Liska, R. *Journal of Polymer Science Part A: Polymer Chemistry* **2013**, *51*, 4261.

[91] Leach, R. H; Armstrong, C; Brown, J. F; Mackenzie, M. J; Randall, L; Smith, H. G., *The Printing Ink Manual*, Springer US, Boston, MA **1988**.

[92] Becker, H; Vogel, H. *Chemical Engineering & Technology* **2006**, *29*, 1227.

[93] Mather, B. D; Viswanathan, K; Miller, K. M; Long, T. E. *Progress in Polymer Science* **2006**, *31*, 487.

[94] Pavlinec, J; Kleinová, A; Moszner, N. *Macromolecular Materials and Engineering* **2012**, *297*, 1005.

[95] Zweifel, H., *Stabilization of Polymeric Materials*, Springer Berlin Heidelberg, Berlin, Heidelberg **1998**.

[96] Mostegel, F. H; Ducker, R. E; Rieger, P. H; el Zubir, O; Xia, S; Radl, S. V; Edler, M; Cartron, M. L; Hunter, C. N; Leggett, G. J; Griesser, T. *Journal of Material Chemistry B* **2015**, *3*, 4431.

[97] Hoyle, C. E; Lowe, A. B; Bowman, C. N. *Chemical Society Reviews* **2010**, *39*, 1355.

[98] Lowe, A. B. *Polymer Chemistry* **2010**, *1*, 17.

[99] Wadu-Mesthrige, K; Amro, N. A; Garno, J. C; Xu, S; Liu, G.-y. *Biophysical Journal* **2001**, *80*, 1891.

[100] Wadu-Mesthrige, K; Xu, S; Amro, N. A; Liu, G.-y. *Langmuir* **1999**, *15*, 8580.

[101] Pavlovic, E; Oscarsson, S; Quist, A. P. *Nano Letters* **2003**, *3*, 779.

[102] Chen, T; Amin, I; Jordan, R. *Chemical Society Reviews* **2012**, *41*, 3280.

[103] Husemann, M; Mecerreyes, D; Hawker, C. J; Hedrick, J. L; Shah, R; Abbott, N. L. *Angewandte Chemie International Edition* **1999**, *38*, 647.

[104] Rühe, J. *Macromolecular Symposia* **1998**, *126*, 215.

[105] Demers, L. M; Ginger, D; Park, S.-J; Li, Z; Chung, S.-W; Mirkin, C. A. *Science* **2002**, *296*, 1836.

[106] Piner, R. D; Zhu, J; Xu, F; Hong, S; Mirkin, C. A. *Science* **1999**, *283*, 661.

[107] Jung, H; Kulkarni, R; Collier, C. P. *Journal of the American Chemical Society* **2003**, *125*, 12096.

[108] Xu, S; Laibinis, P. E; Liu, G.-y. *Journal of the American Chemical Society* **1998**, *120*, 9356.

[109] Liu, G.-y; Xu, S; Qian, Y. *Accounts of Chemical Research* **2000**, *33*, 457.

[110] Xu, S; Liu, G.-y. *Langmuir* **1997**, *13*, 127.

[111] Adams, J; Tizazu, G; Janusz, S; Brueck, S. R. J; Lopez, G. P; Leggett, G. J. *Langmuir* **2010**, *26*, 13600.

[112] Alang Ahmad, S. A; Wong, L. S; Ul-Haq, E; Hobbs, J. K; Leggett, G. J; Micklefield, J. *Journal of the American Chemical Society* **2009**, *131*, 1513.

[113] Pavlovic, E; Quist, A. P; Gelius, U; Nyholm, L; Oscarsson, S. *Langmuir* **2003**, *19*, 4217.

[114] Balachander, N; Sukenik, C. N. *Langmuir* **1990**, *6*, 1621.

[115] Bhatia, S. K; Hickman, J. J; Ligler, F. S. *Journal of the American Chemical Society* **1992**, *114*, 4432.

[116] Ding, Y.-X; Streitmatter, S; Wright, B. E; Hlady, V. *Langmuir* **2010**, *26*, 12140.

[117] Chamoulaud, G; Bélanger, D. *Langmuir* **2004**, *20*, 4989.

[118] Langmuir, I. *Journal of the American Chemical Society* **1917**, *39*, 1848.

[119] Langmuir, I. *Transactions of the Faraday Society* **1920**, *15*, 62.

[120] Blodgett, K. B. *Journal of the American Chemical Society* **1934**, *56*, 495.

[121] Blodgett, K. B. *Journal of the American Chemical Society* **1935**, *57*, 1007.

[122] Bigelow, W; Pickett, D; Zisman, W. *Journal of Colloid Science* **1946**, *1*, 513.

[123] Schreiber, F. *Progress in Surface Science* **2000**, *65*, 151.

[124] Ulman, A. *Chemical Reviews* **1996**, *96*, 1533.

[125] Wasserman, S. R; Tao, Y. T; Whitesides, G. M. *Langmuir* **1989**, *5*, 1074.

[126] Le Grange, J. D; Markham, J. L; Kurkjian, C. R. *Langmuir* **1993**, *9*, 1749.

[127] Mathauer, K; Frank, C. W. *Langmuir* **1993**, *9*, 3002.

[128] Yanker, D. M; Maurer, J. A. *Molecular BioSystems* **2008**, *4*, 502.

[129] Kessel, C. R; Granick, S. *Langmuir* **1991**, *7*, 532.

[130] Silberzan, P; Leger, L; Ausserre, D; Benattar, J. J. *Langmuir* **1991**, *7*, 1647.

[131] Pavlovic, E., *Spatially controlled covalent immobilization of biomolecules on silicon surfaces*, Uppsala **2003**.

[132] Barness, Y; Gershevitz, O; Sekar, M; Sukenik, C. N. *Langmuir* **2000**, *16*, 247.

[133] Bierbaum, K; Kinzler, M; Woell, C; Grunze, M; Haehner, G; Heid, S; Effenberger, F. *Langmuir* **1995**, *11*, 512.

[134] Pavlovic, E; Quist, A. P; Gelius, U; Oscarsson, S. *Journal of Colloid and Interface Science* **2002**, *254*, 200.

[135] Rühe, J., *Polymer brushes: Polymer Brushes: On the Way to Tailor-Made Surfaces*, Wiley-VCH, Weinheim **2004**.

[136] van der Waarden, M. *Journal of Colloid Science* **1950**, *5*, 317.

[137] van der Waarden, M. *Journal of Colloid Science* **1951**, *6*, 443.

[138] Ji, H; Gennes, P. G. de *Macromolecules* **1993**, *26*, 520.

[139] Raphael, E; Gennes, P. G. de *The Journal of Physical Chemistry* **1992**, *96*, 4002.

[140] Amiji, M; Park, K. *Journal of Biomaterials Science, Polymer Edition* **1993**, *4*, 217.

[141] Joanny, J. F. *Langmuir* **1992**, *8*, 989.

[142] MILNER, S. T. *Science* **1991**, *251*, 905.

[143] Zhao, B; Brittain, W. *Progress in Polymer Science* **2000**, *25*, 677.

[144] Boven, G; Folkersma, R; Challa, G; Schouten, A. J. *Polymer Communications* **1991**, *32*, 50.

[145] Boven, G; Oosterling, M. L; Challa, G; Jan Schouten, A. *Polymer* **1990**, *31*, 2377.

[146] Fery, N; Laible, R; Hamann, K. *Angewandte Makromolekulare Chemie* **1973**, *34*, 81.

[147] Prucker, O; Rühe, J. *Macromolecules* **1998**, *31*, 592.

[148] Prucker, O; Rühe, J. *Macromolecules* **1998**, *31*, 602.

[149] Biesalski, M; Rühe, J. *Macromolecules* **1999**, *32*, 2309.

[150] Peng, B; Johannsmann, D; Rühe, J. *Macromolecules* **1999**, *32*, 6759.

[151] Prucker, O; Rühe, J. *Langmuir* **1998**, *14*, 6893.

[152] Bertin, A; Schlaad, H. *Chemistry of Materials* **2009**, *21*, 5698.

[153] Löbbicke, R; Chanana, M; Schlaad, H; Pilz-Allen, C; Günter, C; Möhwald, H; Taubert, A. *Biomacromolecules* **2011**, *12*, 3753.

[154] Yang, W. J; Neoh, K.-G; Kang, E.-T; Lay-Ming Teo, S; Rittschof, D. *Polymer Chemistry* **2013**, *4*, 3105.

[155] Pyun, J; Kowalewski, T; Matyjaszewski, K. *Macromolecular Rapid Communications* **2003**, *24*, 1043.

[156] Barbey, R; Lavanant, L; Paripovic, D; Schüwer, N; Sugnaux, C; Tugulu, S; Klok, H.-A. *Chemical Reviews* **2009**, *109*, 5437.

[157] Jordan, R; Ulman, A. *Journal of the American Chemical Society* **1998**, *120*, 243.

[158] Jordan, R; Ulman, A; Kang, J. F; Rafailovich, M. H; Sokolov, J. *Journal of the American Chemical Society* **1999**, *121*, 1016.

[159] Weck, M; Jackiw, J. J; Rossi, R. R; Weiss, P. S; Grubbs, R. H. *Journal of the American Chemical Society* **1999**, *121*, 4088.

[160] Lee, K.-B; Lim, J.-H; Mirkin, C. A. *Journal of the American Chemical Society* **2003**, *125*, 5588.

[161] Liu, X; Guo, S; Mirkin, C. A. *Angewandte Chemie International Edition* **2003**, *42*, 4785.

[162] Case, M. A; McLendon, G. L; Hu, Y; Vanderlick, T. K; Scoles, G. *Nano Letters* **2003**, *3*, 425.

[163] Bano, F; Fruk, L; Sanavio, B; Glettenberg, M; Casalis, L; Niemeyer, C. M; Scoles, G. *Nano Letters* **2009**, *9*, 2614.

[164] Kenseth, J. R; Harnisch, J. A; Jones, V. W; Porter, M. D. *Langmuir* **2001**, *17*, 4105.

[165] Hirtz, M; Brinks, M. K; Miele, S; Studer, A; Fuchs, H; Chi, L. *Small* **2009**, *5*, 919.

[166] Bernard, A; Renault, J. P; Michel, B; Bosshard, H. R; Delamarche, E. *Advanced Materials* **2000**, *12*, 1067.

[167] James, C. D; Davis, R. C; Kam, L; Craighead, H. G; Isaacson, M; Turner, J. N; Shain, W. *Langmuir* **1998**, *14*, 741.

[168] Madou, M. J., *Fundamentals of microfabrication: The science of miniaturization*, CRC Press, Boca Raton **2002**.

[169] Tizazu, G; el Zubir, O; Patole, S; McLaren, A; Vasilev, C; Mothersole, D. J; Adawi, A; Hunter, C. N; Lidzey, D. G; Lopez, G. P; Leggett, G. J. *Biointerphases* **2012**, *7*, 1.

[170] Reynolds, N. P; Tucker, J. D; Davison, P. A; Timney, J. A; Hunter, C. N; Leggett, G. J. *Journal of the American Chemical Society* **2009**, *131*, 896.

[171] Ahmad, S. A; Leggett, G. J; Hucknall, A; Chilkoti, A. *Biointerphases* **2011**, *6*, 8.

[172] Reynolds, N. P; Janusz, S; Escalante-Marun, M; Timney, J; Ducker, R. E; Olsen, J. D; Otto, C; Subramaniam, V; Leggett, G. J; Hunter, C. N. *Journal of the American Chemical Society* **2007**, *129*, 14625.

[173] Montague, M; Ducker, R. E; Chong, K. S. L; Manning, R. J; Rutten, F. J. M; Davies, M. C; Leggett, G. J. *Langmuir* **2007**, *23*, 7328.

[174] Pease, A. C; d. Solas; Sullivan, E. J; Cronin, M. T; Holmes, C. P; Fodor, P. A. *Proceedings of the National Academy of Sciences* **1994**, *91*.

[175] Schuh, C; Santer, S; Prucker, O; Rühe, J. *Advanced Materials* **2009**.

[176] Born, M; Wolf, E., *Principles of optics: Electromagnetic theory of propagation, interference and diffraction of light*, Pergamon Press, Oxford, New York **1980**.

[177] Sun, S; Leggett, G. J. *Nano Letters* **2002**, *2*, 1223.

[178] Sun, S; Chong, K. S. L; Leggett, G. J. *Journal of the American Chemical Society* **2002**, *124*, 2414.

[179] Sun, S; Thompson, D. G; Graham, D; Leggett, G. J. *Journal of Materials Chemistry* **2011**, *21*, 14173.

[180] el Zubir, O; Barlow, I; Ul-Haq, E; Tajuddin, H. A; Williams, N. H; Leggett, G. J. *Langmuir* **2013**, *29*, 1083.

[181] Alang Ahmad, S; Hucknall, A; Chilkoti, A; Leggett, G. J. *Langmuir* **2010**, *26*, 9937.

[182] Alang Ahmad, S. A; Wong, L. S; Ul-Haq, E; Hobbs, J. K; Leggett, G. J; Micklefield, J. *Journal of the American Chemical Society* **2011**, *133*, 2749.

[183] Hurley, C. R; Ducker, R. E; Leggett, G. J; Ratner, B. D. *Langmuir* **2010**, *26*, 10203.

[184] Wong, L. S; Janusz, S. J; Sun, S; Leggett, G. J; Micklefield, J. *Chemistry - A European Journal* **2010**, *16*, 12234.

[185] Li, L; Gattas, R; Fourkas, J. *SPIE Newsroom* **2009**.

[186] Wollhofen, R; Katzmann, J; Hrelescu, C; Jacak, J; Klar, T. A. *Optics Express* **2013**, *21*, 10831.

[187] Wiesbauer, M; Wollhofen, R; Vasic, B; Schilcher, K; Jacak, J; Klar, T. A. *Nano Letters* **2013**, *13*, 5672.

[188] Wolfesberger, C; Wollhofen, R; Buchegger, B; Jacak, J; Klar, T. A. *Journal of Nanobiotechnology* **2015**, *13*, 132.

[189] Michael, A. *Journal für Praktische Chemie* **1886**, *35*, 349.

[190] Mather, B. D; Viswanathan, K; Miller, K. M; Long, T. E. *Progress in Polymer Science* **2006**, *31*, 487.

[191] Nair, D. P; Podgórski, M; Chatani, S; Gong, T; Xi, W; Fenoli, C. R; Bowman, C. N. *Chemistry of Materials* **2014**, *26*, 724.

[192] Chan, J. W; Hoyle, C. E; Lowe, A. B; Bowman, M. *Macromolecules* **2010**, *43*, 6381.

[193] Liu, M; Tan, B. H; Burford, R. P; Lowe, A. B. *Polymer Chemistry* **2013**, *4*, 3300.

[194] Chan, J. W; Yu, B; Hoyle, C. E; Lowe, A. B. *Polymer* **2009**, *50*, 3158.

[195] Lowe, A. B; Hoyle, C. E; Bowman, C. N. *Journal of Materials Chemistry* **2010**, *20*, 4745.

[196] Fairbanks, B. D; Scott, T. F; Kloxin, C. J; Anseth, K. S; Bowman, C. N. *Macromolecules* **2009**, *42*, 211.

[197] Fairbanks, B. D; Sims, E. A; Anseth, K. S; Bowman, C. N. *Macromolecules* **2010**, *43*, 4113.

[198] Bardwell, J. C; Lee, J. O; Jander, G; Martin, N; Belin, D; Beckwith, J. *Proceedings of the National Academy of Sciences* **1993**, *90*, 1038.

[199] Åslund, F; Beckwith, J. *Cell* **1999**, *96*, 751.

[200] Ostergaard, H; Henriksen, A; Hansen, F. G; Winther, J. R. *The EMBO Journal* **2001**, *20*, 5853.

[201] Bardwell, J. C; Beckwith, J. *Cell* **1993**, *74*, 769.

[202] Konigsberg, W.

[203] Parker, A. J; Kharasch, N. *Chemical Reviews* **1959**, *59*, 583.

[204] Mandal, B; Basu, B. *RSC Advances* **2014**, *4*, 13854.

[205] Brändle, A; Khan, A. *Polymer Chemistry* **2012**, *3*, 3224.

[206] De, S; Khan, A. *Chemical Communications* **2012**, *48*, 3130.

[207] Carioscia, J. A; Stansbury, J. W; Bowman, C. N. *Polymer* **2007**, *48*, 1526.

[208] Fringuelli, F; Pizzo, F; Tortoioli, S; Vaccaro, L. *Tetrahedron Letters* **2003**, *44*, 6785.

[209] Nakayama, N; Hayashi, T. *Progress in Organic Coatings* **2008**, *62*, 274.

[210] Kosaka, M; Kageyama, Y. US 5744568, *Process for the Production of Polyurethane Lens* 28. Apr. **1998**.

[211] Rosen, B. M; Lligadas, G; Hahn, C; Percec, V. *Journal of Polymer Science Part A: Polymer Chemistry* **2009**, *47*, 3940.

[212] Ledung, G; Bergkvist, M; Quist, A. P; Gelius, U; Carlsson, J; Oscarsson, S. *Langmuir* **2001**, *17*, 6056.

[213] Aswal, D. K; Lenfant, S; Guerin, D; Yakhmi, J. V; Vuillaume, D. *Small* **2005**, *1*, 725.

[214] Corum, L. E; Hlady, V. *Biomaterials* **2010**, *31*, 3148.

[215] Janssen, D; Palma, R. de; Verlaak, S; Heremans, P; Dehaen, W. *Thin Solid Films* **2006**, *515*, 1433.

[216] Bain, C. D; Troughton, E. B; Tao, Y. T; Evall, J; Whitesides, G. M; Nuzzo, R. G. *Journal of the American Chemical Society* **1989**, *111*, 321.

[217] Joanny, J. F; Gennes, P. G. de *The Journal of Chemical Physics* **1984**, *81*, 552.

[218] Huang, L; Li, Y; Yang, J; Zeng, Z; Chen, Y. *Polymer* **2009**, *50*, 4325.

[219] Beuermann, S; Buback, M. *Progress in Polymer Science* **2002**, *27*, 191.

[220] Sun, S; Montague, M; Critchley, K; Chen, M.-S; Dressick, W. J; Evans, S. D; Leggett, G. J. *Nano Letters* **2006**, *6*, 29.

[221] Pandya, R; Murashima, T; Tedeschi, L; Barrett, A. G. M. *The Journal of Organic Chemistry* **2003**, *68*, 8274.

[222] Wright, S. W; Hallstrom, K. N. *The Journal of Organic Chemistry* **2006**, *71*, 1080.

[223] Lee, J. W; Louie, Y. Q; Walsh, D. P; Chang, Y.-T. *Journal of Combinatorial Chemistry* **2003**, *5*, 330.

[224] Frost, C. G; Hartley, J. P; Griffin, D. *Synlett* **2002**, *2002*, 1928.

[225] Deng, X; Mani, N. S. *Green Chemistry* **2006**, *8*, 835.

[226] Caddick, S; Wilden, J. D; Judd, D. B. *Journal of the American Chemical Society* **2004**, *126*, 1024.

[227] Hutt, D. A; Leggett, G. J. *Langmuir* **1997**, *13*, 2740.

[228] Prime, K; Whitesides, G. *Science* **1991**, *252*, 1164.

[229] Bryant, S. J; Anseth, K. S. *Biomaterials* **2001**, *22*, 619.

[230] Bryant, S. J; Anseth, K. S. *Biomaterials* **2001**, *22*, 619.

[231] Danos, L; Greef, R; Markvart, T. *Thin Solid Films* **2008**, *516*, 7251.

[232] Höhne, G; Hemminger, W; Flammersheim, H.-J., *Differential scanning calorimetry: An introduction for practitioners*, Springer, Berlin, New York **2003**.

[233] Netzsch-Gerätebau GmbH, *DSC 204 F1 Phoenix - Differential Scanning Calorimetry: Method, Technique, Applications* **2015**.

[234] Ullrich, G; Ganster, B; Salz, U; Moszner, N; Liska, R. *Journal of Polymer Science Part A: Polymer Chemistry* **2006**, *44*, 1686.

[235] Carlson, T. A., *Photoelectron and Auger Spectroscopy*, Springer Verlag **2013**.

[236] Moulder, J. F; Chastain, J., *Handbook of x-ray photoelectron spectroscopy: A reference book of standard spectra for identification and interpretation of XPS data*, Physical Electronics Division, Perkin-Elmer Corp., Eden Prairie, Minn **1992**.

[237] Binnig, G; Rohrer, H; Gerber, C; Weibel, E. *Applied Physics Letters* **1982**, *40*, 178.

[238] Binnig, G; Quate, C. F; Gerber, C. *Physical Review Letters* **1986**, *56*, 930.

[239] Carpick, R. W; Salmeron, M. *Chemical Reviews* **1997**, *97*, 1163.

[240] Jalili, N; Laxminarayana, K. *Mechatronics* **2004**, *14*, 907.

[241] Tamayo, J; García, R. *Langmuir* **1996**, *12*, 4430.

[242] Bennewitz, R. *Materials Today* **2005**, *8*, 42.

[243] Williams, P. *Annual Review of Materials Science* **1985**, *15*, 517.

[244] Sodhi, R. N. S. *The Analyst* **2004**, *129*, 483.

[245] Tadmor, R. *Langmuir* **2004**, *20*, 7659.

[246] Gao, L; McCarthy, T. J. *Langmuir* **2006**, *22*, 6234.

[247] Stauffer, C. E. *The Journal of Physical Chemistry* **1965**, *69*, 1933.

[248] Pascu, R; Dinescu, M. *Romanian Reports in Physics* **2012**, *64*, 135.

[249] Fujiwara, H., *Spectroscopic ellipsometry: Principles and applications*, John Wiley & Sons, Chichester, England, Hoboken, NJ **2007**.